

SLOPE STABILITY ANALYSES IN PART OF THE YAMUNA VALLEY, GARHWAL HIMALAYA

Thesis
Submitted to



Nagaland University, India

In partial fulfilment of the requirement for the Degree of
Doctor of Philosophy (Ph. D)
in
Geology

BY

IMLIRENLA JAMIR

DST INSPIRE Fellow



Wadia Institute of Himalayan Geology,
Dehradun, Uttarakhand, India

2019

NAGALAND UNIVERSITY

March 2019

DECLARATION

I, Miss Imlirenla Jamir, hereby declare that the subject matter of this thesis is the record of work done by me, during the period May 2014 to October 2018. That the contents of this thesis did not form the basis of the award of any previous degree to me or to the best of my knowledge to anybody else, and that the thesis has not been submitted by me for any research degree in any other University/ Institute.

This thesis is submitted to the Nagaland University, in partial fulfilment for the degree of Doctorate in Philosophy in Geology under the joint supervision of Dr. Vikram Gupta, Scientist F (Wadia Institute of Himalayan Geology, Dehradun) and Professor Glenn T. Thong (Nagaland University).

Date: 28th March 2019
Place: Department of Geology
Nagaland University,
Kohima Campus, Meriema



IMLIRENLA JAMIR
DST Inspire Fellow (IF130881)
Department of Geology
Reg. No. 610/2014 (20th May 2014)



Head
Professor B.V. Rao
Department of Geology,
Nagaland University,
Kohima Campus, Meriema



Co-Supervisor
Professor G.T. Thong
Department of Geology,
Nagaland University,
Kohima Campus, Meriema

NAGALAND

Glenn T. Thong
Professor of Geology



UNIVERSITY

☎ : 0370-2240515
Mobile : 09436000479
E-mail : glen2t03@yahoo.com
nagalandslide@yahoo.com

Dated Kohima the 28 March 2019

CERTIFICATE

The thesis presented by Miss Imlirenla Jamir, M.Sc., bearing Registration No. 610/2014 (20th May 2014) embodies the results of investigations carried out by her under my supervision and guidance.

I certify that this work has not been presented for any degree elsewhere and that the candidate has fulfilled all conditions laid down by the University.


(G.T. THONG)

Acknowledgement

The completion of this Ph.D thesis was possible by the grace of God and support of many people whom I would like to thank sincerely. At the very outset, I would like to express my heartfelt gratitude to my supervisor, **Dr. Vikram Gupta**, Scientist F, Wadia Institute of Himalayan Geology, Dehradun, for his constant guidance, support and patience at all stages of this study. My heartfelt gratitude also goes to my co-supervisor, **Prof. Glenn T. Thong**, Nagaland University, for his invaluable time, support and guidance whenever it was required. Their able supervision, guidance and invaluable time were an important part for the completion of this thesis.

I sincerely express my gratitude to **Dr. Khayingshing Luirei**, Scientist E, Wadia Institute of Himalayan Geology for the discussions and his constructive suggestions. The discussions enabled me to widen my horizons of understanding and perspectives during the course of this study. I am also deeply humbled and grateful to **Prof. D. Vaughan Griffiths**, Colorado School of Mines, USA for his invaluable time, for the discussions and his keen interest to go through some of my important chapters of the manuscript.

The conducive, academic and resourceful environment, the laboratory and other research facilities provided to me by the Wadia Institute of Himalayan Geology, Dehradun enabled me to carry out my research work smoothly. I therefore, would like to express my gratitude to the scientists and other staff who had, in one way or the other, rendered their help and support during this journey.

I would like to thank the faculties of the Department of Geology, Nagaland University, **Prof. B.V. Rao**, **Prof. Santosh K. Singh**, **Dr. Vikoleno Rino**, **Dr. Sanjai K. Srivastava**, **Dr. Temsulemba Walling** and **Dr. Ch. Mangi Khuman** for nurturing us during the initial stage of this research journey. The staff and students of the department are also heartily acknowledged for always being so helpful and hospitable.

I am extremely indebted to **Mr. Vipin Kumar** and **Mr. Pranay Diwate** for their consistent help and support throughout my research work. The discussions and

sometimes disagreements which eventually often turned out to be constructive had played a major role during this work.

My sincere gratitude goes to **Dr. Supongtemjen** and **Mr. Samuel Thong**, NGIS & RS Centre, Department of Planning and Coordination, Nagaland, Kohima and **Dr. Rakesh Bhamri**, Scientist B, Wadia Institute of Himalayan Geology, Dehradun for their assistance and help rendered to all my queries related to Remote Sensing and GIS.

I also thank the **Director**, National Geotechnical Facility, Dehradun for providing me the facility to carry out the analyses. The scientists and technical staff, who were always there to help and assist me with my queries, are also sincerely acknowledged.

The grant from the **DST-INSPIRE Fellowship** (No. DST/INSPIRE Fellowship/2013/965) is sincerely acknowledged. The financial support had made the research work and challenges a lot smoother.

My special gratitude goes to **Mrs. Deepa Jain Gupta** for the hospitality and her constant encouragement. I am also thankful to my lab mates for their help and moral support.

I am very grateful to all my friends who had been instrumental in keeping me sane and being there to support me consistently.

I owe my heartfelt gratitude and love to my loving parents, sisters and other family members who have ceaselessly supported me throughout this journey. Their constant support, love and encouragement have helped me complete this journey.



(IMLIRENLA JAMIR)

Preface

Since time immemorial, landslides have been part and parcel of the mountain ecosystems. However, it was not considered a threat as long as it did not impact on the human population or cause socio-economic loss. Over the past decades, with the ever growing population and demand for more land to accommodate the population and its ambition for development, exploitation of resources and land knew no limit, even to the extent of migrating to higher treacherous terrains. The repercussions caused by such developmental activities have eventually led to more disasters including landslides, particularly in developing countries such as India. As such, the Himalayan terrain is one of the most vulnerable regions, which is highly prone to landslides. The complexity of its geomorphic setting and varying litho-tectonic regime makes it all the more vulnerable to landslide phenomena. However, a great extent of the disaster can be prevented if the geological and mechanical conditions are understood and mitigated.

In as much as developmental activities are concerned, thorough investigation of the area with regard to its stability is the pre-requisite for decision makers. The analysis and solution of landslide problems as well as prevention or mitigation of landslides requires an understanding of geology, hydrology, seismology, geotechnical exploration and engineering, computerized analytical methods and practical and constructible engineering solutions. The engineering approach to landslide studies has focused attention on analysis of individual slope failure and their remedial/mitigation measures.

The Yamuna Valley in the Garhwal Himalaya is subject to anthropogenic activities for developmental schemes in the form of road widening, damming for upcoming hydroelectric power projects, etc. It is of strategic importance as it links to the Char Dham Yatra (Hindu Pilgrimage) route which, during the Yatra season (May-July) is flocked by pilgrims and heavy vehicular movement. However, negligence may cause the area to become vulnerable to landsliding and other mass movements. Hence, there is a need for identification of potential landslide zones.

The purpose of this study was to prepare a landslide susceptibility map of the Yamuna Valley in the Garhwal Himalaya and determine the contribution of various causative

factors responsible for the landslides in the area. An attempt was made to understand the interrelationship between landslides and the litho-tectonic regime, which further helped in evaluating the stability of the individual slopes in the region. The thesis comprises six chapters that have been structured as follows:

Chapter 1 introduces the subject and provides a comprehensive idea of the causes of landslides and the various approaches for landslide studies. This chapter gives an insight about the motivation and the nature of the study. It also gives an account about the study area, its physiography and climatic condition. The climatic condition of the valley has been discussed as per literature available. **Chapter 2** gives an account of the regional geological setup of the Himalaya, followed by a detailed account of the Garhwal Himalaya and the Yamuna Valley. A discussion of the geology of the area has been made based on the regional geological maps available from previous literature and verification from various field traverses. **Chapter 3** elaborates the quantitative approach of Landslide Susceptibility Zonation mapping using the Frequency Ratio method. It was determined by establishing the relationship between landslides and the causative factors. It gives a detailed account of the methods and data used. The accuracy of a susceptibility map was evaluated using success rate curves. **Chapter 4** gives an insight on the spatial interrelationship of the landslides with the litho-tectonic regime and precipitation of the region. Geomorphic proxies such as longitudinal profile of the river (L-profile), topographic swath profile, valley floor width to height ratio (V_f), stream length gradient index (SL) and channel steepness index (K_s) were used to understand the tectonic regime. Tropical Rainfall Measurement Mission (TRMM) and normalized difference vegetation index (NDVI) were used to discern the precipitation condition of the region. A Schmidt Hammer Rebound (SHR) and geological strength index (GSI) were used as lithological strength proxies. **Chapter 5** deals with slope stability analysis of both debris slides and rock falls using analytical techniques such as Finite Element Method, Kinematic Analysis and Rock Mass classification (Rock Mass Rating and Slope Mass Rating). This is followed by a case study for slope stability evaluation of a selected slope (Wariya landslide) and also to suggest mitigation measures. **Chapter 6** is the synthesis of the results drawn from the previous chapters along with conclusions and a general recommendation for the landslides of the study area.

TABLE OF CONTENTS

	Page No.
Declaration	i
Certificate	ii-iii
Acknowledgement	iv-v
Preface	vi-vii
Lists of Tables	viii
List of Figures	ix-xi
Particulars of the candidate	xii
CHAPTER 1 INTRODUCTION	1-7
1.1 Statement of the problem and motivation	4-5
1.2 Study area	5-7
1.2.1 Physiography and climate	6-7
1.3 Aim and objectives	7
CHAPTER 2 GEOLOGICAL SETTING	8-19
2.1 Introduction	8
2.2 Litho-tectonic divisions of the Himalaya	8-11
2.2.1 Sub Himalaya	9
2.2.2 Lesser Himalaya	9-10
2.2.3 Higher Himalaya	10
2.2.4 Tethyan Himalaya	10
2.2.5 Trans Himalaya	10-11
2.3 Geological setting of the Garhwal Himalaya	11-14
2.4 Geological setup of the Yamuna Valley and the study area	14-19
2.4.1 Autochthonous Zone	16-17
2.4.2 Allochthonous Zone	18
2.4.3 Central Crystalline	18-19
CHAPTER 3 LANDSLIDE SUSCEPTIBILITY ZONATION MAPPING	20-48
3.1 Introduction	20-21
3.2 Methodology	21-25

3.2.1	Data generation	
3.2.1.1	Landslide inventory	21-22
3.2.1.2	Spatial database preparation/ Thematic maps	23
3.2.1.3	Digital Elevation Model generation	23-25
3.3	Landslide Susceptibility Zonation Mapping	25-26
3.3.1	Frequency Ratio method	25
3.3.2	Validation and evaluation	26
3.4	Results	27-38
3.4.1	Landslide inventory	27
3.4.2	Spatial database/ Thematic maps	27-38
3.4.2.1	Relationship between elevation and landslides	27-28
3.4.2.2	Relationship between slope angle and landslides	28-29
3.4.2.3	Relationship between slope aspect and landslides	29
3.4.2.4	Relationship between lithology and landslides	29-30
3.4.2.5	Relationship between land use / land cover and landslides	30
3.4.2.6	Relationship between proximity to lineament and landslides	30-31
3.4.2.7	Relationship between proximity to drainage and landslides	31
3.4.2.8	Relationship between proximity to road and landslides	31
3.5	Landslide Susceptibility map	39-41
3.5.1	Application of frequency Ratio	
3.6	Validation and evaluation	41-42
3.7	Discussion	42-48
3.7.1	Limitations	48

CHAPTER 4 SPATIAL INTERRELATIONSHIP OF LANDSLIDES, LITHO-TECTONIC AND PRECIPITATION REGIME 49-64

4.1	Introduction	49-50
4.2	Methodology	50-56
4.2.1	Landslide inventory	50-51
4.2.2	River long profile and topographic swath profile	51
4.2.3	Stream Length Gradient index	51-52
4.2.4	Steepness index	52-53

4.2.5	Valley floor width to valley height ratio	53-54
4.2.6	Rainfall and Normalized Difference Vegetation Index	54-55
4.2.7	Rockmass Strength	55-56
4.2.7.1	Schmidt Hammer Rebound (R)- value	55
4.2.7.2	Geological Strength Index (GSI)	55-56
4.3	Results	57-61
4.3.1	Landslide inventory	57
4.3.2	River long profile and topographic swath profile	57-58
4.3.3	Stream Length Gradient index	58-59
4.3.4	Steepness index	59
4.3.5	Valley floor width to valley height ratio	59-60
4.3.6	Rainfall and Normalized Difference Vegetation Index	60
4.3.7	Rockmass Strength	61
4.4	Discussion	62-64
4.4.1	Higher Himalaya	62
4.4.2	Lesser Himalaya	62-63
4.4.3	Limitations	63-64
CHAPTER 5 SLOPE STABILITY EVALUATION		65-101
5.1	Introduction	65
5.2	Methodology	66-79
5.2.1	Kinematic analysis of discontinuities	66-68
5.2.2	Rock Mass Rating (RMR) classification	68-69
5.2.3	Slope Mass Rating (SMR) classification	69-70
5.2.4	Geological Strength Index (GSI) classification	70
5.2.5	Finite Element Method	72-79
5.3	Results	79-94
5.4	Discussion	95-101
5.4.1	Scope of the study	97-100
5.4.2	Limitations	100-101
CHAPTER 6 CONCLUSIONS		102-107
6.1	Conclusions	102-104
6.2	Prospect of the work	104-107
BIBLIOGRAPHY		108-139

APPENDIX 1

140-142

BIO-DATA OF THE CANDIDATE

xiii-xiv

LIST OF TABLES

	Page No.
Table 2.1: Generalized litho-stratigraphy of the Garhwal Group (Kumar, 2005)	13
Table 2.2: Regional litho-tectonic setting of the Yamuna Valley (modified after Pachuari, 1972 and Valdiya, 1980)	16
Table 3.1: Details of satellite imagery and topographic maps used in the study	22
Table 3.2: Details of thematic map used in the present study	24-25
Table 3.3: Computed ratios for classes of various data layers based on landslide occurrences	36-38
Table 3.4: Different classes of landslide susceptibility zone	41
Table 5.1: The relative weight of observational and laboratory- determined parameters used to calculate RMR_{basic} (Bieniawski, 1979)	71
Table 5.2: Values of adjustment Factors for F1, F2, F3 and F4 (Romana, 1985)	72
Table 5.3: Values of stability classes as per SMR values (Romana, 1985)	72
Table 5.4: Details of parameters used in FEM	77-78
Table 5.5: Details of rock mass exposures in the study area and results of kinematic analysis.	79-87
Table 5.6: Geomechanical classification of the rockmass in the study area	89-91
Table 5.7: Details of debris slide and result of FEM analysis	92-93
Appendix 1: Landslide details: HH, Higher Himalaya; LH, Lesser Himalaya. The classification of landslide type is based on Varnes, (1978)	140-142

LIST OF FIGURES

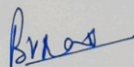
	Page No.
Fig. 1.1: Location map of the study area	6
Fig. 1.2: Spatial variation of valley width along the river. Inset: a) narrow gorge; b) widening of the valley	7
Fig 2.1: Generalized litho-stratigraphic divisions of the Himalaya (after Searle et al., 2003; Yin, 2006)	9
Fig. 2.2: Geological map of the Garhwal Himalaya (After Valdiya 1980; Kumar, 2005)	12
Fig. 2.3: Geological setting after Pachuari (1972), Valdiya (1980) and Saklani et al. (1991). The red rectangle (inset) denotes position of the study area in the NW Himalaya. F-F: fault, MCT- Main Central Thrust; NAT-North Almora Thrust; HH-Higher Himalaya; LH- Lesser Himalaya	15
Fig. 3.1: Inventory of landslides indicating the spatial distribution in the study area	28
Fig.3.2: Thematic maps of the study area: (1) Elevation map; (2) Slope map; (3) Slope aspect map; (4) Lithological map; (5) Land use/Land cover map; (6) Proximity to lineaments map; (7) Proximity to drainage map; (8) Proximity to road map	32-35
Fig. 3.3: Landslide susceptibility map of the study area; the map was validated in the field (Photos 1-6)	40-41
Fig. 3.4: Success rate curve	42
Fig. 3.5: Spatial distribution of landslides with causative factors and frequency ratio analysis	43
Fig. 3.6: (a) Damaged retaining wall below Wariya village. (b) Erosional deposits on the NH-94. Photograph of November 2014, prior to the disaster (November, 2017)	47
Fig.3.7: Magnified view of Wazri landslide (Inset: images prior to	

field mapping and post-field mapping)	47
Fig. 4.1: Spatial variation of valley width along the river (Inset: Mean and maximum topographic swath profile along the stream)	53
Fig.4.2: Quantification of GSI chart (Cai et al., 2007)	56
Fig.4.3: Tectonic regime of the Yamuna Valley. Spatial variability of stream length gradient index (SL), topographic swath profile, valley floor width to valley floor height (V_f), steepness index (K_s), area and volume of individual landslides along the river longitudinal (L) profile. The gradient change along the river profile is measured in m/km. F-F denotes fault, MCT and NAT refers to the Main Central Thrust and the North Almora Thrust respectively.	58
Fig.4.4: Comparison of steepness index (k_s) at $\theta=0.45$ and $\theta=0.6$. k_{sn} refers to normalized steepness index	59
Fig.4.5: Precipitation regime of the Yamuna Valley. Spatial variability of topographic swath profile, normalized difference vegetative index (NDVI), annual rainfall, area and volume of individual landslides along the river longitudinal (L) profile. F-F denotes fault, MCT and NAT refers to the Main Central Thrust and the North Almora Thrust respectively	60
Fig. 4.6: Proxy for rockmass strength. GSI and SHR-Geological strength index and Schmidt hammer rebound. (a) Spatial variability of GSI and SHR. Red dashed line indicates average value; (b) correlation of SHR and GSI	61
Fig. 5.1: Geometric representation and stereo-plots of structural discontinuities for (a) planar failure (b) wedge failure and (c) toppling failure. ϕ is the angle of internal friction	67
Fig 5.2: General finite element model configuration of slope using 6-noded triangular elements in uniform meshing	73

Fig 5.3: Flowchart in FEM used in the present study	74
Fig.5.4: Standard roughness profile (After Jang et al., 2014)	75
Fig 5.5: Results of FEM analysis in terms of FoS and displacement (m)	88
Fig. 5.6: Correlation between FoS, landslide area and volume. (a-b) FoS vs landslide area and FoS vs volume for 29 slopes (c-d) FoS vs landslide area and FoS vs volume in the HH. (e-f) FoS vs landslide area and FoS vs volume in the LH The dashed line represents linear regression	94
Fig 5.7: Results of slope stability evaluation. HH-Higher Himalaya; LH-Lesser Himalaya; L_d - Landslide density	94
Fig 5.8: Results of the rockmass classification using RMR, SMR and GSI	95
Fig. 5.9: Field exposures: (a) Highly fractured quartzite at location 21; (b) Highly fractured slate along NH-94	96
Fig. 5.10: (a) Present landslide at Wariya village; (b) Illustration for remedial/mitigation measures	99
Fig. 6.1: Overhanging slope along part of the Char Dham Yatra route	105

PARTICULARS OF THE CANDIDATE

NAME OF THE CANDIDATE : Miss Imlirenla Jamir
DEGREE : Ph.D.
DEPARTMENT : Geology
TITLE OF THE THESIS : Slope stability analyses in part of the
Yamuna Valley, Garhwal Himalaya
DATE OF ADMISSION : 25th March, 2013
APPROVAL OF RESEARCH PROPOSAL : 16th June 2014
REGISTRATION NUMBER & DATE : 610/2014 (20th May, 2014)



Head of the Department

HEAD
Department of Geology
Nagaland University, Kohima

Chapter-1

INTRODUCTION

Landslide as defined by Cruden (1991) is “the movement of a mass of rock, debris or earth down a slope”. It is a natural geological process that is generally controlled by a variety of factors including geological condition, groundwater condition, topography, intense rainfall, earthquake, land use (Varnes, 1984; Cruden, 1991; Dai et al., 2002). Depending on the type of material (debris, rock) and mechanisms involved, landslides may be classified as flow, slide, topple or fall (Varnes, 1978). However, if a landslide exhibits a combination of more than two types of movements, it is a complex slide (Varnes, 1978; Cruden and Varnes, 1996).

Landslides are responsible for hillslope development and are an important part of mass movement (Harmon et al., 2001; Glade and Crozier, 2005; Petley, 2010). These are some of the most important, long term evolutions of landscapes, providing major means for sediment release from slopes to permit transportation through the fluvial system (Van Westen, 1993). Generally, such processes are common in areas of weak lithology and steep slopes. These are common in the mountainous terrain and to a great extent, pose threat to lives and the economy. These become hazardous when they interfere with human activities.

The Himalaya is orogenically active and is constantly undergoing deformation, with rupturing in the thrust belt zones due to which earthquakes and mass movements occur frequently. Both these phenomena are responsible for continued modification of the landscape. Because of relatively high relief, immature terrain and highly multifaceted tectonic setting, this region assumes greater significance for the mass wasting processes, including landslides. The terrain in the Himalayan is traversed by a number of neotectonically active thrusts and faults, hence the slopes along or in the vicinity of these discontinuities are highly unstable and prone to landslides (Sarkar et al., 1995; Gupta and Sah, 2008a). This is possibly due to the weak lithology comprising shattered rock masses and unfavourable geomorphological setup in the form of steep slopes and high relief in the vicinity of these discontinuities (Koukis et al., 2009). Due to the diverse geological conditions in the Himalaya, it offers a good laboratory to study the various geological processes and landform developments. It has thus, been of keen interest to many workers for decades. Nonetheless, a concise

idea of the geological setup of an area would lend insight on the sensitivity of the slope failure, which would help in identifying remedial and/or mitigation measures.

Over the past decades, several techniques and approaches have been used to assess and monitor landslides. The conventional approach of studying a particular landslide site is through extensive fieldwork and subsequently monitoring the particular slope over a period of time. This conventional approach is still being used and is widely accepted, particularly for studying a particular landslide. However, in order to study landslides which, cover a large area, this approach is very tedious, time consuming and very costly. With the advancement of remote sensing and geospatial technology, these have become convenient to study and monitor landslides over large areas.

Landslide study comprises pre- and post-failure evaluation (Skempton and Hutchinson, 1969). Pre-failure evaluation involves the preparation of small or regional scale maps, ranging from 1: 50,000 to 1: 15,000 scales for feasibility studies, in the form of Landslide Susceptibility Map (LSM), followed by field verifications. These maps, generally used for regional planning, give a synoptic view of the areas susceptible to landslides. Post-failure evaluation involves the preparation of large or local scale maps ranging from 1:15,000 to 1: 5,000, or even larger, depending on the scope of the study, for detailed studies of the landslides. Such maps that give detailed geological and geotechnical information of slopes are used for mitigation purpose.

Ideally, regional scale studies involve generation of landslide susceptibility, hazard, risk and vulnerability maps (Guzzetti et al., 1999; Fell et al., 2008). However, preparation of landslide hazard and risk maps becomes difficult due to insufficient temporal data as well as analysis of triggering factors, such as earthquakes and rainfall, in relation to landslides. In general, determining the time frame for a landslide to occur is difficult, even under ideal conditions. This is probably due to lack of historical records or insufficient length of historical record. In such cases, landslide susceptibility mapping has been recommended (Van Westen et al., 2006; Fell et al., 2008), which is limited to the spatial likelihood of occurrence of landslides.

The regional study of landslides in an active river valley includes the distribution of landslides with the relative influence of factors such as lithology, tectonics, structure, and anthropogenic activity in the area. For preparation of a landslide inventory, numerous remotely sensed data products, including satellite imagery on the Google

Earth (GE) platform are used. GE images are extensively used due to their high resolution, free access, and wide coverage (Fisher et al., 2012; Blöthe et al., 2015; Cascini et al., 2015; Kumar et al., 2018a). To assess the interrelationship of landslide distribution with the litho-tectonic regime, various geomorphic proxies have been used by several researchers (Bull and McFadden, 1977; Seeber and Gornitz, 1983; Gregory and Schumm, 1987; Rhea, 1993; Silva et al., 2003; Burbank and Anderson, 2011; Grohmann, 2011; Telbisz et al., 2013; Kumar et al., 2018b). To evaluate the influence of precipitation, rainfall data are used as a means to quantify it and understand its spatial distribution pattern. Earlier studies for precipitation were usually carried out on the basis of climate prediction models and sparsely distributed surface rain gauges (Xie and Arkin, 1997; Chen et al., 2002; Yatagai et al., 2010) covering only a small portion of an area, which over the course of time proved to be quite erroneous. However, with the advent of time, satellite-based precipitation data, documentation sensors such as the Tropical Rainfall Measuring Mission (TRMM) has made it possible to study the rainfall pattern on a regional scale. The TRMM is dedicated to observing and evaluating tropical rainfall and its effects on global climate (Simpson et al., 1996; Kummerow et al., 1998; Wolff et al., 2005).

Site-specific landslide studies on local scale involve detailed investigation of individual slopes. These include slope stability analyses of individual slopes, generally carried out to determine the possible causes of slope failure (Kanungo et al., 2013; Gupta et al., 2016a; Jamir et al., 2017; Kumar et al., 2018a). Rock slope stability analysis is an age old practice in geotechnical engineering, especially for developmental projects in hilly terrain. There are several methods available for stability analysis of rock slopes. These are mainly kinematic analysis (Hoek and Bray, 1981; Goodman, 1989; Pettifer and Fookes, 1994), limit equilibrium (Fredlund and Krahn, 1977; Duncan, 1996; Cheng et al., 2007) and various numerical modelling techniques (Griffith and Lane, 1999; Bhasin and Kaynia, 2004; Eberhardt et al., 2004; Singh et al., 2010; Gupta et al., 2016a). Among the various numerical methods, the Finite Element Method (FEM) has widely been accepted due to its capability to simulate complex geometry (Jing, 2003; Kanungo et al., 2013; Gupta et al., 2016a; Jamir et al., 2017).

There exist various rock mass classifications to assess the condition of rock masses. This is the preliminary step to assess the condition of slopes that give a precise

quantitative idea about the strength of the rock mass (Bieniawski, 1979, 1989). These are the Rock Mass Rating (RMR) of Bieniawski (1976), Q-classification system of Barton et al. (1974), and Geological Strength Index (GSI) of Hoek (1994). The concept was originally introduced for underground excavations, but it was later modified as the Slope Mass Rating (SMR) for the stability analyses of slopes (Romana, 1985, 1993). These are primarily based on field data, orientation of discontinuities and their relation with the slope.

1.1. Statement of the problem and motivation

Landslide incidences are common in the Indian landmass. They are among the major hazards in the country and account for loss of lives and adversely impacting the economy by damaging roads, settlements, agricultural land and other natural resources. According to the Geological Survey of India (GSI) report (www.gsi.gov.in, retrieved on December 2016), ~200 human lives are loss annually, along with crores of rupees in monetary loss. A large contribution to the increase in frequency and magnitude of landslides is due to anthropogenic activities, mainly in the form of road cutting, deforestation and hydroelectric and tunnel projects (Siddique et al., 2015; Singh et al., 2015; Sarkar et al., 2016). Over the years, landslide incidences have increased exponentially and have become a major concern. In the Indian landmass, these are mainly concentrated in the Himalayan mountain ranges, Western Ghats, the Nilgiri Hills (Parkash, 2011) and the Indo-Myanmar Range (Aier et al., 2012). It has been observed that ~15% of the land cover in the country is vulnerable to landslides, out of which 80% is spread over the Himalayan mountain range (www.gsi.gov.in, retrieved on December 2016). Many researchers have worked in different parts of the Himalayan terrain and have documented these events: 1994 Urni rockfall in the Satluj Valley (Gupta, 1998), 1998 Malpa rockfall in the Kali Valley (Paul et al., 2000), 2003 Pareechu rockfall in the Spiti Valley (Gupta and Sah, 2008b), seismicity-induced landslide in Kashmir (Ray et al., 2009), 2013 Kedarnath disaster (Dobhal et al., 2013; Prakash, 2018), 2011 Sikkim earthquake-triggered landslides (Gupta et al., 2015) and Urni landslide (Kumar et al., 2018b). A detailed compilation of the historical records of landslides in India has been given by Parkash (2011) and the National Institute of Disaster Management (Parkash and Kathait, 2014).

There are records of numerous fatal landslides in the NW Himalaya and a number of events have been reported since the 1970's (Parkash and Kathait, 2014). With the ever increasing developmental activities and changing climate pattern in the region, the frequency and magnitude of landslides have increased (Gupta and Joshi, 1990; Mehrotra et al., 1994; Sharma and Kandpal, 1996; Parkash, 2011). However, several parts of the Himalaya still remain unattended and unheard of. The Yamuna River valley is one such neglected area, despite its strategic importance. It links with the Char Dham Yatra route (Hindu Pilgrimage) route, which houses numerous heritage sites. During the Yatra season (May-July) the area flocks with pilgrims, involving heavy vehicular movement. Occurrences of landslides are very common in this region, yet detailed landslide studies are lacking. Moreover, the LSM of the Yamuna Valley carried out by the Geological Survey of India (Sanwal et al., 2005) has not been updated since 2005 and records exist for few selected landslides (Anantharaman, 1980; Pachuari et al., 1998; Gupta and Sah, 2008b; Parkash and Kathait, 2014; Gupta et al., 2017). In view of this, a comprehensive study was taken up to determine the causes of landslides in the Yamuna Valley.

1.2. Study area

The location of the study area is between latitudes 30°38'54"- 30°59'59"N and longitudes 78°01'01"- 78°26'46"E in the Yamuna River Valley of the Garhwal Himalaya. It is part of the Survey of India (SoI) topographic maps nos. 53F/14, 53I/8, 53J/1, 53J/2 and 53J/5. It is situated between the pilgrimage township of Yamunotri in the northeast and Damta in the southwest. It encompasses a length of ~75 km along the Yamuna River (Fig. 1.1), which is the major drainage of the area. It is a perennial river that originates from the Saptrishi Kund (lake) which is situated at an altitude of 4200 m. This, in turn, is fed by the Bander Punch glacier (6315 m) (Agarwal and Kumar, 1973). The river flows towards the SW between Yamunotri (~3150 m asl) and Naugaon (1135 m). Thereafter it flows towards the SSW till Damta and then abruptly changes direction towards the south. Several tributaries, such as the Unta Gad, Hanuman Ganga, Wazri Gad, Pali Gad, Badiyar Gad, Kuthnaur Gad, Kamal River, Asnol Gad, Barni Gad and Sauri Gad drain into the Yamuna River from both sides. The National Highways (NH-123 and NH-94) run alongside the river till Janki Chatti. The NH-123 connects Vikasnagar-Barkot and terminates at the NH-94 junction near the Barkot Bend.

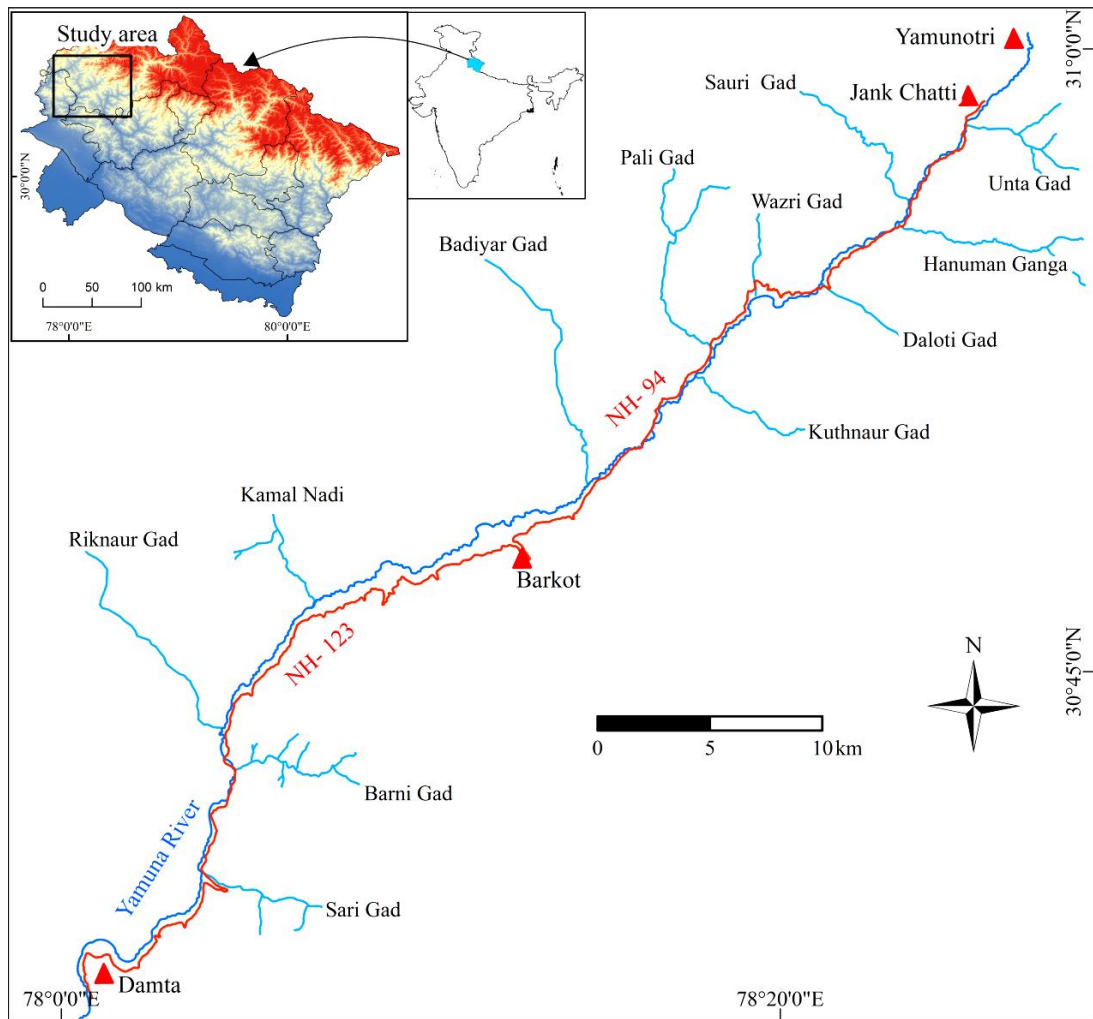


Fig. 1.1: Location map of the study area

1.2.1. Physiography and climate

Physiographically, the study area is characterized by deeply incised river valleys that are sporadically wide at places, and a number of terraces all along the valley. The upper reaches of the area, which form a part of the Higher Himalaya, represents a very rugged topography with very high relief. Altitudes range from 1200 m to 4100 m. The valleys are generally V-shaped, with profound narrow gorges and relatively steep slopes ($>60^\circ$) due to rapid down-cutting by the river. The lower reaches of the valley is infested by sporadic distribution of deep narrow gorges (Fig. 1.2a). In general, the valley gradually widens downstream of the Yamuna River, which is dominated by terraces (Fig. 1.2b). These terraces all along the valley are used for settlements and agriculture all along the valley.



Fig.1.2: Spatial variation of valley width along the river. Inset: a) narrow gorge; b) widening of the valley

The climate in the area varies with altitude from the Lesser Himalaya (735 m) to the Higher Himalaya (>3150 m). In the lower reaches, the area experiences sub-tropical conditions, while at the upper reaches it is entwined with warm, cold and temperate conditions. During the winters, the temperature falls as low as -6°C while in the summers, it rises to a maximum of 20°C (www.environmentclearance.nic.in, retrieved on 20th December 2016). Monsoonal season generally sets in between June to September. Annually the total precipitation in the area is about 2000 mm, with most of it falling during the monsoon, between July and September. Winter season in the upper reaches of the valley is experienced by heavy snowfall.

Aim and Objectives

The Yamuna River Valley is undergoing extensive developmental activities. It is therefore, essential to understand the landslide scenario in the area. In view of this, the following objectives were chosen for the present study:

1. Preparation of a landslide susceptibility map of the area.
2. To determine the spatial distribution of landslides and their interrelationship with tectonics and precipitation.
3. Model the unstable slopes to evaluate their behaviour under different sets of environmental conditions.

Chapter 2

GEOLOGICAL SETTING

2.1. Introduction

The Himalaya forms an important part of the Alpine-Himalayan chain and is one of the youngest mountain belts. It was formed due to the Indian and Eurasian continental plates collision during the early Cenozoic, ~55 Ma. The collision resulted in large-scale crustal shortening, with thrusting towards the south, against the northward push of the Indian Plate (Lefort, 1975; Garzanti et al., 1987; Hodges, 2000). The regional strike length of the Himalaya is about 2400 km, extending from the Nanga-Parbat in the west to the Namcha Barwa in the east. The width of this belt, from north to south, varies from 250 to 300 km. The Himalaya is bounded by the Indo-Gangetic plains in the south, the Tibetan Plateau in the north and the Karakoram-Hindukush mountain ranges in the northwest.

Prolific works have been carried out by several researchers from all over the world on the Himalaya, which is active since the geologic past (Medlicott, 1864; Griesbach, 1880, 1891; Oldham, 1883; Middlemiss, 1887; Hayden, 1904; Pilgrim, 1906; Pilgrim and West, 1928; Wadia, 1931; Auden, 1935; Heim and Gansser, 1939; Wadia, 1953; Gansser, 1964; LeFort, 1975). The northwestern part of the Himalaya, consisting mainly of the Garhwal and Kumaun Himalaya, has also been studied on different scales for more than a century (Middlemiss, 1885; Holland, 1908; Auden, 1935; Heim and Gansser, 1939; Misra and Sharma, 1967; Jain, 1971; Rupke, 1974; Valdiya, 1980; Thakur, 1992; Srivastava and Mitra, 1994; Valdiya, 1995; Srikantia and Bhargava, 1998; Marquer et al., 2000; Islam and Gururajan, 2003; Jayangondaperumal et al., 2018).

2.2. Litho-tectonic divisions of the Himalaya

The Himalaya is litho-tectonically divided into the following five units. These, from south to north are the Sub Himalaya, Lesser Himalaya, Higher Himalaya, Tethyan Himalaya and Trans Himalaya (Gansser, 1964; LeFort, 1975; Thakur, 1992; Yin, 2006). The southern front of these litho-tectonic units are marked by the Himalayan Frontal Thrust (HFT), Main Boundary Thrust (MBT), Main Central Thrust (MCT), South Tibetan Detachment (STD) and Indus-Tsangpo Suture Zone (ITSZ) (Fig. 2.1).

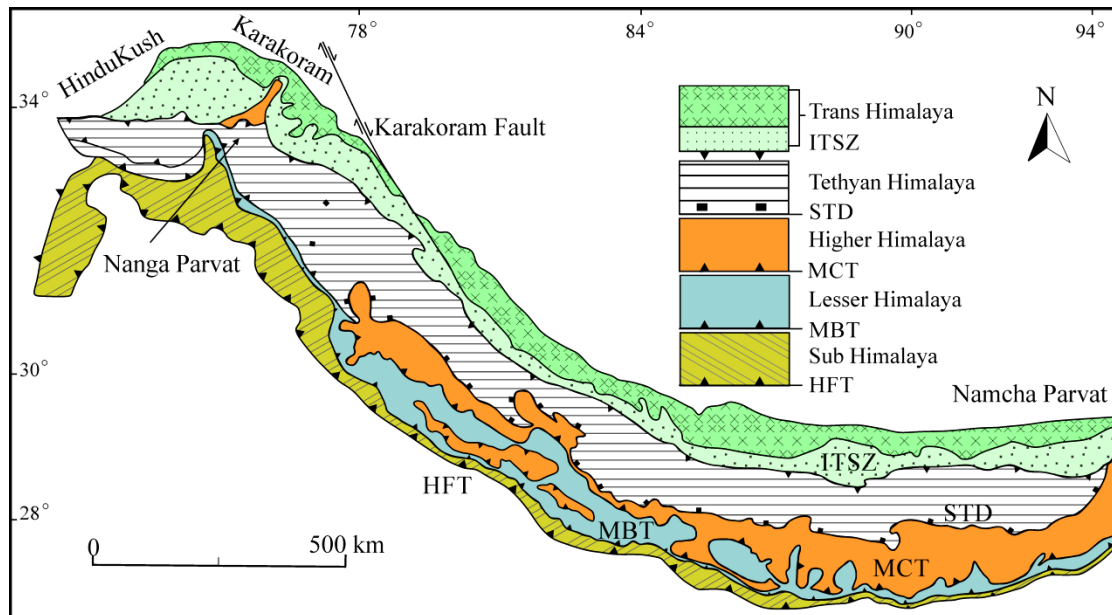


Fig 2.1: Generalized litho-stratigraphic divisions of the Himalaya (after Searle et al., 2003; Yin, 2006)

These are the major tectonic discontinuities that divide the Himalaya into different litho-tectonic zones. These litho-tectonic zones are briefly described below.

2.2.1. Sub Himalaya

The Sub Himalaya is the southernmost part of the Himalaya. It is separated from the Indo-Gangetic plains in the south by the HFT and from the Lesser Himalaya in the north by the MBT. It consists of Neogene-Quaternary (20-2 Ma) molasse sediments (Yin, 2006). It varies in width from 8-10 km and is exposed in the low elevated Siwalik hills and the intermontane valleys called the duns (e.g., Dehra Dun) (Saxena, 1971).

2.2.2. Lesser Himalaya

The Lesser Himalaya is separated from the Sub Himalaya by the MBT and from the Higher Himalaya by the MCT. It is mainly composed of Cambrian clastic sediments with minor occurrences of displaced crystallines and is 50-80 km wide (Valdiya, 1980). This zone has the largest exposed width of ~80 km in the Kumaun and Garhwal region (Thakur, 1992). The Lesser Himalaya has been sub-divided into the Inner Lesser Himalaya and Outer Lesser Himalaya (Jain, 1971; Valdiya, 1980). The Inner Lesser Himalaya lies to the south of the Higher Himalaya. It comprises mainly

Paleoproterozoic rocks; the Outer Lesser Himalaya overlying the Sub-Himalaya is composed of Mesoproterozoic to Tertiary rocks (Kumar, 2005).

2.2.3. Higher Himalaya

The Higher Himalaya is demarcated by the STD in the north that separates the Higher Himalaya from the Tethyan Himalaya (Fig. 2.1). It consists of a 15-20 km thick slab of crystalline rocks dipping northward and thrusting southwardly along the MCT over the Lesser Himalayan rocks. It is characterized by a tectonically active topography comprising very thick piles of high-grade Precambrian metamorphic and granitic gneisses. These are the oldest rocks of the Himalaya, which are also known as the Higher Himalayan Crystallines (HHC). These crystallines are associated with a number of igneous intrusives of varying ages (Valdiya, 1980, 1998). The rocks of the Higher Himalaya (HH) show an inverted disposition of metamorphic isograds, which gives the HH the distinction of the world's largest terrain of inverted metamorphism (Arita, 1983; Harrison et al., 1999; Kohn, 2014).

2.2.4. Tethyan Himalaya

The Tethyan Himalaya, also referred to as the Tibetan Himalaya, is named after the ancient intercontinental Tethyan Sea. It is confined between the Trans Himalaya and the Higher Himalaya and separated by the ITSZ and STD (also known as the Trans Himadri Fault) respectively (Fig. 2.1). It is mainly made up of 10-12 km thick fossiliferous sedimentary rocks of Late Proterozoic to early Eocene age (Valdiya, 1980). These sediments are characteristic of the marine environment representing the Tethys sea regime, which shows a drastic contrast to that of the sedimentary facies in the Lesser Himalaya (Thakur, 1992). The Tethyan Himalaya extends all along the southern margin of the Tibetan Plateau in the east to the Zaskar Mountains in the west. In the western Himalaya, the Tethyan zone is well exposed in the Kumaun, Spiti and Zaskar mountains.

2.2.5. Trans Himalaya

The Trans Himalaya is the northern margin of the Tethyan Himalaya. It is an assemblage of remnants of Mesozoic ocean, plutonic-volcanic arc, fore-arc and post orogenic molasse sedimentaries (Thakur and Mishra, 1984; Sorkhabi et al., 1999). It is formed due to partial melting of a subducting Tethyan slab beneath the Eurasian

Plate. It is mainly present in the Kohistan area, Indus and Shyok sutures of Ladakh and the Karakoram Zones of the western Himalaya. The Indus and Shyok sutures run parallel to each other in northern Kashmir, pointing to complex evolutionary processes that operated in the western Himalaya.

2.3. Geological setting of the Garhwal Himalaya

The Garhwal Himalaya is part of the Northwest Himalaya and Uttarakhand Himalaya (Uttarakhand state of India). The Uttarakhand Himalaya is administratively divided transversally into the Garhwal Himalaya and the Kumaun Himalaya. The Garhwal Himalaya extends from the Alaknanda Valley in the east to the Tons Valley in the west, whereas the Kumaun Himalaya extends from the Alaknanda Valley in the west to the Kali Valley in the east (Kumar, 2005). It occupies parts of the Sub Himalaya, Lesser Himalaya, Higher Himalaya and the Tethyan Himalaya (Fig. 2.2). The southernmost part of the Garhwal Himalaya is the Sub Himalaya, comprising the Sirmur and Siwalik groups (Medlicott, 1864). The Sirmur Group is divisible into the Subathu Formation, Dagshai Formation and Kasauli Formation of Paleocene age (Najman and Garzanti, 2000). The Subathu Formation is dominantly made up of shale, the Dagshai Formation of red mudstone, siltstone and grey sandstone and the Kasauli Formation is dominantly made up of sandstone. Pilgrim (1910) classified the Siwalik Group into three sub-groups: the Lower Siwalik, Middle Siwalik and the Upper Siwalik. The Lower Siwalik rocks are dominantly made up of sandstone with alternations of clay and claystone. The Middle Siwalik consists of micaceous sandstone while the Upper Siwalik is made up mainly of conglomerates.

Further northward, the Cambrian sequence of the Lesser Himalaya is exposed. It is sandwiched between the MBT in the south and the MCT in the north. Auden (1936) first referred to the sediments of this region as the “Barahat Series” but later called it the “Garhwal Series” (Auden, 1949) after the name of the region where it is extensively exposed. Later, Kumar (1970) grouped these sediments under the “Garhwal Group”. Kumar (2005) sub-divided the Garhwal Group into four formations; the Uttarkashi Formation, Rautgara Formation, Tejam Formation and Berinag Formation. These formations are further sub-divided into members based on different lithologies. The generalized litho-stratigraphic succession of the Garhwal Group depicting formations, members and lithology is presented in Table 2.1. The

two stratigraphic zones of the Inner Lesser Himalaya and Outer Lesser Himalaya are separated from each other by the North Almora Thrust (NAT). The NNW-SSE trending NAT has been variably referred to as the Nalupani Fault (Dhoundial and Ali, 1967), Dharkot Dislocation (Saklani and Pande, 1970), Dharasu Thrust (Jain, 1971), Dharkot Thrust (Saklani, 1971), Shrinagar Thrust (Mehta, 1971) and Shrinagar Shear (Bhargava, 1972). The Inner Lesser Himalaya comprises the Berinag Formation, the Damtha Group (Chakrata and Rautgara formations) and the Tejam Group (Deoban and Mandhali formations). The Outer Lesser Himalaya consists of the Dudatoli Group (Chandpur, Nagthat and Blaini formations), Infra-Krol, Krol and Tal formations of the Krol Supergroup (Valdiya, 1980; Thakur, 1992).

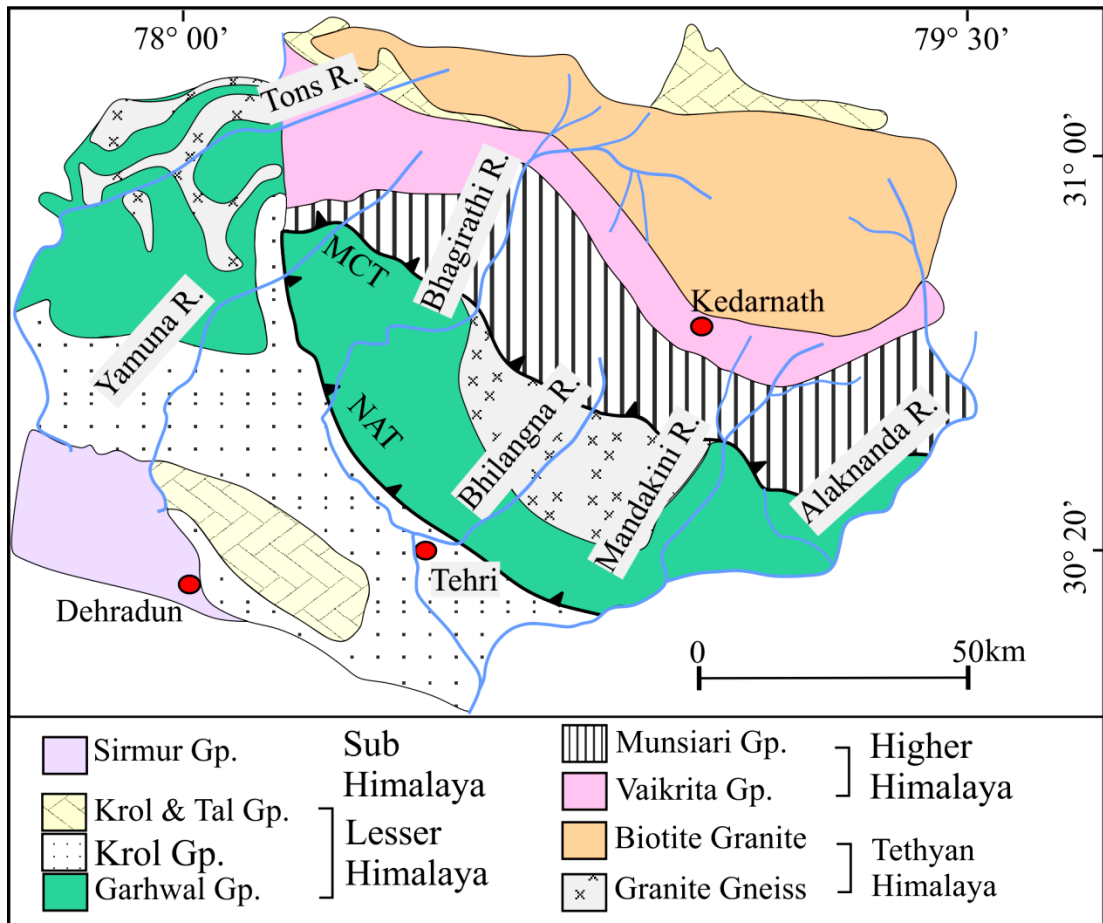


Fig. 2.2: Geological map of the Garhwal Himalaya (After Valdiya 1980; Kumar, 2005)

Table 2.1: Generalized litho-stratigraphy of the Garhwal Group (Kumar, 2005)

Formation	Member	Lithology
Berinag	Hudoli	Thick bedded massive quartzite and phyllite
	Nawagaon	White, massive, fine grained to gritty, current-bedded quartzite with lenticular intra-formational conglomerate, phyllite partings and mafic metavolcanics
Tejam	Patet Slate	Black carbonaceous slate/phyllite and bluish grey limestone, with bands of magnesite and talc-schist
	Balga	Massive dolomite with limestone and talc-chlorite-sericite schist
	Naulara Phyllite	Black carbonaceous phyllite and green slate, chlorite phyllite, quartzite and feldspathic grit
	Tejam Dolomite	Massive dolomite with dolomitic limestone and talc-sericite-schist
	Simgad	Purple quartz-peidmonite siltstone and phyllite, banded greenish quartzite and calcareous phyllite and dolomite
Rautgara	Bhekuna metavolcanics	Mafic amygdaloidal lavas (spilitic) altered to hornblende-actinolite-chlorite phyllite with veins of epidote and tourmaline
	Nagnath Quartzite	Interbedded fine grained quartzite and phyllite, with marble and calc silicate in the upper part
	Karanprayag metavolcanics	Mafic spilitic lava and keratophyre, amygdaloidal occasionally porphyritic, chlorite phyllite, actinolite-biotite- albite phyllite with veins of epidote; Interappean purple phyllite
	Haryali Quartzite	Massive, gritty, coarse to fine grained, with occasional pebble beds; current and graded bedded, ripple marked with thin partings of chocolate phyllite, lenticular dolomite/limestone
	Dhari metavolcanics	Mafic amygdaloidal lava flows, altered to drab green chlorite phyllite, with phyllite and bands of quartzite
Uttarkashi	Khattukhal Limestone	Greyish black to greyish blue limestone with thinly bedded grey slate
	Dhaneri Slate	Banded, grey green and purple slates, interbedded with quartzite
	Netala Quartzite	White to buff, fine grained, current bedded quartzite and interbedded slate with minor lenses of limestone

The Lesser Himalayan rocks are overlain by the Higher Himalayan Crystallines, which is differentiated by the MCT towards north. The Vaikrita Group, Jutogh Group (Munsiari Formation) and Chail Group are the three litho-stratigraphic units recognized in the Higher Himalaya Crystallines (Thakur, 1992). The Vaikrita Group consists of high grade metamorphic rocks of the upper amphibolite facies-mica schist, amphibolite, quartzite and gneiss. The Jutogh Group comprises medium to high grade metamorphic rocks (quartzite, kyanite-bearing schist, granite gneiss, marble and augen gneiss), whereas the Chail Group consists of metamorphic rocks of the green-schist facies metamorphic rocks (phyllite, phyllitic quartzite, chlorite-sericite schist and occasional limestone). These three groups are separated from each other by the Vaikrita Thrust, Jutogh/Munsiari Thrust and the Chail Thrust respectively. There are several propositions regarding the MCT; however, there is general agreement that the MCT is a duplex structure and not a single thrust plane. The MCT is a ~10-12 km thick, NNE dipping high strain ductile shear zone, which is referred to as the “MCT Zone” (Bouchez and Pecher, 1981; Metcalfe, 1993; Searle et al., 1993; Singh and Thakur, 2001; Bhattacharya and Weber, 2004, Srivastava and Tripathy, 2007). Thakur (1992) and Yin (2006) have given a detailed account of the various definitions of the MCT.

The Tethyan Himalaya, overlying the Higher Himalayan rocks along the STD, lies in the northernmost part of the Garhwal Himalaya. It dominantly consists of thick un-metamorphosed to feebly metamorphosed rocks (phyllite and ortho-quartzite).

2.4. Geological setup of the Yamuna Valley and the study area

The Yamuna River valley comprises rocks of the Lesser Himalaya and the Higher Himalaya, which are separated by the NW-SE trending MCT, locally known as the Munsiari Thrust (MT), passing near Wazri village (Fig. 2.3). The rocks of the Lesser Himalaya are overlain by the Central Crystallines of the Higher Himalaya (Pachuari, 1972). The physical geology and rock types have been briefly described by Middlemiss (1887), Rao et al. (1981) and Pati and Rao (1983). A broad outline of the tectonic setup and the stratigraphy of the area have been given by Dhoundial and Ali (1967), Jain (1971) and Saklani (1971). Geological mapping of the area from Naugaon to Wazri was carried out by Srivastava (1974) who classified the rocks of the region into five distinct stratigraphic units: the Central Crystallines, Naugaon

Formation, Simla Slate, Deoban Formation and the Garhwal Group. Pachuari (1972) and Valdiya (1975) suggested that the Barkot sheet of the Yamuna Valley is an extension of the Chail Nappe of the Shimla Hills. Rupke (1974) opines that the Barkot sheet is actually the Deoban. Raina (1978) also proposed that the rocks between Barkot and Barni Gad along the Yamuna River valley are members of the Deoban Formation. Biyani (1995) described the geology of the Yamuna Valley.

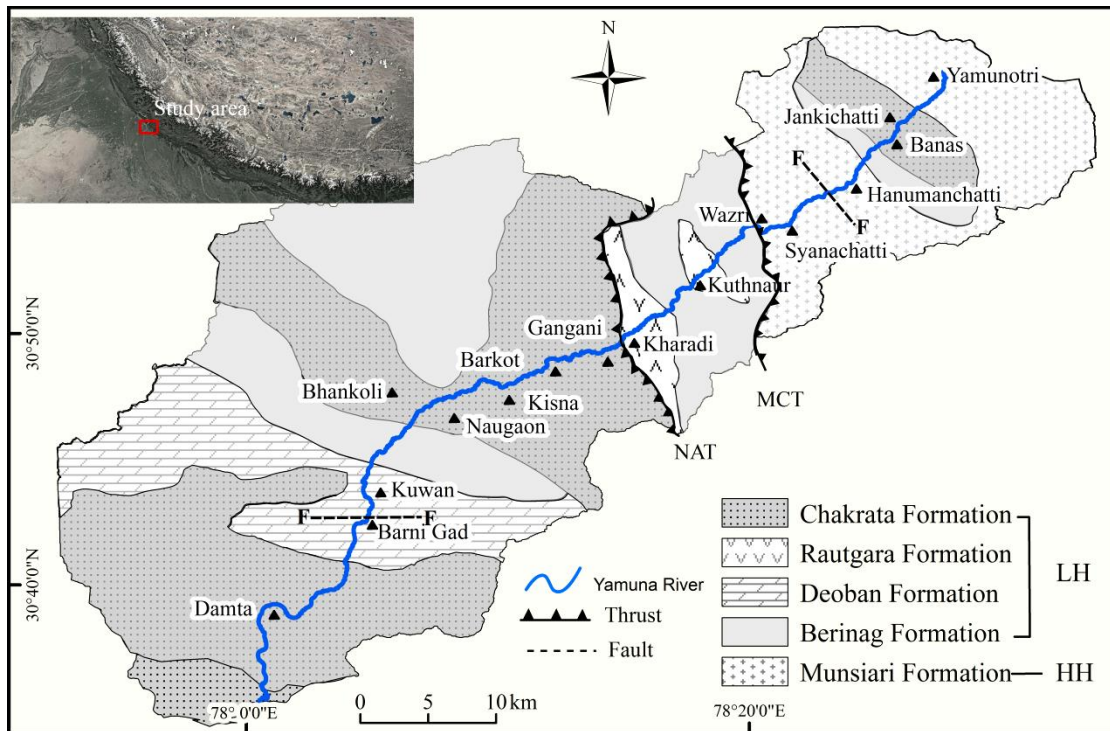


Fig. 2.3: Geological setting after Pachuari (1972), Valdiya (1980) and Saklani et al. (1991). Red rectangle (inset) denotes position of study area in the NW Himalaya. F-F: fault; MCT-Main Central Thrust; NAT-North Almora Thrust; HH- Higher Himalaya; LH-Lesser Himalaya

The litho-tectonic units of the Yamuna Valley can be grouped into four zones: the Krol Nappe, Autochthonous Zone, Allochthonous Zone and the Central Crystallines (Table 2.2). The Krol Nappe comprises the Mandhali, Chandpur and Nagthat formations. It is delineated from the Autochthonous Zone by the Tons Thrust. The Autochthonous Zone is represented by the Morar-Chakrata Formation, Barni Gad Formation (Lower Deoban), Bhankoli-Barkot Formation (Middle Deoban) and Sauli Formation (Upper Deoban). The Allochthonous Zone includes Nawagaon, Hudoli (Berinag Quartzites) and Rama Serai formations. The Nawagaon Formation is a klippe, which is probably detached from the Hudoli Formation (Pachuari, 1972). The metamorphic and crystalline rocks (Central Crystallines) form the uppermost tectonic

unit. The Autochthonous Zone forms a syncline, which is flanked on both sides by anticlines. The Allochthonous zone has been thrust upon the Autochthonous Zone, while the Central Crystallines have been thrust upon the Allochthonous Zone. The Krol Nappe is not exposed in the study area, so it has not been discussed.

Table 2.2: Regional litho-tectonic setting of the Yamuna Valley (modified after Pachuari, 1972 and Valdiya, 1980)

Tectonic Zone	Formation
Central Crystalline Zone	Central Crystallines
-----Main Central Thrust-----	
	Berinag Formation
Allochthonous Zone	Rama Serai Formation
	Hudoli Formation
	Nawagaon Formation
-----Thrust-----	
Autochthonous Zone	Deoban Formation
	Sauli Formation (Upper Deoban)
	Bhankoli-Barkot Formation (Middle Deoban)
	Barnigad Formation (Lower Deoban)
	Morar-Chakrata Formation
	Rautgara Formation
	Chakrata Formation
-----Tons Thrust-----	
Krol Nappe	Nagthat Formation
	Chandpur Formation
	Mandhali Formation

2.4.1. Autochthonous Zone

Morar-Chakrata Formation

The Morar-Chakrata Beds, as described by Auden (1934), has been designated the Damtha Group by Rupke (1974) after Damta village in the Yamuna Valley. Valdiya (1980) later enlarged the stratigraphic extent by including both the Chakrata and Rautgara formations. The Morar-Chakrata Formation consists essentially of purple to green slate, greywacke and siltstone. Based on sedimentary characteristics, the Morar-Chakrata Formation has been divided into two units, the Damtha Unit and the Kunnan

Unit (Pachuari, 1972), which are equivalent to the Chakrata Formation and Rautgara Formation respectively of Valdiya (1980).

- 1) *Chakrata Formation*: It is represented by bedded limestone, deep brown and purple slate and greywacke (Pachuari, 1972). These rocks are exposed around Sauri Gad and further extend up to the Naugaon-Gangani region. The Chakrata Formation window is also exposed in the Banas-Janki Chatti region. This unit refers to the Chhaosa-type of Simla Slate of Auden (1934).
- 2) *Rautgara Formation*: It is represented by moderately thick-bedded shale, siltstone and subordinate greywacke. The Kuthnaur and Gangani windows (Valdiya, 1980) expose the rocks of the Rautgara Formation. This unit also corresponds to the Sauri Gad Formation of Rupke (1974).

Deoban Formation

The Deoban Formation, viz., Barni Gad Formation (Lower Deoban), Bhankoli-Barkot Formation (Middle Deoban) and Sauli Formation (Upper Deoban), consists of thick sequences of dolomitic limestone, phyllite and slate. It is exposed around Barni Gad and extends up to Gangani, towards the north.

- 1) *Barni Gad Formation*: The Barni Gad Formation is equivalent to the Lower Deoban (Rupke, 1974). Bedded limestone and slate are well exposed between Barni Gad and Kuwan, and a section stretching for about 2-3 m is also exposed in the Gangani region. It is however, not mappable in the study area.
- 2) *Bhankoli-Barkot Formation*: It is equivalent to the Middle Deoban (Rupke, 1974). It conformably overlies the Barni Gad Formation (Pachuari, 1972) and consists of black carbonaceous slate and quartzite. It is well exposed between Naugaon and Barkot. It is also exposed in Bhankoli; small segments are exposed near Kuwan, Kisna and Badiyar Gad.
- 3) *Sauli Formation*: Rupke (1974) defined it as equivalent to the Lower Deoban. It consists of thick sequences of dolomitic limestone, slate and quartzite. The Sauli Formation conformably overlies the Bhankoli-Barkot Formation and is well exposed around Naugaon.

2.4.2. *Allochthonous Zone*

The Deoban Group is overlain by a huge succession of massive, coarse-grained sericitic quartzarenite, which has been named the Berinag Formation (Valdiya, 1965). Heim and Gansser (1939) named it the Quartzite Series. It is divisible into the Nawagaon, Hudoli and Rama Serai formations (Kumar, 2005). The Nawagaon Formation, resting upon the Deoban Formation, is composed of green phyllite and quartzite. It is well developed downstream of Naugaon and in the Wazri-Kharadi and Banas-Hanuman Chatti regions. The Hudoli Formation is distinctly arenaceous and represented by quartzite, serite quartzite, quartz schist, phyllite and basic amphibolite. Most of the northern and northeastern parts are covered by this formation (Pachuari, 1972). The Quartzite Series is variously known as Bawar Quartzite (Oldham, 1883), Gamri Quartzite (Jain, 1971), Pratapnagar Quartzite (Saklani, 1971) and Berinag Quartzite (Valdiya, 1962). The Rama Serai Formation is a thick succession of biotite schist, quartz schist and gneiss. This formation is however, seen in Purola, Chandeli and Kalsi Dhar, which is further west of the study area.

2.4.3. *Central Crystallines*

The Central Crystallines of the HH is thrust over the Berinag Formation along the MCT. It is composed of huge crystalline augen gneiss, mica schist, marble and quartzite (Gansser, 1964). These metamorphosed rocks are well exposed from Wazri to Yamunotri. In the Syanachatti region, augen gneisses and porphyroblastic gneiss are well exposed, while schist and calc-silicate rocks are exposed further upstream from Jankichatti (Pachuari, 1972); marble, schist and quartzite are observed at Yamunotri.

The rocks of the Yamuna Valley are exposed in a large syncline flanked by anticlines on either side (Pachuari, 1972; Valdiya, 1980; Saklani et al., 1991). The tectonic units are accounted in Table. 2.2. In the Allochthonous Zone, the Morar-Chakrata Formation is unconformably overlain by the Lower Deoban (Barni Gad Formation). Dhoundial and Ali (1967) referred to the unconformability of various formations in this zone, except for some local dislocations. Minor faults such as the Barni Gad Fault are noted in the zone (Pachuari, 1972). The Autochthonous Zone consists of the Berinag Formation (Nawagaon, Hudoli and Rama Serai formations). The Nawagaon Formation is thrust over the Sauli Formation of the Deoban Group. The Nawagaon

thrust mass is an asymmetrical syncline, with the axial planes striking E-W, NW-SE and NNE-SSW (Pachuari, 1972). The Hudoli Formation is also a syncline with its axis trending N-S. Further north, the Hudoli Formation is thrust upon by the Central Crystallines along the MCT. In the southernmost part of the study area is the Krol Nappe (Mandhali, Chandpur and Nagthat formations), which forms the northern limb of the Mussoorie Syncline (Auden, 1934) and demarcated by the southerly dipping Tons Thrust.

The area comprises of two major thrusts, the NNW-SSE trending NAT and the NW-SE trending MCT, near Gangani and Wazri villages respectively. The NAT separates the two sedimentary suites of the shallow water Autochthonous Zone (Garhwal Group) and deeper water sequence of the Krol Nappe. The general trend of the fault plane is 70° - 80° towards WSW (Agarwal and Kumar, 1973) whereas, the MCT is a steep (40° - 60°) northerly dipping thrust, which trends parallel to the NAT. Considered to be a duplex structure, Saklani et al. (1991) characterized the planes at Yamunotri, Jankichatti-Phulchatti and Wazri. However, the present study takes into consideration the MCT (Munsiari Thrust) based on the observations of Agarwal and Kumar (1973) and Pachuari (1972). A detailed structural study of the area has been carried out by Agarwal and Kumar (1973) and Biyani (1995).

Chapter 3

Landslide Susceptibility Zonation Mapping

3.1. Introduction

Landslides are naturally recurring phenomena particularly in hilly terrain that cause loss to lives and major substantial economic loss. It is often considered insignificant until a catastrophic event takes human lives. However, with ever growing human activity and the demand for more land, the losses due to landslides have grown rapidly. According to Brabb (1993), at least 90% of landslide losses are avoidable if the problem is recognized before planning any developmental activities. Hence, it is necessary to identify zones or areas which are susceptible to landslides.

As a pre-requisite to any landslide study, an overall regional perspective of the landslide prone areas is required. This regional understanding requires a detailed insight into various influencing factors responsible for landslides. Basically, the fundamental assumption of any landslide zonation map is build on the concept that “the past is the key to the future” (Varnes, 1984; Hutchinson, 1995). The Landslide Susceptibility Map (LSM) depicts an area of relative landslide susceptibility. A LSM is prepared using either of the following two approaches:

1. *Qualitative heuristic approach*: This is a direct mapping method, whereby the causative factors such as geology, slope, aspect, curvature, drainage and land use/land cover of the landslides are given ratings based on expert knowledge and experience (Brabb et al., 1972; Wright et al., 1974; Van Westen et al., 2008).
2. *Quantitative statistical approach*: This statistical approach takes into account the statistical relationship between slope instability and its causative factors (Carrara, 1983; Brand, 1988; Gupta and Joshi, 1990; Aleotti and Chowdhury, 1999; Saha et al., 2005; Anbalagan et al., 2015; Chen et al., 2016).

Owing to subjectivity and uncertainty associated with the qualitative approach, quantitative methods have been observed to provide more realistic results (Kanungo et al., 2009). The quantitative methods are generally statistical, including bivariate, multivariate (Carrara, 1983; Sarkar et al., 1995; Aleotti and Chowdhury, 1999), probabilistic (Lee et al., 2002) and distribution-free approaches, that is, fuzzy-based and artificial neural network (Kanungo et al., 2006). Although multivariate, fuzzy-

based and artificial neural network methods provide more realistic results (Arora et al., 2004; Ercanoglu and Gokceoglu, 2004) they involve voluminous data and are time consuming. The probabilistic approach includes a certain degree of subjectivity in weight assignment procedures for the existing causative factors that exist (Kanungo et al., 2009).

Over the past decade several techniques for LSM have been adopted by researchers around the world (Brabb et al., 1972; Radbruch-Hall and Crowther, 1973; Nilsen et al., 1979; Ives and Messerli, 1981; Choubey and Litoria, 1990; Gupta and Joshi, 1990; Anbalagan, 1992; Pachuari and Pant, 1992; Mehrotra et al. 1994; Van Westen, 1994; Sarkar et al. 1995; Pachuari et al., 1998, Aleotti and Chowdhury, 1999; Sarkar and Kanungo, 2004; Saha et al., 2005). However, so far, no general agreement exists about the ideal method for preparing landslide susceptibility maps (Guzzetti et al., 2000). The applicability of the techniques varies from place to place, depending on terrain conditions, geological factors and most importantly, the availability of data. Detailed accounts of different methods and guidelines for preparation of LSM have been reviewed and summarized by Guzzetti et al. (2000), Fell et al. (2008) and Kanungo et al. (2009).

The present study aims to prepare a LSM (1:25,000) of the study area using the frequency ratio approach. This would help in delineating potential landslide zones, which will be useful for a variety of general planning purposes and also form the basis for further detailed studies, if required.

3.2. Methodology

The preparation of a LSM involves the generation of a digital database, application of statistical methods, validation and evaluation of the results. These are briefly described herein under:

3.2.1 Data Generation

3.2.1.1 Landslide inventory

A landslide inventory essentially depicts the spatial distribution, type and dimension of a landslide, which is a prerequisite for defining any landslide type in a region (Wieczorek, 1984; Soeters and Van Westen, 1996). Although there is no standardized method for the preparation of a landslide inventory, historical data can be used to

individual landslide events, satellite imagery, field surveys and aerial photographs (Ayalew and Yamagishi, 2005; Kanungo et al., 2006; Kayastha et al., 2013; Xu et al., 2014). In the present study, a high-resolution Linear Imaging Self Scanner (LISS-4) imagery (5.8 m resolution), ortho-image of Cartosat-1 (2.5 m), Google Earth (GE) imagery, Survey of India (SoI) topographic maps (53J/1, J/2, J/5 and I/8) and detailed field surveys using a Global Positioning System (GPS) were used to prepare a landslide inventory. The minutiae of the satellite images used are presented in table 3.1. The satellite-based landslide inventory was rectified with extensive fieldwork in the Yamuna Valley during 2014-2017. The locations of the landslides were measured in the field using a handheld GPS with an accuracy of ~5 m. The classifications of the landslides were based on Varnes (1978) and Hungr et al. (2014). The landslide datasets were then rasterized and resampled into grid size of 10x10 m resolution.

Table 3.1: Details of satellite imagery and topographic maps used in the study

Satellite data / Source	Date acquired	Spatial resolution (m)
Google Earth Imagery	17 th December 2016	1.0-2.5*
	26 th November 2011	
Cartosat-1 (ISRO)	8 th December 2011	2.5
	27 th April 2014	
	6 th June 2014	
LISS 4 (ISRO)	2 nd December 2011	5.8
	11 th November 2013	
	26 th November 2013	
	26 th November 2014	
Topographic map (SoI)	53J/1 1987	Scale: 1:50,000
	53J/2 1986	
	53J/5 1967	
	53I/8 1966	

ISRO - Indian Space Research Organization; SoI-Survey of India;

* Fisher et al. (2012) have related this level of resolution to Worldview-1, 2, and Quick bird imagery (Digital Globe, Inc.)

3.2.1.2 Spatial database preparation/thematic maps

Landslides and related mass movements are, to a great extent controlled by numerous factors. In the present study, the spatial database representing the contributing factors for landslides like elevation, slope angle, slope aspect, lithology, land use/land cover, proximity to lineaments, proximity to drainage and proximity to roads have been used. These causative factors were prepared in a GIS platform in the form of thematic maps. The thematic maps used for analysis are given in table 3.2. All these parameters were digitized and rasterized using ArcGIS 10.5 software. The topographic data used in the analysis (elevation, slope angle, slope aspect) were derived from the Cartosat-1 digital elevation model (DEM) with a spatial resolution of 10 m. Details of the generation of DEM is explained in section 3.2.1.3. Other ancillary data (lithology, land use/land cover, distance to lineament, distance to drainage and distance to road) were generated using high resolution LISS 4 and GE imagery.

3.2.1.3 Digital elevation model

A DEM is a three dimensional raster file representing terrain surface with height at regularly spaced horizontal intervals. It can be generated by various techniques such as ground surveys using DGPS, GPS, Total Station, etc., topographic maps and aerial photogrammetry, and optical satellite sensor data from World View-1, Quick bird, IKONOS, ASTER, Cartosat-1. In this study a DEM was generated using high resolution Cartosat-1 stereo image. The DEM is used for evaluating terrain parameters such as elevation, slope, contours and drainage patterns. These are the input parameters used for landslide susceptibility mapping and numerical modeling of slopes.

A Leica Photogrammetry Suite (LPS) version, ERDAS-11 software package was used to generate DEM using the following steps:

- For the generation of DEM from stereo images (bands A and F) geometric model, and tie points were used. The tie points and GCPs were used as seed vertices.
- A block project file with UTM-44 N projection and WGS 1984 datum was created that defines the geometric model as a Rational Polynomial Coefficient (RPC) model.

- The GCPs and tie points were generated using the classical point measurement too. The GCPs were acquired using a high performance Garmin hand-held GPS with ~5 m vertical accuracy and ~50 cm horizontal accuracy .
- A total of ~1005 tie points were generated, both automatically and manually, for even distribution. Tie points are those points whose ground coordinates are unknown and can be identified in the overlap area of stereo images.
- After the addition of GCPs and tie points, the triangulation was run to improve the accuracy. This was followed by extraction of DEM with cell size of 10 m.

Table 3.2: Details of thematic maps used in the present study

Sl. No.	Parameters	Definition	Source	Remarks
1.	Elevation	Height of the area above mean sea level	DEM (IRS-P5, Cartosat-1 stereo data)	Increased height may correlate with increased likelihood of failure
2.	Slope angle	Ratio of altitude change to the horizontal distance	DEM (IRS-P5 Cartosat-1 stereo data)	Increased slope may correlate with increased likelihood of failure
3.	Slope aspect	Slope azimuth	DEM (IRS-P5 Cartosat-1 stereo data)	Divided into nine classes- Flat, N, NE, E, SE, S, SW, W and NW
4.	Lithology	Gross physical characteristics of a rock or rock formation	Geological map (GSI)	Some lithologies such as phyllite and slate are more prone to failure than the others
5.	Proximity to lineament	Mappable, linear features on the surface caused by drainage, faults, lithological condition, etc.	Digitized lineament layer (IRS-P5 Cartosat-1 and IRS-P6 LISS-IV image)	Proximity to faults identified by buffering from lineament or fault map
6.	Proximity to drainage	Streams and river channels	Digitized drainage layer (IRS-P5 Cartosat-1 and IRS-P6 LISS-IV images and SoI topographic map)	Proximity to streams was identified by buffering drainage map
7.	Proximity to road	Slopes cut for transportation	Digitized drainage layer (IRS-P5 Cartosat-1 and IRS-P6 LISS-IV images and SoI topographic map)	Anthropogenically induced slope instability

8.	Land use and land cover	Land use is the human utilization of land and land cover refers to the physical material on the surface of the earth	Land use / land cover map (IRS-P5 Cartosat-1 and IRS-P6 LISS-IV images and SoI topographic map)	Classified into 6 classes- snow cover, water body, settlement, dense forest, sparse vegetation and barren land
----	-------------------------	--	---	--

3.3. Landslide Susceptibility Zonation Mapping

3.3.1 Frequency ratio method

The frequency ratio (FR) method or bivariate method is one of the most popularly used statistical methods, basically due to its user friendly approach and its simplicity in the implementation of data (Lee and Pradhan, 2007; Yilmaz, 2009; Li et al., 2017). The FR method is based on the spatial distribution between landslides and their causative factors (Lee, 2005). It is the ratio of the percentage of the area of landslide occurrences to the total percentage of the factor influencing it in the study area (Lee and Talib, 2005; Pradhan and Lee, 2010; Solaimani et al., 2013; Regmi et al., 2014). The FR is expressed as:

$$FR = PLO / PIF \quad (3.1)$$

where PLO is the relative area where landslide occurred, in percent, for the given category of influencing factor, and PIF is the relative area of the influencing factor for the given category of influencing factor. A FR value less than 1 (below 0.85) indicates low correlation, a value of 1 indicates an average value and a value greater than 1 indicates higher correlation (Erener et al., 2007; Oh et al., 2010).

The landslide susceptibility value represents the relative susceptibility to landslide occurrence. The lower the value, the lower is the susceptibility to landsliding and the greater the value, the higher is the susceptibility to landsliding (Pradhan and Lee, 2010). In order to obtain the landslide susceptibility index (LSI), the frequency ratios of the factors were summed with equation 3.1 (Lee and Talib, 2005). This LSI was used to map the landslide susceptibility as

$$LSI = \sum (FR)_i \quad (i=1, 2, 3 \dots n) \quad (3.2)$$

where 'n' is the total number of input factors.

3.3.2 *Validation and evaluation*

After preparation of the LS map of the area, its evaluation for accuracy is important. It can be evaluated in several ways, such as partitioning the population of landslides (Lee and Min, 2001; Fabbri et al., 2003; Lee and Pradhan, 2006; Lee, 2007; Pradhan et al., 2010), statistical verification (Chung and Fabbri, 1999, 2003) and field verification.

For verification of the LS map, the population of landslides is partitioned by dividing the landslide inventory into two random parts, one for use as training data and the other part for validation (Fabbri et al., 2003). The thumb rule of this concept is that a LS map would be good if the majority of the actual landslides are to be found in the pixels belonging to the high susceptibility classes and that these classes occupy very small area (Can et al., 2005; Duman et al., 2006). For the statistical and knowledge-driven method, the best way is to use the success rate curve (Chung and Fabbri, 1999; Lee et al., 2002). The statistical based success rate method is used to determine how well the resulting susceptibility map has classified the areas of existing landslides as susceptible areas. The cumulative percentage of the observed landslide area is plotted against the cumulative percentage of the susceptibility map area in order to obtain the success rate. The LSI was sorted in descending order (i.e., very high susceptibility to very low susceptibility classes) and divided into 100 equal areas classes. The same was done for the percentage of landslide area. The cumulative percentage of the susceptibility index (x-axis) corresponding to the cumulative percentage of landslide area (y-axis) was then plotted.

For an ideal accuracy analyses, AUC is calculated with a hypothetical validation curve coinciding with a diagonal ranging from 0.5 to 1 (Remondo et al., 2003; Lee, 2007). If the AUC is close to one, the test result is considered accurate while for that close to 0.5, it is fair (Das et al., 2010). All the analyses are finally validated in the field to evaluate and ascertain the LS map generated.

3.4. Results

The aim of this work is to prepare a LS map of the area, for which a landslide inventory map and various thematic maps such as elevation, slope angle, slope aspect, lithology, land use/land cover, proximity to lineament, proximity to drainage, and proximity to road were generated. All these maps were rasterized and resampled to 10x10 m resolution. This was followed by computing the percentage of the distribution of landslides in each thematic class, which gives an idea of the relationship between the different themes and landslides. In order to characterize the spatial distribution of landslides, a FR analysis was carried out using equation 3.1 (section 3.3.1), the value of which was superimposed on the thematic layers. Finally, the LSI was calculated using equation 3.2 (section 3.3.1). The validation of the map was done by partitioning landslide population distribution and success rate curve, and followed by field verification.

3.4.1 *Landslide inventory*

A landslide inventory of 154 landslides was prepared, covering an area of 4.11 km² (41080 pixels) in a total area of 1440.22 km² (14402168 pixels). The minimum, mean and maximum landslide areas are 1.8×10^{-4} km², 2.66×10^{-2} km² and 3.47×10^{-2} km² respectively. Of the total landslides, 52 are debris slides and 102 are rockfalls. From the total landslides, 124 (80%) were randomly selected for preparing a landslide susceptibility model and the remaining 30 (20%) were used to validate the model. Figure 3.1 illustrates the distribution of landslides in the study area. Most of these slides were mapped using satellite imagery, topographic maps and Google Earth images and those along road-cuts and accessible areas were verified in the field.

3.4.2 *Spatial database/thematic maps*

The landslide causative factors spatial database was prepared and the relationship between landslide occurrences in each causative factor was analyzed.

3.4.2.1 *Relationship between elevation and landslides*

Elevation is an important component in the classification of local relief and significantly contributes to the hydrological regime and slope instability (Yilmaz, 2009). With increase in the height of a terrain, the possibility of landsliding also

increases. For the present study, an elevation model with 30 m contour intervals was extracted. On the basis of elevation range, the entire area was classified into ten classes each with elevation difference of 500 m (Fig. 3.2.-1). A major portion (19%) of the study area lies at elevations of 1500-2000 m (279.9 km²), 18% (264.1 km²) at elevations of 1000-1500 m and 14% (197.2 km²) at elevations of 2500-3000 m. The remaining areas occupy less than 10% at different elevations and quite a negligible area at elevations of <500 m (0.01 km²).

Spatial distribution of landslides in the different elevation classes is presented in Table 3.3. The highest (34%) number of landslides occurs in the 1500-2000 m elevation range, followed by 30% in 1000-1500 m, 13% in 3000-3500 m, 7% each at elevations of 2500-3000 m, 3500-4000 m and 500-1000 m, 2% at 4000-4500 m elevations and no landslides in elevations below 500 m and above 4500 m.

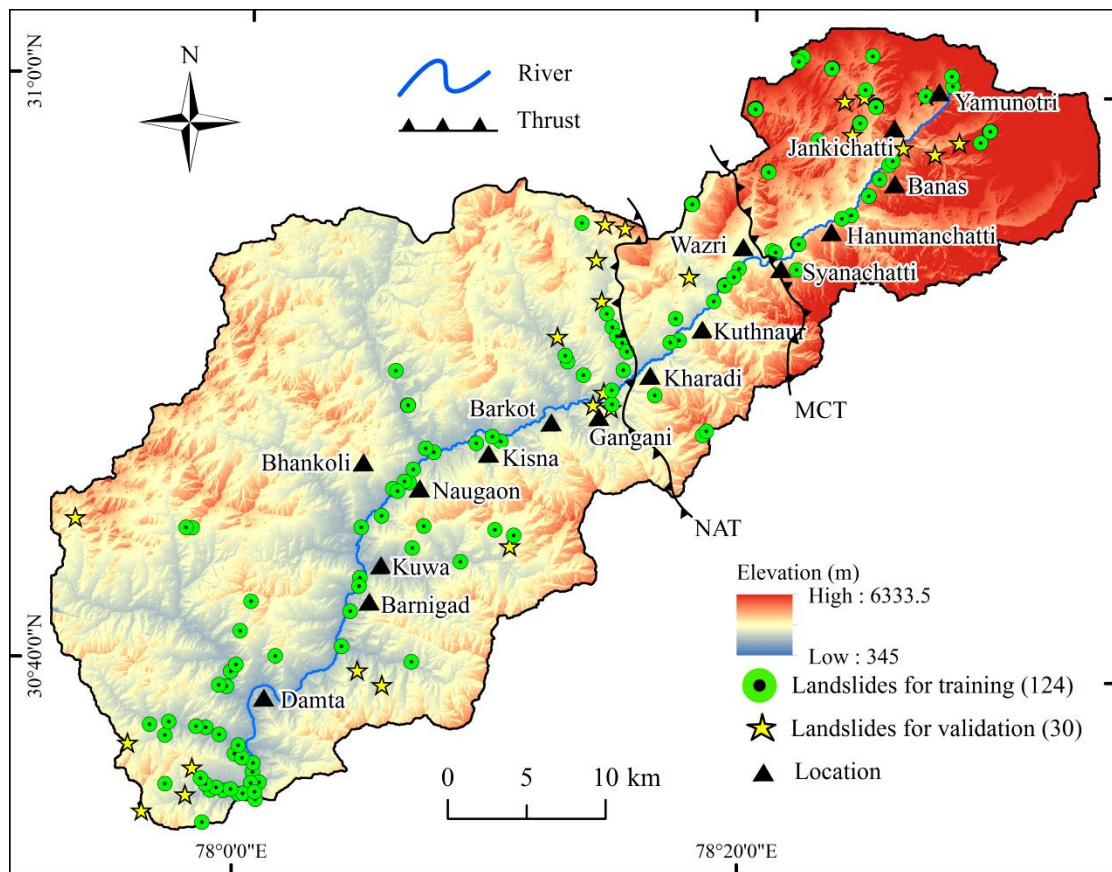


Fig. 3.1: Inventory of landslides indicating their spatial distribution in the study area

3.4.2.2 Relationship between slope angle and landslide

Slope angle is one of the major factors responsible for slope instability. In this study, slopes have been classified into nine categories: 0°-5°, 5°-10°, 10°-15°, 15°-20°, 20°-

25°, 25°-30°, 30°-45°, 45°-60°, >60° (Fig. 3.2.-2). A major portion (24%) of the study area lies in the category of 25°-30°, followed by 19% in slopes with angles of 5°-10°, 18% in 20°-25°, 17% in 15°-20°, 14% in 10°-15°, 7% in 30°-45°, 0.9% in 45°-60° and a very negligible area is occupied by slopes at angles <60° (0.2%) and >5° (0%).

The spatial distribution of landslides in the different slope classes is presented in Table 3.3. It is observed that the maximum distribution of landslides occurs in slopes lying between 25°-30° (37%), followed by 21% in slopes angles between 20°-25°, 13% in slopes of 30°-45°, 12% in 15°-20°, 11% in 5°-10°, 6% in 10°-15°, 1% in slope angles of 55°-60° and no landslides above 60°.

3.4.2.3 Relationship between slope aspect and landslides

Aspect is the slope direction which controls solar insolation and is indirectly related to the geochemical processes, which plays a decisive role in slope instability (Pandey et al., 2018). In the study, the slope aspect has been classified into nine directional classes as flat (-1°), north (337.5°-360°, 0°-22.5°), northeast (22.5°-67.5°), east (67.5°-112.5°), southeast (112.5°-157.5°), south (157.5°-202.5°), southwest (202.5°-247.5°), west (247.5°-292.5°), and northwest (292.5°-337.5°) (Fig. 3.2.-3). The southwest-facing slopes are dominant, covering an area of 196 km² (14%), followed by north-facing slopes, which cover about 13% of the area (191.6 km²), 13% each by west- and northwest-facing slopes, 12% each by northeast-, south- and east- facing slopes, 11% in the southeast and very negligible in the flat areas (0.0018 km²).

The distribution of the landslides in the different slope directions is presented in Table 3.3. It is observed that the southwest-, west-, south- and northwest-facing slopes have comparatively higher percentage of landslides in the study area (22%, 18%, 16% and 14% respectively) as compared to the others.

3.4.2.4 Relationship between lithology and landslides

Lithology of a region, to a great degree, controls the geomorphological features of a landscape (Dai et al., 2001; Lan et al., 2004). The erosion-resistant rocks contribute more to the stability of a slope as compared to the weak rocks (Kanungo, 2006). Hence, lithology is an important component for LS mapping. A lithological map was prepared by field mapping on 1:50,000 using a SoI topographic map. The study area is composed mostly of slate, quartzite, platy limestone and limestone of the Lesser

Himalaya and gneiss and quartzite of the Higher Himalaya (Fig. 3.2.-4). A major portion (25%) of the study area is composed of platy limestone (353.24 km²) followed by 23% each of quartzite and slate occupying an area of 330.3 km² and 325.3 km² respectively; 21% is composed of gneiss (303.85 km²) and 9% by limestone (127.55 km²).

The spatial distribution of landslides in the different lithological sections is given in Table 3.3. The maximum number (29%) of landslide incidences have occurred in areas composed of platy limestone, followed by 24% in slate, 22% in quartzite, 19% in gneiss and 7% in limestone.

3.4.2.5 Relationship between land use/land cover and landslides

Land use/land cover is another component that induces slope instability. It is generally observed that barren and modified slopes are more prone to landslides than vegetated slopes (Kanungo, 2006). In the study area, based on field surveys and use of satellite imagery, six categories were identified (Fig. 3.2.-5). A maximum area of 46% is covered by sparse vegetation (662.23 km²), 45% by barren land (642.86 km²), 8% by forest (117.90 km²) and very negligible area by snowcover, water bodies and settlements (1.18 km², 0.16 km² and 0.15 km² respectively).

The distribution of landslides in the different land use/land cover is presented in Table 3.3. Results show that 53% of the total landslides are distributed in sparse vegetation, followed by 38% in barren land, 9% in forest covered areas and very negligible or no landslides are seen in areas of snowcover, settlements and water bodies.

3.4.2.6 Relationship between proximity to lineament and landslides

Lineaments are linear features of the terrain, which may be due to faults or stratigraphic boundaries (Xu et al., 2012). These plays an imperative role in assessing slope instability as the material around the lineaments are weak due to high degree of shearing and fracturing. In the study area, the major trends of the lineaments are along NE-SW and NW-SE. Lineament buffers of 50 m, 100 m, 150 m, 200 m, 250 m, 300 m, 400 m, 500 m, 1000 m and 1500 m were created (Fig. 3.2.-6).

The distribution of landslides in these buffered categories is presented in Table 3.3. The maximum percentage (29%) of landslides lie within a vicinity of 50 m from

lineaments, followed by 25% within 100 m, 14% within 150 m, 7% within 200 m, 5% within 250 m, 4% within 300 m, 6% within 400 m, 4% within 500 m, 4% within 1000 m and very negligible within 1500 m. Basically, landslide distribution decreased with increase in distance.

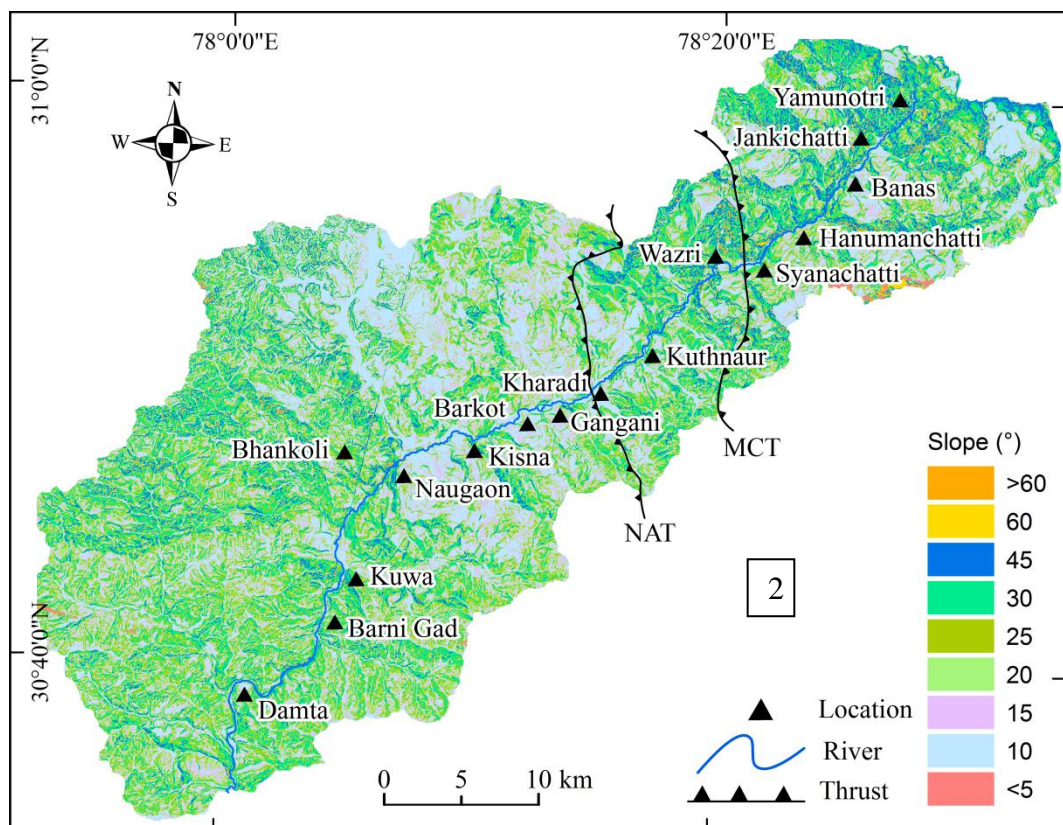
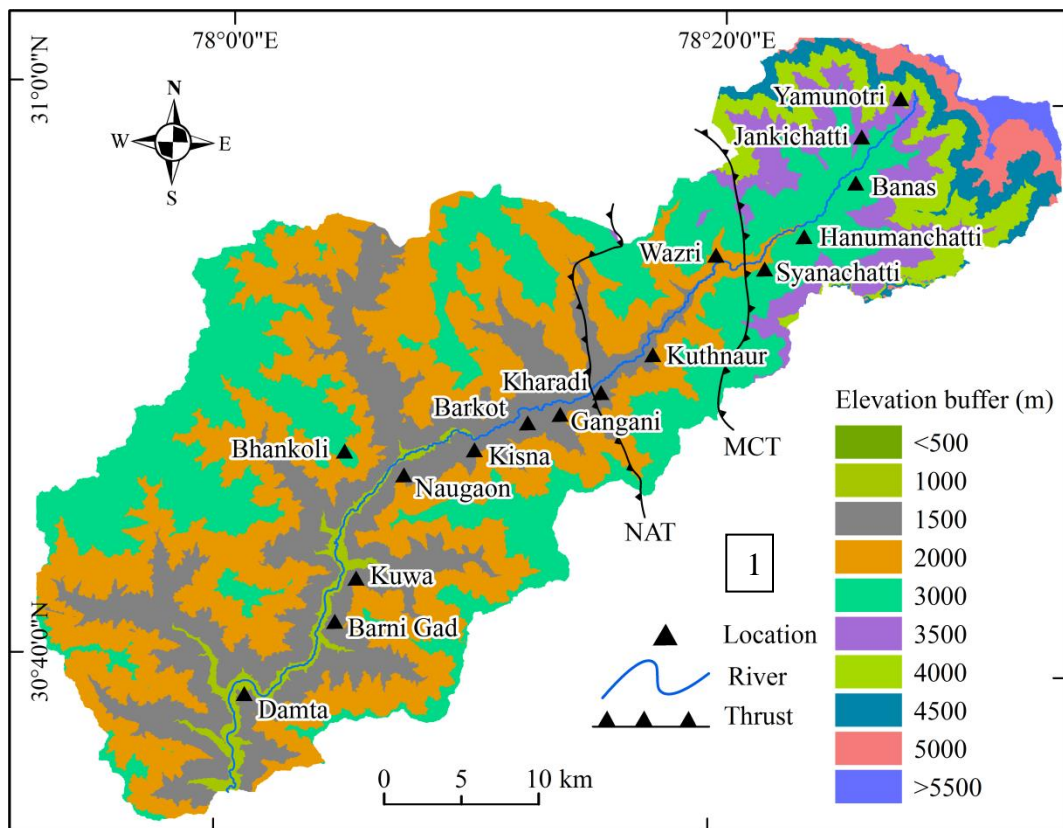
3.4.2.7 Relationship between proximity to drainage and landslides

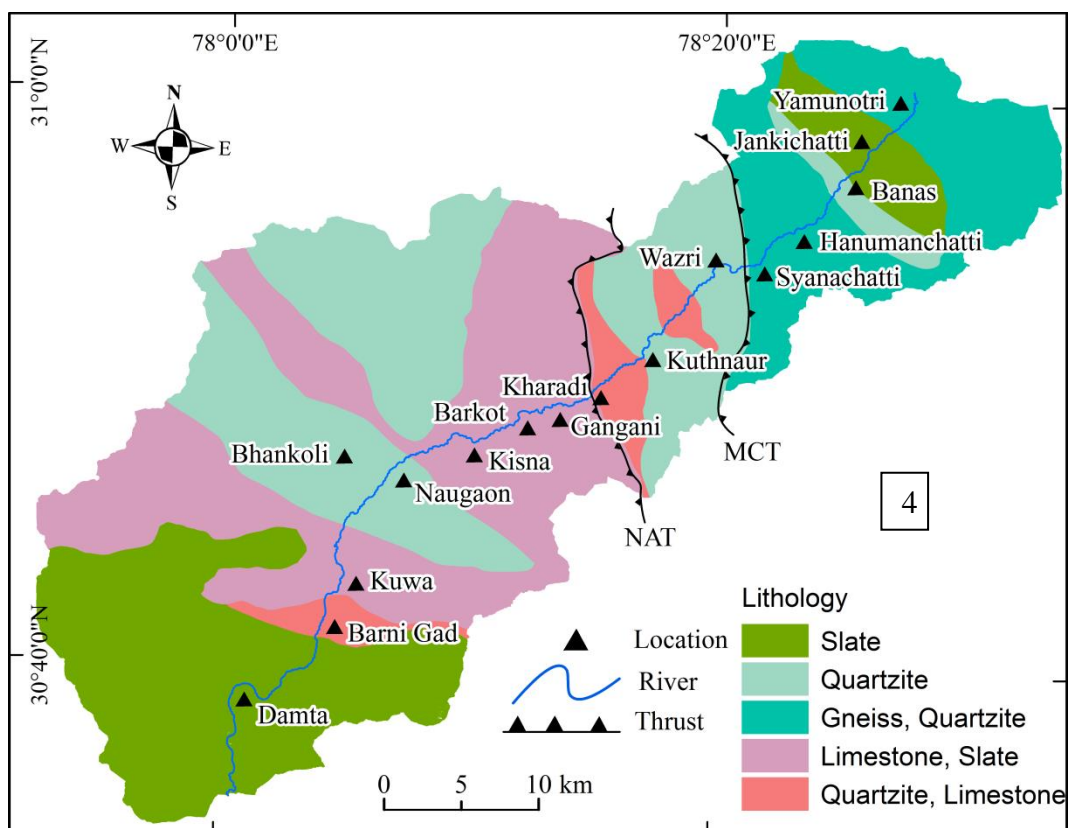
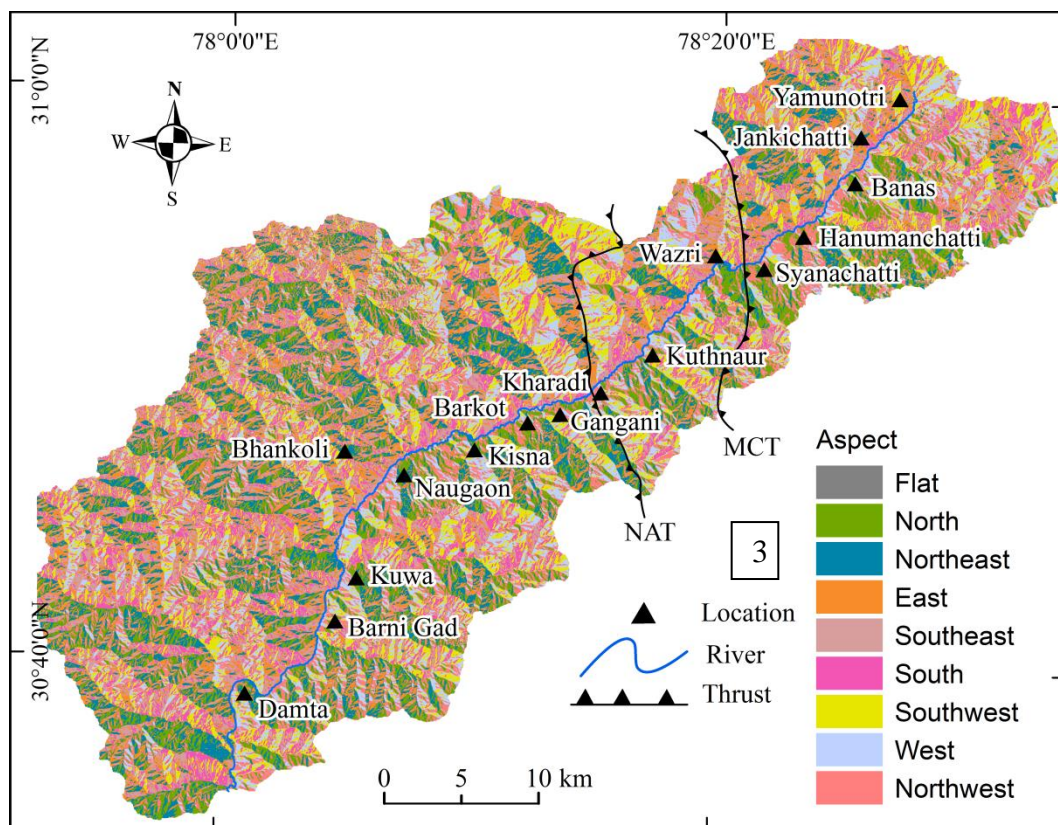
Landslides are often part of the erosional activity of streams or by saturation at the toes of slopes (Gokeceoglu and Aksoy, 1996; Nandi and Shakoor, 2010). Nine classes of drainage buffer from the drainage lines were prepared (Fig. 3.2.-7). Spatial distribution of the landslides in the buffer zones is presented in Table 3.3. The majority of the landslides are distributed in the vicinity of 50 m and 100 m (29% and 24% respectively). This is followed by 150 m (16%), 200 m (10%) and so on in decreasing order, with the increase in proximity to streams.

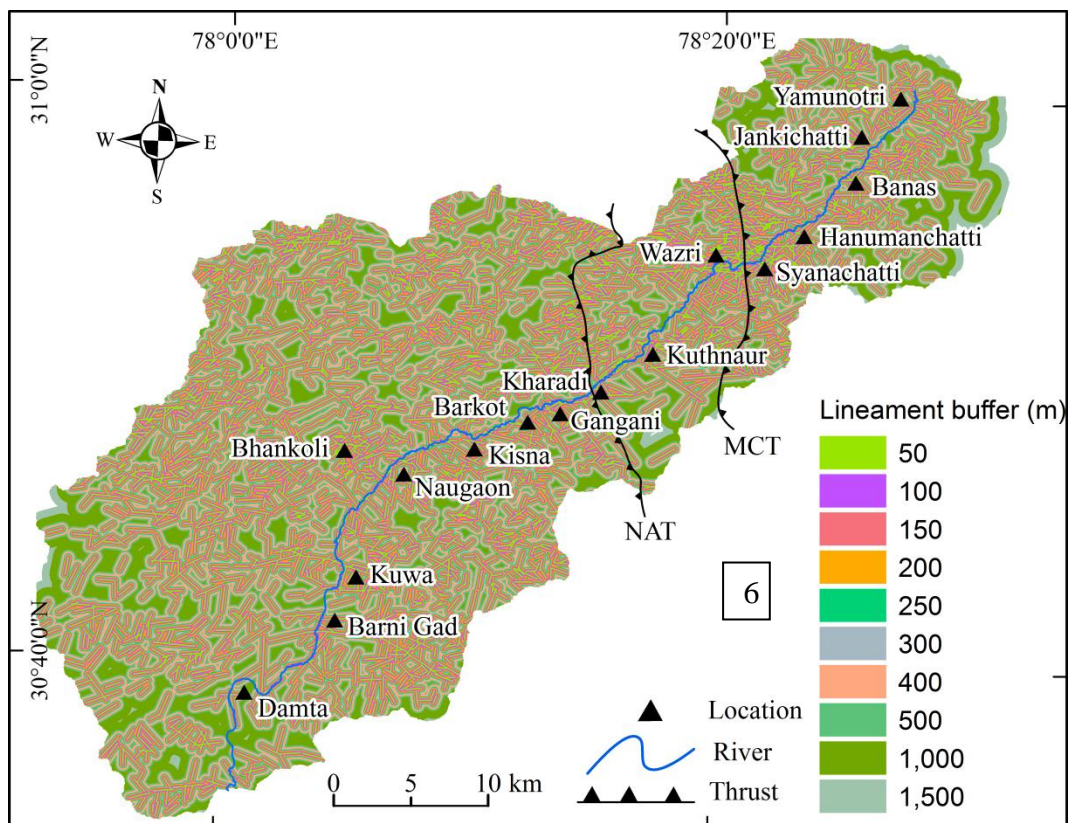
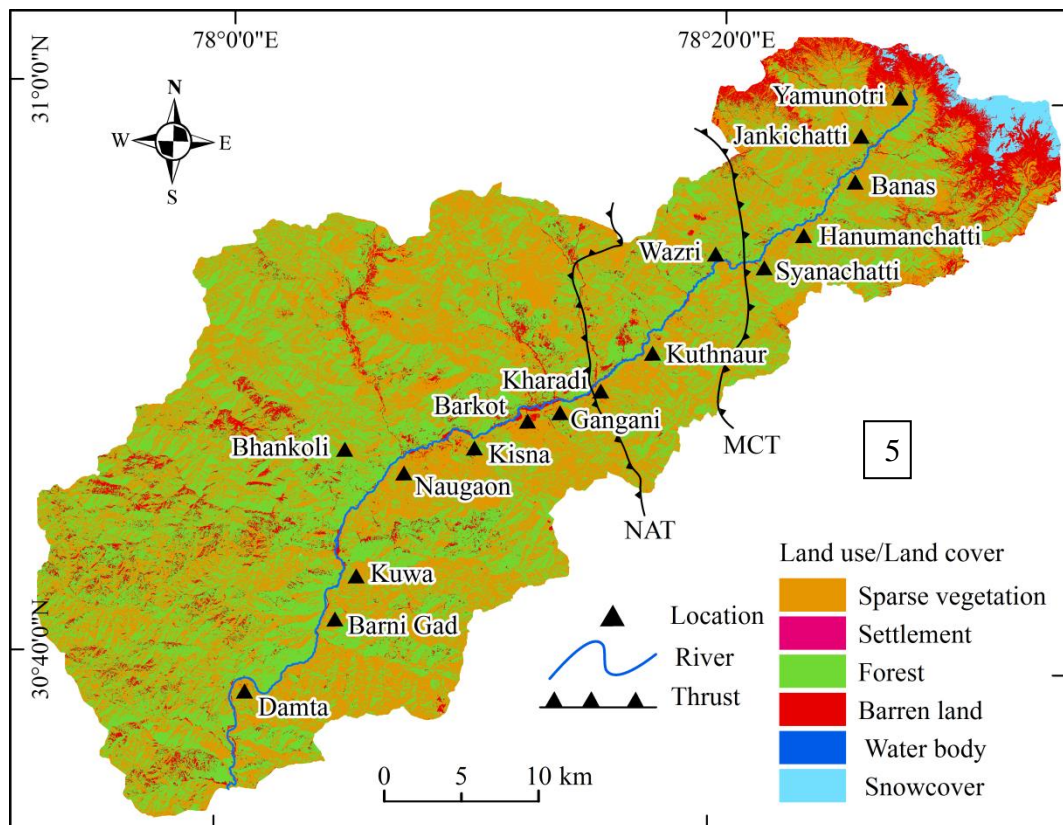
3.4.2.8 Relationship between proximity to road and landslides

One of the components controlling slope instability is human interference in the form of road cuts and other activities. This severely impacts slopes and hence, is considered an essential factor for mapping. In this study, 32 categories of buffers from the road were created (Fig. 3.2.-8). Though the surface may not be affected by landslides with increase in distance from the road, the buffers were made to cover the entire study area for further stability analysis.

The spatial distribution of landslides with road buffers is given in Table 3.3. Results show that landslide area percentage decreases with increase in proximity from the road. The maximum landslide area is observed in the proximity of 50 m from the road (15%), followed by 100 m (9%), 150 m (7%), 200 m (6%) and so on. The landslide population gradually decreases with increase in the distance from the road.







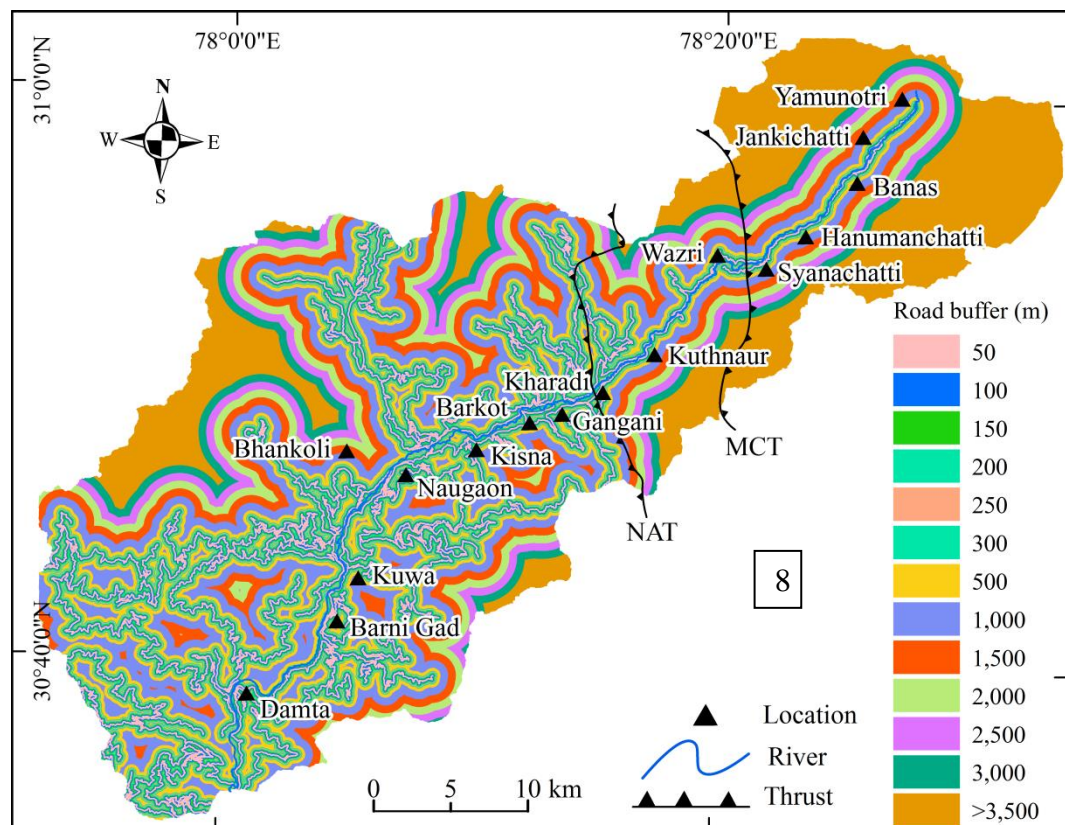
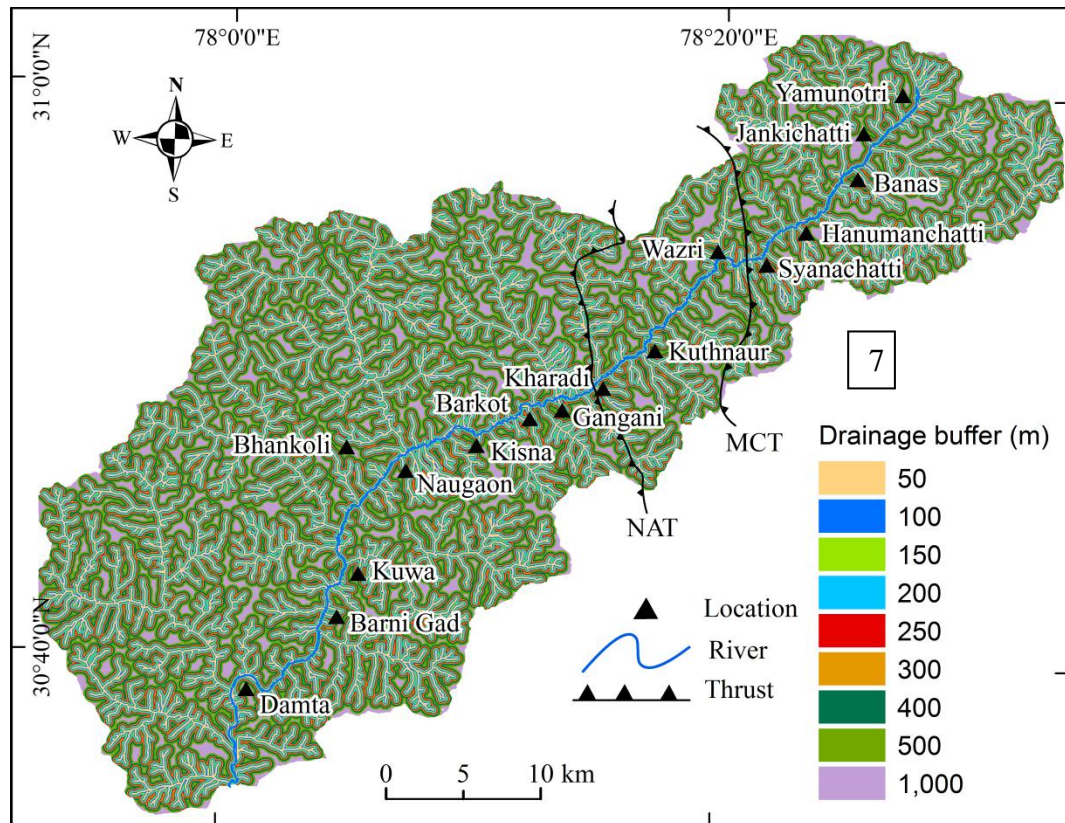


Fig.3.2: Thematic maps of the study area: (1) Elevation map; (2) Slope map; (3) Slope aspect map; (4) Lithological map; (5) Land use/Land cover map; (6) Proximity to lineaments map; (7) Proximity to drainage map; (8) Proximity to road map

Table 3.3: Computed ratios for classes of various data layers based on landslide occurrences

Category	No. of pixels in each class	Area of class (km ²)	% of class	No. of pixel occupied by landslide	Landslide area per unit class	% of landslide	FR
1. Elevation							
500	105	0.01	0	0	0	0.00	0.00
500-1000	1201886	120.19	8.35	2988	0.30	7.27	0.87
1000-1500	2640495	264.05	18.33	12140	1.21	29.55	1.61
1500-2000	2798781	279.88	19.43	13823	1.38	33.65	1.73
2500-3000	1971917	197.19	13.69	3042	0.30	7.41	0.54
3000-3500	1261457	126.15	8.76	5412	0.54	13.17	1.50
3500-4000	1265123	126.51	8.78	2967	0.30	7.22	0.82
4000-4500	1390400	139.04	9.65	708	0.07	1.72	0.18
4500-5000	1009681	100.97	7.01	0	0	0	0
>5000	862323	86.23	5.99	0	0	0	0
2. Slope angle							
<5°	3	0.00	0	0	0	0	0
5°-10°	2756380	275.64	19.14	4314	0.43	10.50	0.55
10°-15°	2002121	200.21	13.90	2642	0.26	6.43	0.46
15°-20°	2427631	242.76	16.86	4912	0.49	11.96	0.71
20°-25°	2616981	261.70	18.17	8441	0.84	20.55	1.13
25°-30°	3437380	343.74	23.87	16152	1.62	39.32	1.65
30°-45°	1032596	103.26	7.17	4280	0.43	10.42	1.45
55°-60°	126806	12.68	0.88	329	0.03	0.80	0.91
>60°	2270	0.23	0.02	10	0	0.03	1.54
3. Aspect classes							
Flat	18	0	0	0	0	0	0
North	948669	94.87	6.58	1383	0.14	3.37	0.51
Northeast	1786181	178.62	12.40	2278	0.23	5.55	0.45
East	1711350	171.14	11.88	3246	0.33	7.90	0.66
Southeast	1625443	162.54	11.29	4526	0.46	11.02	0.98
South	1732220	173.22	12.03	6535	0.65	15.91	1.32
Southwest	1960248	196.02	13.61	8835	0.88	21.51	1.58
West	1849269	184.93	12.84	6569	0.66	15.99	1.25
Northwest	1821187	182.12	12.65	5854	0.59	14.25	1.13
North	967583	96.76	6.72	1854	0.19	4.51	0.67
4. Lithology							
Slate, Limestone	3253308	325.33	22.59	9717	0.97	23.65	1.05

Quartzite	3302486	330.25	22.93	9037	0.90	22.00	0.96
Gneiss, Quartzite	3038472	303.85	21.10	7712	0.77	18.77	0.89
Limestone, Slate	3532381	353.24	24.53	11863	1.19	28.88	1.18
Quartzite, Limestone	1275521	127.55	8.86	2751	0.28	6.70	0.76
5. Land use / land cover							
Sparse Vegetation	6622285	662.23	45.98	22852	2.29	53.29	1.16
Forest	6428558	642.86	44.63	16129	1.61	37.61	0.84
Water body	1641	0.16	0.01	0	0	0.00	0
Barren land	1179025	117.90	8.19	3850	0.39	8.98	1.10
Settlement	1549	0.15	0.01	3	0	0.01	0.65
Snowcover	169810	16.98	1.18	46	0	0.11	0.09
6. Proximity to lineament							
50	2093204	209.32	14.53	12045	1.20	29.32	2.02
100	2050957	205.10	14.24	10158	1.02	24.73	1.74
150	1852210	185.22	12.86	5859	0.59	14.26	1.11
200	1595823	159.58	11.08	3241	0.32	7.89	0.71
250	1339004	133.90	9.30	2222	0.22	5.41	0.58
300	1097236	109.72	7.62	1711	0.17	4.17	0.55
400	1570554	157.06	10.91	2459	0.25	5.99	0.55
500	967710	96.77	6.72	1488	0.15	3.62	0.54
1000	1096187	109.62	7.61	1897	0.19	4.62	0.61
1500	739283	73.93	5.13	0	0	0.00	0
7. Proximity to road							
50	1019957	102.00	7.08	6001	0.60	14.61	2.06
100	799706	79.97	5.55	3794	0.38	9.24	1.66
150	672035	67.20	4.67	2827	0.28	6.88	1.48
200	581241	58.12	4.04	2276	0.23	5.54	1.3
250	504438	50.44	3.50	2102	0.21	5.12	1.46
300	443874	44.39	3.08	1746	0.17	4.25	1.38
400	751141	75.11	5.22	2285	0.23	5.56	1.07
500	629917	62.99	4.37	1575	0.16	3.83	0.88
600	548202	54.82	3.81	1059	0.11	2.58	0.68
700	475680	47.57	3.30	718	0.07	1.75	0.53
800	421398	42.14	2.93	769	0.08	1.87	0.64
900	376670	37.67	2.62	669	0.07	1.63	0.62
1000	342432	34.24	2.38	603	0.06	1.47	0.62

1500	1330018	133.00	9.24	2939	0.29	7.15	0.78
2000	973470	97.35	6.76	3028	0.30	7.37	1.09
2500	909088	90.91	6.31	2389	0.24	5.82	0.92
3000	713711	71.37	4.96	2158	0.22	5.25	1.06
3500	614069	61.41	4.26	1658	0.17	4.04	0.95
4000	450063	45.01	3.13	0	0.00	0	0
4500	358937	35.89	2.49	0	0.00	0	0
5000	192301	19.23	1.34	0	0.00	0	0
5500	147255	14.73	1.02	256	0.03	0.62	0.61
6000	198765	19.88	1.38	761	0.08	1.85	1.34
7000	292555	29.26	2.03	670	0.07	1.63	0.80
7500	218988	21.90	1.52	0	0.00	0	0
8000	115749	11.57	0.80	193	0.02	0.47	0.59
8500	103908	10.39	0.72	180	0.02	0.44	0.61
9000	77934	7.79	0.54	424	0.04	1.03	1.91
9500	56026	5.60	0.39	0	0.00	0	0
10000	43571	4.36	0.30	0	0.00	0	0
10500	30169	3.02	0.209	0	0.00	0	0
8. Proximity to drainage							
50	2010596	201.06	14.02	9965	1.00	24.26	1.73
100	1840796	184.08	12.83	9994	1.00	24.33	1.90
150	1692884	169.29	11.80	6743	0.67	16.41	1.39
200	1559556	155.96	10.87	3924	0.39	9.55	0.88
250	1428406	142.84	9.96	2452	0.25	5.97	0.60
300	1289255	128.93	8.99	1685	0.17	4.10	0.46
400	2113410	211.34	14.73	2223	0.22	5.41	0.37
500	1381047	138.10	9.63	2305	0.23	5.61	0.58
1000	1029155	102.92	7.17	1789	0.18	4.36	0.61

3.5 Landslide susceptibility zonation map

3.5.1. Application of frequency ratio

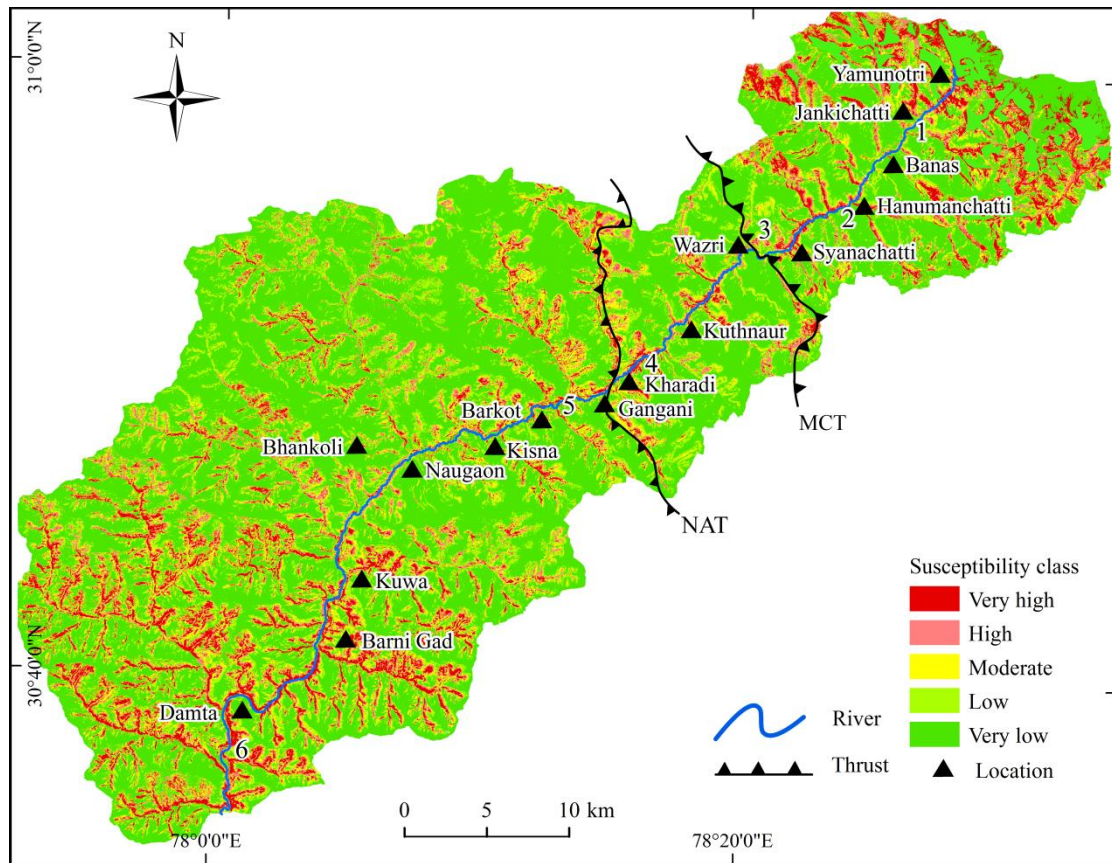
The FR method for evaluating landslide susceptibility of an area is based on the relative importance of the factors in contributing to landslides. In this study, the frequency ratios of each controlling factor was calculated and then added to calculate the LSI. The results of the distribution of landslides in each class of the different causative factors and their relationship with each factor using the FR method are given in table 3.3.

The highest FR of 1.7 is observed in the elevation range 1500-2000 m; it gradually decreases with increase in altitude. Slope angle of 25°-30° exhibit the maximum FR of 1.6. It decreases with decrease in slope angle. These also decrease with increase in slope angle, exceptionally at slope angle >60° with FR of 1.44. The FR for slope aspect shows maximum affinity towards southwest with a value of 1.58 followed by south with an FR of 1.32. Flat areas do not contribute to slope instability. The slopes facing north, northeast, east and southeast have FR <1. The highest FR value of 1.17 in the lithologic variables is found in the Lesser Himalayan rocks, i.e., limestone and slate of the Chakrata Formation, followed by slate and limestone of the Deoban Formation (1.05). Other rock types have FR values of <1.

The FR values for the different classes of land use/land cover show that the region with sparse vegetation has the maximum value of 1.16, followed by barren land (1.10); in the rest of the classes FR is <1. The proximity from lineaments shows that at distances 0-50 m, the FR is the highest (2.02), which decreases with increase in the proximity to the lineament. FR values for the drainage buffer also show similar results as lineaments, with a maximum at a distance of 50-100 m (1.9); it gradually decreases with the increase in the proximity to the drainage. In the case of proximity from the road, FR values are highest at distances of 0-50 m (2.06). The FR for this category is quite random with respect to distance to the road.

After calculation of the frequency ratios of each cell for all the influencing factors, the LSI was calculated using the formula given in equation 3.2. The value of LSI varies from 0.524 to 5.73, which is further classified into five categories based on defined intervals namely, very high susceptibility (VHS), high susceptibility (HS), moderate susceptibility (MS), low susceptibility (LS) and very low susceptibility (VLS). Figure

3.3 illustrates the classified LS map of the study area. The major portion (55%) of the study area lies in the VLS zone and 15% of the area lies in the LS zone, while 10% each of the area lies in the VHS, HS and MS zones (Table 3.4).



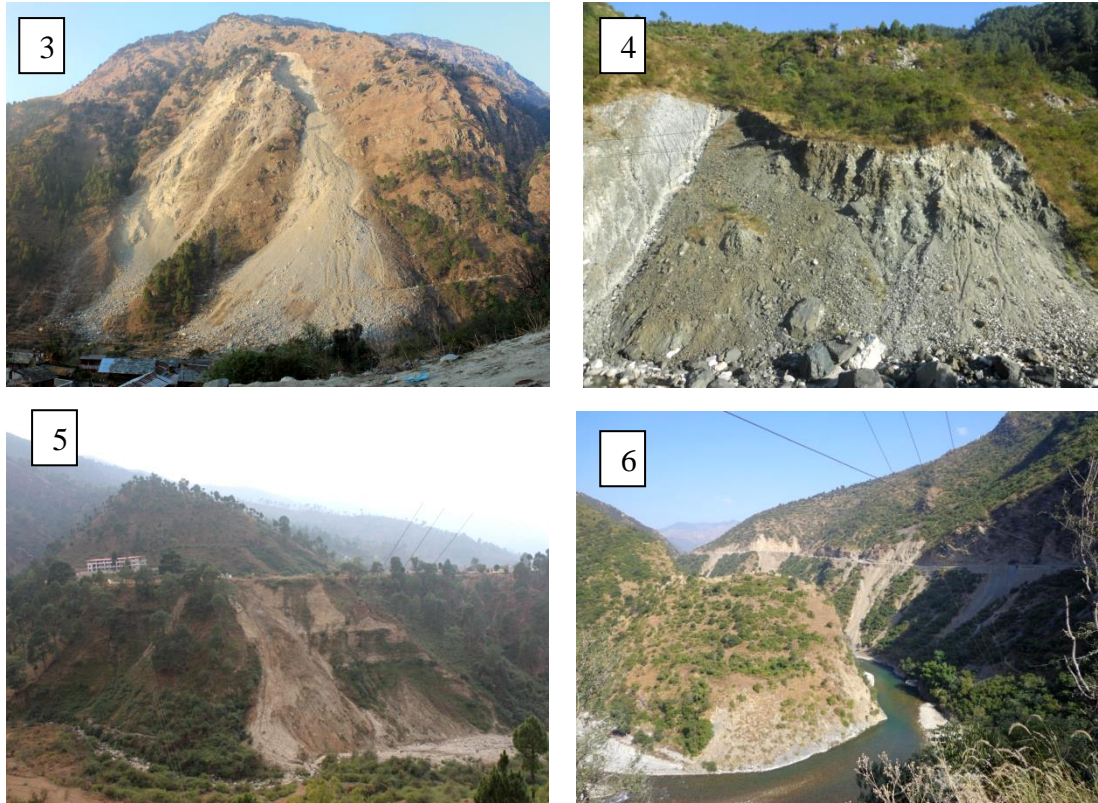


Fig. 3.3: Landslide susceptibility map of the study area; the map was validated in the field (Photos 1-6)

Table 3.4: Different classes of landslide susceptibility zones

Class	No. of pixels in each class	Area (%)	Area (km ²)
VHS	1430843	10	143.08
HS	1438934	10	143.89
MS	1431397	10	143.14
LS	2146153	15	214.62
VLS	7891136	55	789.11

3.6. Validation and evaluation

For validation of the LS map, landslide population partition and success rate curve methods were used, followed by field verification. For the first part, the total landslide population was randomly divided into two parts of 124 and 30 landslides. The 124 landslides were used to generate the LS map and the other 30 landslides were used for validation of the output map. Results show that the majority of the landslides used for validation occurred in the high and very high susceptibility zones. Only two landslides occurred in the moderately susceptible zones.

The success rate curve method graphically ascertains the accuracy of the generated map (Van Westen et al., 2003). The graphical representation of the success rate curve for the study area is given in Fig. 3.4. Results indicate that 10% of the VHS zones account for about 48% of the total landslide area. The

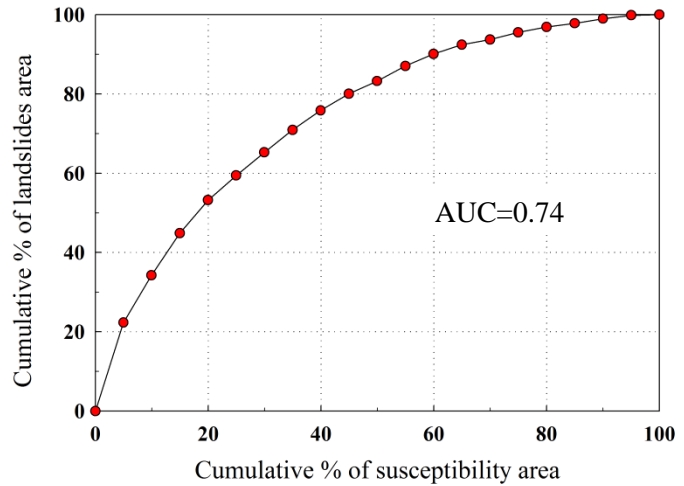


Fig. 3.4: Success rate curve

next 20% of the HS zones account for about 58% of the total landslide area. 40% of the MS zones account for about 78% of the total landslide area; 60% of the LS zones which have comparatively low values, account for about 90% of the landslide area. The remaining 75% of the susceptible landslide areas are classified as VLS zones, which account for about 95% of the total landslide area. The ROC plot analysis, with an AUC of 0.74, accounted to about 74% accuracy of the generated map.

The landslides at a few locations, particularly in the VHS and HS zones, were physically verified in the field. The field-verified photos of six landslides are presented in figure 3.3. The first landslide is located in Kharsali village that falls in the VHS zone. The second landslide lying in Wariya village is classed in the HS zone. The third landslide lies near Wazri village, which lies between the VHS and HS zones. The fourth landslide lies downstream of Kuthnaur village, falling in the VHS zone. The fifth landslide is about 1 km downstream from Tunalka village, and is categorised as a HS zone. The sixth landslide, about 500 m downstream of Naingaon village, lies in the VHS zone.

3.7. Discussion

Landslide susceptibility is the spatial likelihood of landslide occurrence under a given set of geo-environmental conditions (Guzzetti et al., 2005). It is based on the hypothesis that the same conditioning factors that caused landslides in the past will also cause landslides in the future (Carrara et al., 1991; Hutchinson, 1995; Aleotti and Chowdhury, 1999; Chung and Frabbri, 1999; Guzzetti et al., 1999; Chen et al., 2016).

For the present study, the LSM was prepared using the bivariate method (frequency ratio) on a 1:25,000 scale. The LS zones were generated based on the relationship between the landslides and each class of causative factor such as elevation, slope angle, slope aspect, lithology, land use/land cover, proximity to lineament, proximity to drainage and proximity to road. Though it is not easy to pinpoint exactly which causative factor is responsible for landsliding, it lends insight of the relative influence of the factor on the landslide. Figure 3.5 is a graphical representation of the spatial distribution of landslides in each class of the causative factors and its corresponding frequency ratios.

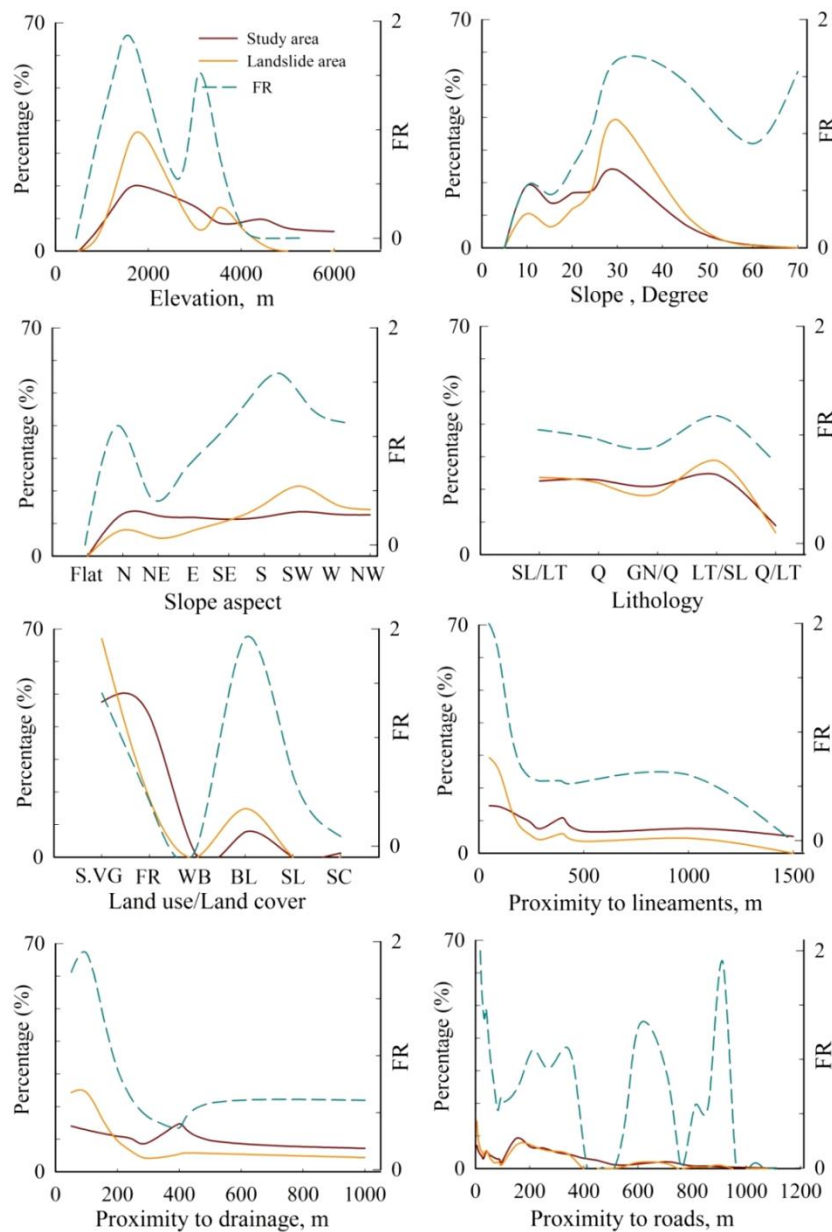


Fig. 3.5: Spatial distribution of landslides with causative factors and frequency ratio analysis

Results show that high correlation is observed in elevations between 1000-2000 m, with FR values ranging between 1.5-1.7. Such elevations in the study area generally comprise cliffs and rocky terrain, particularly in the Higher Himalaya. Rock fall is the dominant mass wasting process in these regions. A major portion of the landslide area (37%) is confined to the slopes ranging between 25-30°, with a high FR of 1.65. These are generally areas of slopes overburdened with slope-wash and river-borne material, which make them susceptible to instability when triggered by an external agent. Such slopes have relatively high moisture retention capacity, thereby increasing the pore pressure and making it liable to instability (Sujatha et al., 2012; Rautela and Thakur, 1999). The outcome of such slopes in relation to landslides distribution has also been reported in other parts of the Himalaya (Sarkar and Gupta, 2005; Kanungo et al., 2006; Sarkar et al., 2008) as well as in other countries (Dai and Lee, 2002; Santacana et al., 2003; Fernandez et al., 2004; Magliulo et al., 2009). It has also been observed that in slopes with angles >60°, the FR value increased to 1.54, though its areal distribution is very less (0.027%). In such slopes, rockfalls are dominant while gentle to moderate slopes show debris slides, which has also been observed by Gupta et al. (2017) in the Yamuna Valley, and others in other parts of the Himalaya (Kanungo and Sarkar, 2003; Ghosh et al., 2009; Sarkar et al., 2013). A major portion of such slopes is seen in the Higher Himalaya, which acts as an orographic front that experiences maximum precipitation.

Lithology of an area plays a key role in the stability of slopes. Variations in lithology define the strength and permeability of the rock and soil in a region, and have been considered as one of the most decisive parameters by several researchers (Gorum et al., 2011; Yalcin et al., 2011; Akgun, 2012; Peruccacci et al., 2012). However, in the present study, the lithological units of the Higher Himalaya and the Lesser Himalaya contribute almost equally to slope instability. In the Higher Himalaya, the rocks comprising gneiss and quartzite have a FR value of 0.89. This may possibly be due to high degree of shearing and mechanical weathering, which is the cause of the rockfalls. The rocks of the Lesser Himalaya, comprising of slate, limestone and quartzite, contribute equally, with FR values ranging from 0.75 to 1.17. It indicates the influence of other factors in conjunction with lithology. Lineaments constitute an important factor in such terrain. Lineaments include joints, fractures, faults and other structural discontinuities, which drastically reduce the strength of rocks and in turn,

increase the probability of failure (Dai et al. 2002; Kayastha et al., 2013; Sarkar et al., 2013). In the present study, the maximum areal distribution of landslides is in the proximity of 0-50 m from lineaments, with the highest FR value of 2.01. The FR values gradually decrease with the increase in distance from lineaments. This implies that areas close to lineaments are highly prone to slope failure. This is evident from the fact that the density of landslides near the MCT, NAT and other local faults is greater compared to areas further from the thrusts and faults. This testifies to the high degree of shearing and weathering in the region infested by faults and thrusts, and thereby causing landslides.

The proximity to drainage is another controlling factor, which is related to the degree of saturation of slopes and the erosive action of rivers (Yalcin, 2008; Pourghasemi et al., 2012). Most landslides are noted between 0-100 m of stream channels; these have high FR values ranging between 1.89 and 1.73. The influence of drainage on slopes decreases with increase in distance. This may possibly be due to toe cutting of the slopes by the streams, which destabilises the slope, resulting in landslides. Anthropogenic activity in the form of road cutting disrupts the natural topography, which increases the instability of slopes (Bernardi De Leon, 2009). In the study area, a high FR value (2.06) is noted at distances of 0-50 m, which gradually decreases with increase in proximity. The modification of slope in the form of road cuts makes the slope highly vulnerable to slope failure, as it fractures rock slopes due to blasting and exposes the surface to weathering and erosion. Over the years, the Yamuna Valley has burst with developmental activities in the form of construction of roads and buildings, mainly for the tourism sector, as this corridor leads to Yamunotri, which is one of the pilgrimage centres of the Char Dham Yatra. Much of the impact of slope cuts is seen at close proximity; FR values decrease with increasing distance. However, at certain distances, 2000-3000 m, 5500-6000 m and 8500-9000 m there is an increase in FR values from 1.06 to 1.9, which may be due to reasons other than the impact of roads. Much of the impact of anthropogenic interference is seen in the Lesser Himalaya and fewer in the Higher Himalaya; however, this may change in the years to come.

Another contributing factor is land use and land cover, which is one of the key factors responsible for landslide occurrences (Koukis and Ziourkas, 1991; Anbalagan, 1992). Sparse vegetation occupies the maximum areal distribution (53%) with a high FR value of 1.159, followed by barren land (FR 1.09), though its areal distribution is only

8.9% of the total study area. Lack of vegetation on the hillslopes has been observed as one of the most common phenomena responsible for hillslope erosion (Kumar et al., 2019).

A major portion of the study area (55%) lies in the VLS zone, followed by the LS zone (15%). Most of these areas lie in the forest and sparse vegetation area, indicating that vegetation cover has a greater role to play in landslide occurrences. The remaining classes (VHS, HS and MS) appear to occupy equal areas of 10% each. The study shows that the HS and VHS zones are mostly confined to areas close to drainage and faults/thrusts, barren land, steep slopes facing south and west and higher elevations.

In order to ascertain the precision of the LSM, the validation sample of landslides was overlain on the susceptibility map; 21 landslides lie in the VHS zone and 4 in the HS zone. The results indicate a high reliability of the LSM. The success-rate curve (Fig. 3.4) further illustrates how close the LSM fits with reality. This curve gives an area ratio of 0.74, which indicates that the LSM generated is fairly good, with an accuracy of 74%. This result was further attested in the field, where five selected landslides occurring in the VHS zone were physically verified (Fig.3.3). The first landslide near Kharsali village lies in the VHS zone. The landslide appears to have an adverse impact on the village, which shows signs of subsidence; houses and other structures, including the age-old Shani Temple are tilted and cracked. Detailed stability analysis of this landslide was carried out by Jamir et al. (2017). The second landslide, located just below Wariya village, lies in the HS zone. This has endangered the whole village, which is evident from the subsidence and cracks developed in most of the dwellings. This landslide, discussed in Chapter 5, has been reactivated, which is evident from the damaged retaining walls (Fig. 3.6a). The third and fourth landslide zones are made up of highly sheared rock masses, which point to tectonic activity in the area. The third landslide, lying near Wazri village, was triggered in November 2017. This area was mapped from satellite imagery and field visits prior to sliding, when the area was affected by gully erosion (Fig. 3.6b). Results show that the area falls in the VHS zone, which proves the reliability of the map. Figure 3.7 shows a magnified view of the landslide area prior to the disaster, and post disaster. Further downstream, the fifth landslide near Tunalka village was caused due to river erosion, i.e., toe cutting of the slope. The sixth landslide represents the combined influence of both tectonic activity

and anthropogenic interference. The highly sheared and pulverised rock slopes here have been extensively modified for development. The tectonic influence on these hill slopes is further verified and discussed in Chapter 4.



Fig. 3.6: (a) Damaged retaining wall below Wariya village; (b) Erosional deposits on the NH-94. Photograph of November 2014, prior to the disaster (November, 2017)



Fig.3.7: Magnified view of Wazri landslide (Inset-images prior to field mapping and post-field mapping)

3.7.1. Limitations

Inasmuch as the quantitative FR method for LSM generation is considered agreeable, there are always limitations in every method. The FR method, though reliable, is based on the hypothesis that landslides that occurred in the past under certain conditions due to certain factors will also happen in the future under the same set of conditions (Carrara et al., 1991; Hutchinson, 1995; Aleotti and Chowdhury, 1999; Chung and Fabbri, 1999; Guzzetti et al., 1999). However, this may not be so in some cases. Though the geological factors (slope, aspect and lithology) may not change in short time spans, stream action, landslides and anthropogenic activities are variables that may change the whole system in short durations. The causative factors too are independent of each other and hence, only a relative idea of the main causative factor for landslide occurrence can be obtained.

Chapter-4

SPATIAL INTERRELATIONSHIP OF LANDSLIDES AND LITHO-TECTONIC AND PRECIPITATION REGIMES

4.1. Introduction

In the geodynamically active Himalayan mountain belt, landslides are an inevitable component of the orogeny (Koukis et al., 2009). Landslides being an outcome of the intertwining of various geological processes, it is important to understand the contribution of factors such as tectonics and precipitation in the region. Hence, concise data on the litho-tectonic and precipitation unpredictability would lend insight on the relative influence of these factors on hillslopes and their relationship with landslides (Hovius et al., 1997; Reichenbach et al., 2004; Borgatti and Soldati, 2010; Crozier, 2010; Kumar et al., 2018b Wang et al., 2018).

Such inter-relationship studies, however, are exceptional in the Himalaya, particularly in the NW Himalaya, despite the active nature of this portion of the Himalaya (Khatttri et al., 1989; Scherler et al., 2014; Mahesh et al., 2015) and high frequency of disastrous landslides (Martha et al., 2015; Gupta et al., 2016b; Gupta et al., 2017). Spatio-temporal altering landslide distribution patterns play a key role in such studies. Temporal data on landslide distribution, however, is not easy to obtain due to limitations such as delineation of individual failure events on reactivated landslide, loss of landslide scarp caused by successive mass movement, vegetation on detached debris and dating constraints (Lang et al., 1999). But spatial distribution can be achieved suitably using high resolution satellite imagery and subsequent ground truthing and hence, the present study pertains to such spatial distribution analysis.

For landslide distribution mapping on a regional scale, Google Earth (GE) images have been used and the uncertainty of GE mapping has been resolved by comparing known ground distances with GE measurements (Mohammed et al., 2013; Kumar et al., 2018b). To determine the interrelationship of landslide distribution with the main causative factors, that is, litho-tectonic and precipitation regime, the following proxies have been used to quantify these factors, longitudinal profile of the river (L-profile), topographic swath profile, stream length gradient index (SL), valley floor width to height ratio (V_f), and channel steepness index (K_s) to discern the tectonic regime (Bull

and McFadden, 1977; Seeber and Gornitz, 1983; Gregory and Schumm, 1987; Rhea, 1993; Silva et al., 2003; Burbank and Anderson, 2011; Grohmann et al., 2011; Telbisz et al., 2013; Kumar et al., 2018b) and snowfall/rainfall, surface temperature (Mach and Mastrandrea, 2014; Bin et al., 2017) and normalized difference vegetation index (NDVI) for precipitation (Yang et al., 1998; Bin et al., 2017). As a lithological proxy, Schmidt Hammer Rebound (SHR) (Schmidt, 1951) has been used in many studies that represent rock strength (Lifton et al., 2009; Gupta, 2009; Goudie, 2016). Similarly, the geological strength index (GSI) (Hoek, 1994; Hoek et al., 2002; Cai et al., 2004; Cai et al., 2007) has also been used as a rock mass strength index.

This study aims to correlate the various multi-proxy components with that of landslides in the Yamuna Valley. The L-profile of the river channel, K_s , V_f , topographic swath profiles and SL are used to understand tectonic unpredictability whereas, Tropical Rainfall Measurement Mission (TRMM) based daily rainfall data of the last 17 years (2000-2016) and the NDVI are used to characterize precipitation variability. SHR and GSI have been used to determine the relative strength of various lithologies. This study will help find out the relative influence of tectonics, structure, precipitation and lithology on landslide distribution and dimensional pattern.

4.2. Methodology

4.2.1. Landslide inventory

In the present study, a landslide inventory along the Yamuna River valley was prepared using high resolution LISS-4 imagery (5.8 m resolution), ortho-image of Cartosat-1 (2.5 m), GE imagery and SoI topographic maps. Landslide locations were marked in the field using a handheld GPS. These landslides were classified following Varnes (1978) and Hungr et al. (2014). A detailed account of the preparation of landslide inventory has been discussed in Section 3.2.1.1 of Chapter 3. The uncertainty (error) in landslide dimensions (total disturbed area) caused by measurement in the GE image was determined by comparing known distances in the study area with those measured in the GE image. The known distances were obtained from the SoI topographic maps. The dimensions of the landslide were determined using area (total disturbed area), shape (length and width) and volume. The approximate thicknesses (with \pm error) of the landslides were ascertained in the field

following Larsen and Torres Sanchez (1998), Guzzetti et al. (2009) and Kumar et al. (2018b).

4.2.2. River long profile and topographic swath profile

The L-profile of a stream is the geometric representation of its gradient that is generally concave upward; any deviation from a concave-up shape indicates a state of disequilibrium, possibly due to tectonic, climatic or lithologic perturbations and landslide damming (Hack, 1973; Seeber and Gornitz, 1983; Molin and Fubelli, 2005; Korup, 2006; Whitakker et al., 2007; Gupta and Sah, 2008a). The profile for the study was extracted from Cartosat DEM to identify over-steepened channel reaches (knickpoints) and to determine their relationship with the other factors. However, the river L-profile covers only minimum elevation conditions along the stream and may not preserve the major topographic changes that may owe their origin to tectonic influences (Grohmann et al., 2011; Telbisz et al., 2013; Kumar et al., 2018a); hence topographic swath profile was also incorporated.

Topographic swath profile refers to generalized elevation profiles along the swath baseline that, unlike a single cross-sectional line, represents multiple parallel cross-sectional lines. A curvilinear (following the river trend) swath polygon was used to reconstruct a topographic profile along the Yamuna Valley using Cartosat DEM, considering a swath width of 4 km and horizontal sampling interval of 10 m along the base line (river). The polygonal swath profile with the river as the baseline is represented in Fig. 4.1. The mean and maximum swath profiles were calculated along the trunk stream to analyze the topography (Fig. 4.1, inset).

4.2.3. Stream Length Gradient index

The SL index is a quantitative measure of gradient change along a river and is calculated by normalizing the river channel against the longest regional drainage (Hack, 1973; Keller and Pinter, 1996). It exhibits the adjustment of a river as it attempts to reach a dynamic equilibrium. The SL index may also be used to detect recent tectonic activity by identifying anomalously high index values on a specific rock type (Merritts and Vincent, 1989; Keller and Pinter, 1996; Brookfield, 1998).

The SL index remains approximately constant along a graded stream and any variations appear to be attributable to tectonic or structural and lithological controls (Lifton and Chase, 1992). It is calculated using the following equation:

$$SL = (\Delta H / \Delta L) * L$$

where ΔH and ΔL are the differences of elevation of the reach and length of the reach, respectively. L is the total channel length from the midpoint of the reach of interest upstream to the highest point on the channel.

The SL index was extracted from Cartosat-DEM along the longitudinal profile of the river, at an interval of 500 m downstream from Yamunotri to Damta.

4.2.4. Steepness index

The k_s and V_f indices were used to evaluate the tectonic regime in the area. The k_s belongs to the ‘stream erosion power law’ and has been widely used as a proxy to study active tectonics in different river valleys (Flint, 1974; Howard and Kerby, 1983; Wobus et al., 2006). Generally, higher k_s represent high uplift regions and low k_s imply low uplift zones (Synder et al., 2000). It is computed using the following equation:

$$S = k_s A^{-\theta}$$

where S is the local channel slope, A is the upstream drainage area, and k_s and θ are the channel steepness and concavity indices respectively. The θ was measured by power regression of slope versus upstream drainage area log-log plots. The S and A values were determined at 500 m horizontal interval between Yamunotri and Damta along the Yamuna River using Cartosat DEM. The slope and upstream drainage area log-log plot resulted in a concavity index (θ) of 0.6. However, for comparison sake, a normalized channel steepness index (k_{sn}) was also calculated using a reference concavity index (θ_{ref}) of 0.45, an estimated value as proposed by Whipple and Tucker (1999) and Snyder et al. (2003). The θ of most streams can vary over a wide range. However, in steady state landscapes, the value may vary between 0.35 and 0.65 (Snyder et al., 2000; Kirby and Whipple, 2001; Roe et al., 2002; Wobus et al., 2006). Thus, the empirical calculation of the normalized steepness index is given as:

$$k_{sn} = S A^{\theta_{ref}}$$

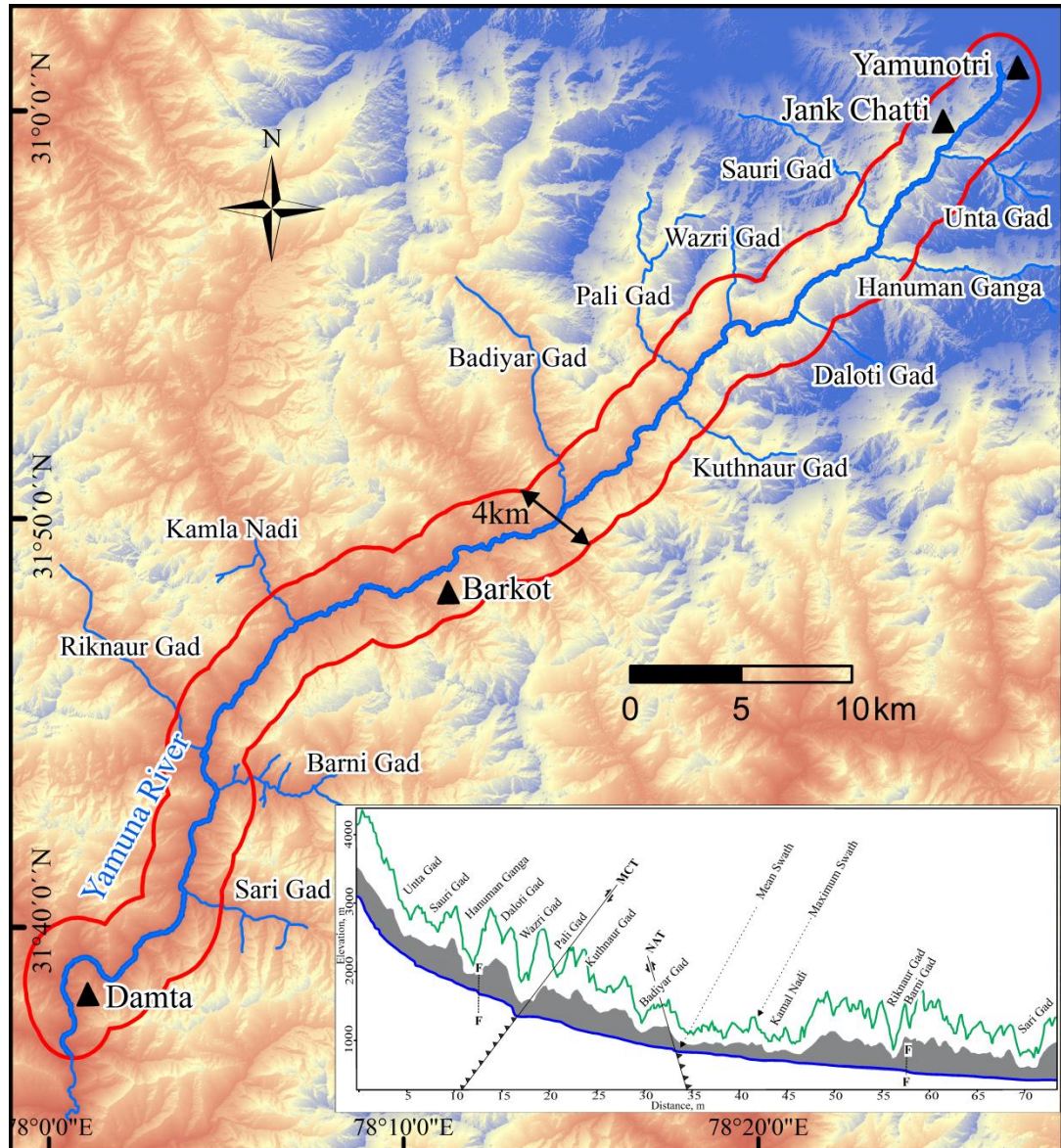


Fig. 4.1: Spatial variation of valley width along the river (Inset: Mean and maximum topographic swath profile along the stream)

4.2.5. Valley floor width to valley height ratio

The V_f ratio (Bull and McFadden, 1977) is used to understand the relation of valley morphology and landslides, and to identify portions that experience more tectonic activity than others. This index differentiates between the broad-floored, U-shaped open valleys that signify relatively low tectonic activity and the V-shaped, deep narrow valleys in response to active uplift due to relatively high tectonic activity (Bull and McFadden, 1977; Keller and Pinter, 1996). The low values of $V_f (<1)$ reflect deep valleys with streams that are actively incising, which is commonly associated with uplift (Keller and Pinter, 1996), whereas the high values ($V_f >1$) reflect lateral erosion

(Wells et al., 1988; Silva et al., 2003; Malik and Mohanty, 2007). The V_f is calculated using the following equation:

$$V_f = 2V_{fw} / [(E_{ld} - E_{sc}) + (E_{rd} - E_{sc})]$$

where V_{fw} is the width of the valley floor, E_{ld} and E_{rd} are the elevations of the left and right valley divides respectively and E_{sc} is the elevation of the valley floor. These parameters were extracted from Cartosat DEM at 500 m horizontal interval.

4.2.6. *Rainfall and Normalized Difference Vegetation Index*

Rainfall data is an indirect means of assessing and quantifying the changing climate and its precipitation regime in a region. The TRMM mainly observes rain structure, rate and distribution in tropical and subtropical regions; the data is expected to play an important role in understanding mechanisms of global climate change and monitoring environmental variation. Spatial variability of the precipitation regime was achieved using TRMM-based daily rainfall data for a time period of sixteen years (2000 to 2016) and NDVI swath profile. Daily rainfall data was used to find out the spatial variation of annual average rainfall and monsoon rainfall (June-September).

The NDVI is a numerical approach that uses the visible and near-infrared bands of the electromagnetic spectrum and is adopted to assess whether the area contains vegetation (greenness) or not (Tucker, 1979; Tucker et al., 1986). The NDVI (Rouse Jr et al., 1974; Deering, 1978; Jackson and Huete, 1991) was used as an indirect proxy and was determined using the following equation:

$$NDVI = (NIR - R) / (NIR + R)$$

where NIR is near infrared and R is red. NIR and R represent bands 5 and 4 respectively of Landsat 8 imagery. To construct the NDVI swath profile, a curvilinear swath of 4 km width with a horizontal sampling resolution of 15 m was used along the valley. A curvilinear polygon was used to eliminate the influence of curvatures on the NDVI along the river (Kumar et al., 2018b). Cloud-free imagery of September was used for maximum vegetation that eliminated seasonal changes, solar angle and bare soil/rock effects on the NDVI (Jackson and Huete, 1991). Given that the NDVI swath also involved river bed and bare hillslopes, only the maximum NDVI profile was used. The spatio-temporal variation in vegetation density and type, generally controlled by climate, has been observed to affect the NDVI (Myneni et al., 1995,

Wessels et al., 2012; Bin et al., 2017). The value of NDVI has also been observed to vary based on the surface ≤ 0.2 bare soil, 0.2-0.5 mixture of bare soil, vegetation and rock surface and > 0.5 dense vegetation (Shao, 2009; Rahman et al., 2014).

4.2.7. Rock mass Strength

4.2.7.1. Schmidt Hammer Rebound value

The Schmidt hammer was originally devised to test the surface rebound hardness of concrete (Schmidt, 1951). In the present study, N-type Schmidt hammer (impact energy of 2.207 Nm) is used on fresh rock exposures to evaluate indirect rock strength. Other studies where SHR values have been used to measure rock strength include that of Lifton et al. (2009) and Goudie (2016). A total of 50 measurements were made at each site, following the methodology of Day and Goudie (1977). Sampling intervals of the measurement was based on conditions such as change in lithology and/or ~500 m interval if same lithology persists. SHR values were not taken in areas of highly sheared rock masses. The tests were performed following the International Society of Rock Mechanics (ISRM) method (Aydin and Basu, 2005); hence, the hammer position was kept in $90 \pm 5^\circ$ relative to the rock surface. The 10 lowest and highest values were not included in the analysis considering the influence of uncertainty (Gupta, 2009).

4.2.7.2. Geological Strength Index

The GSI was introduced by Hoek (1994) to provide a practical means to estimate the strength and deformation modulus of jointed rock masses for use with the Hoek-Brown failure criterion (Hoek and Brown, 1980, 1997; Hoek, 1988, Hoek et al., 2002). It basically characterizes rock masses depending on the condition of joint surfaces and blocky nature of rock masses to estimate the deformability and strength indirectly. GSI values range from 0 to 100. The GSI system consolidates various versions of the Hoek-Brown criterion into a single simplified and generalized criterion that covers all of the rock types normally encountered in underground engineering. The early version of the GSI system was presented as a table (Hoek et al., 1995) and a revised version was presented as a chart (Hoek and Brown, 1997). It was subsequently modified by Hoek (1998), Hoek et al. (2002), Cai et al. (2004), Marinos et al. (2005) and Cai et al. (2007). It classifies rock masses ranging from unweathered, massive to highly weathered, crushed rock masses. In this study, GSI is

quantified using the method proposed by Cai et al. (2004) and Cai et al. (2007). The modified chart proposed by Cai et al., 2007 is given in Fig.4.2. GSI was measured at the same sampling sites where SHR values were measured.

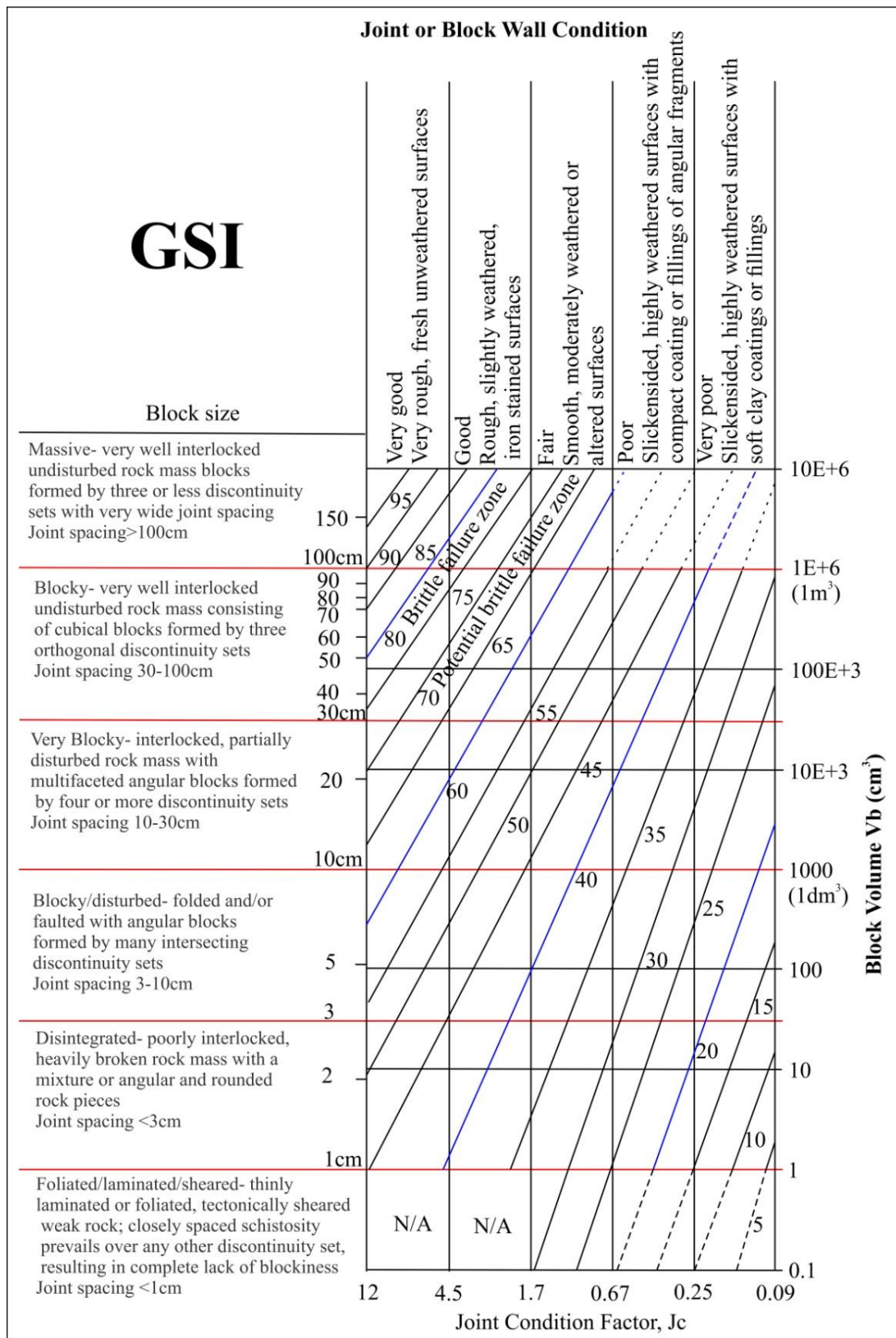


Fig.4.2: Quantification of GSI chart (Cai et al., 2007)

4.3. Results

4.3.1. Landslide inventory

An inventory of 70 landslides was mapped in the study area, occupying a surface area of $\sim 1.5 \times 10^6 \text{ m}^2$ and volume of $4.7 \times 10^6 \text{ m}^3$. Out of the total landslides, 29 are debris slides and 41 are rockfalls. It has been noted that 22 landslides are distributed along a stretch of 16 km in the Higher Himalaya, while 48 landslides are present along a length of 59 km in the Lesser Himalaya. The concentration of landslides in terms of landslide density (L_d) in the Higher Himalaya is 1.3 and that in the Lesser Himalaya is 0.8. Here, the landslide density (L_d) refers to the ratio of the number of landslides in a region to the total extent (length) of the region. Dimensionally, the Higher Himalaya landslides (12 debris slides and 10 rockfalls) contribute $\sim 59\%$ and $\sim 75\%$ to the total area and volume respectively, whereas the Lesser Himalaya (20 debris slides and 28 rockfalls) occupy 41% and 25% of the total area and volume, respectively. APPENDIX 1 gives the details of the landside inventory. A difference of 1.11% was noted between the known distances (from topographic map) and those measured in the GE.

4.3.2. River long profile and topographic swath profile

The L-profile of the Yamuna River in general, shows a typical concave-up profile; with minor convexities in the form of knickpoints (Fig. 4.3). It is observed that the channel gradient in the Higher Himalaya, upstream of Wazri, is comparatively steeper than in the Lesser Himalaya, downstream of Wazri. Further downstream, the river profile is gentler. The channel gradient is high, of the order of 175 m/km between Yamunotri and Janki Chatti, which gradually decreases to 75 m/km between Janki Chatti and Wazri, and 29 m/km between Wazri and Gangani. Further downstream it attains a low gradient value of the order of 5.7 m/km. A total of eight knickpoints (K-1, K-2, K-3, K-4, K-5, K-6, K-7 and K-8) have been observed along the longitudinal river profile. Of these, four knickpoints (K-1, K-2, K-3 and K-4) are located within a stretch of 16 km in the Higher Himalaya, between Yamunotri and Wazri, while the other four (K-5, K-6, K-7 and K-8) lie within a stretch of 59 km in the Lesser Himalaya, between Wazri and Damta.

A pronounced increase (2000-4000 m) in the topography is observed from Wazri upstream in the Higher Himalaya (Fig. 4.3), whereas downstream of Wazri, the area

exhibits moderate relief (2000-1300 m). However, the Naugaon-Damta region in the Lesser Himalaya also shows an abrupt increase in relief (1300-1900 m).

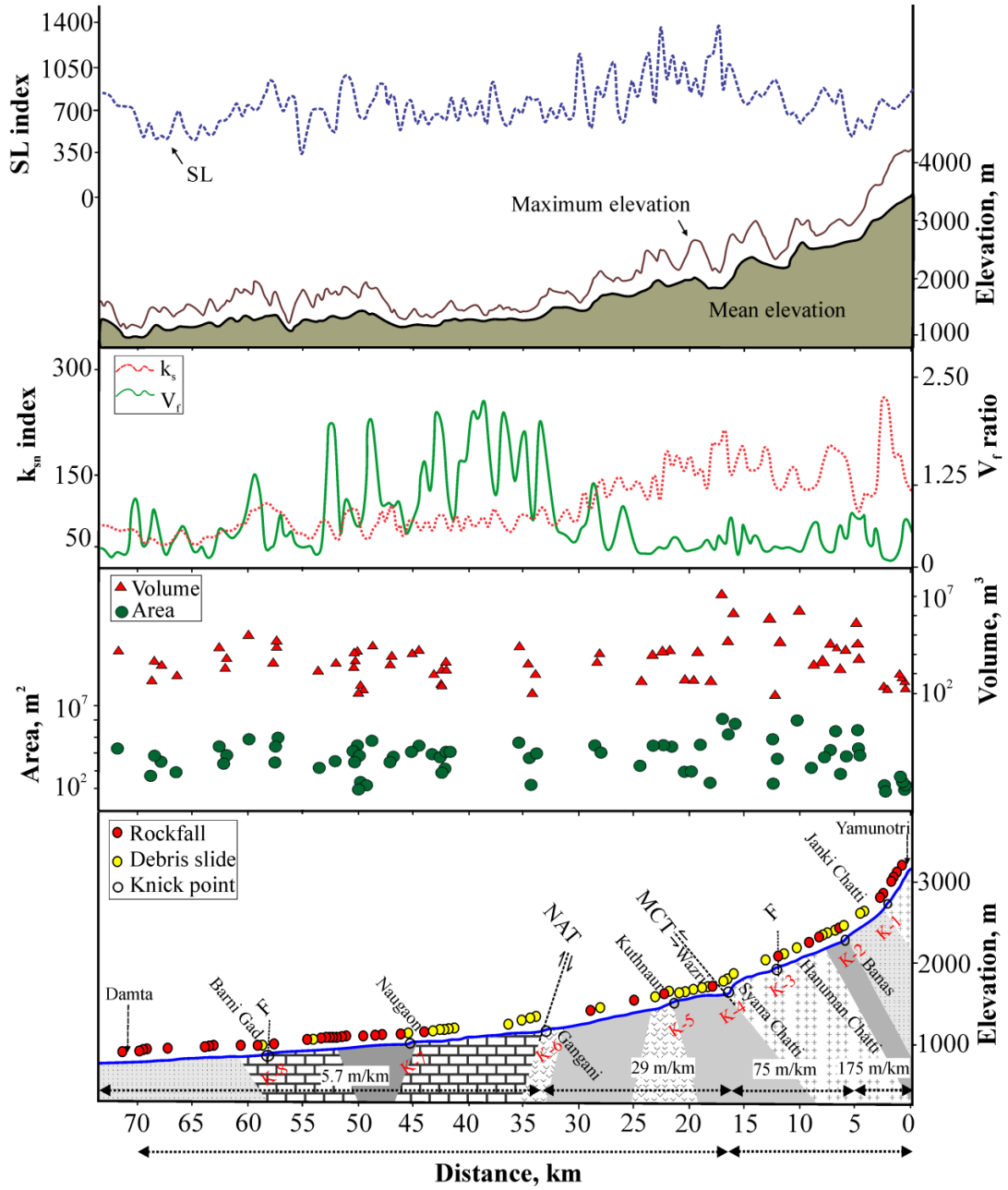


Fig.4.3: Tectonic regime of the Yamuna Valley. Spatial variability of stream length gradient index (SL), topographic swath profile, valley floor width to valley floor height (V_f), steepness index (K_s) and area and volume of individual landslides along the river longitudinal (L) profile. The gradient change along the river profile is measured in m/km. F-F denotes fault, MCT and NAT refer to Main Central Thrust and North Almora Thrust respectively.

4.3.3. Stream Length gradient index

SL values along the valley vary from 9 to 1425 m, with an average of 597 m (Fig. 4.3). The areas around the MCT-NAT exhibit comparatively high SL values (1032,

1425, 1116, 1098, 1407, 1130, 1070, 1037 and 1127 m). The highest SL values of 1425 m are observed near Wazri and 1407 m near Kuthnaur. It is observed that areas with remarkably high SL values lie near the intersections of tributaries and/or lithologic contacts. An SL value as low as 90 m is observed in the Barni Gad region. SL values gradually increase from Damta downstream.

4.3.4. Steepness index

The values of K_s , with an estimated θ of 0.6, range from 230 to 4015 $\text{m}^{1.2}$ (Fig. 4.3). Normalized steepness index was also calculated using reference concavity value θ_{ref} 0.45. Values along the main trunk river range from 24 to 272 $\text{m}^{0.9}$, with an average of 92 $\text{m}^{0.9}$. The patterns of K_{sn} obtained from both the concavity values follow a similar trend (Fig. 4.4); hence, θ_{ref} 0.45 has been used for further analysis. K_{sn} values as high as 272 and 217 are observed around K-1 and K-4 respectively in the Higher Himalaya, which gradually decrease downstream from Wazri to Damta in the Lesser Himalaya. Two distinct regions are observed from the spatial pattern of K_{sn} . A relatively high-peaked zone is observed in the Yamunotri-Wazri of the Higher Himalaya region, with K_{sn} values ranging between 272 and 180 $\text{m}^{0.9}$. Further

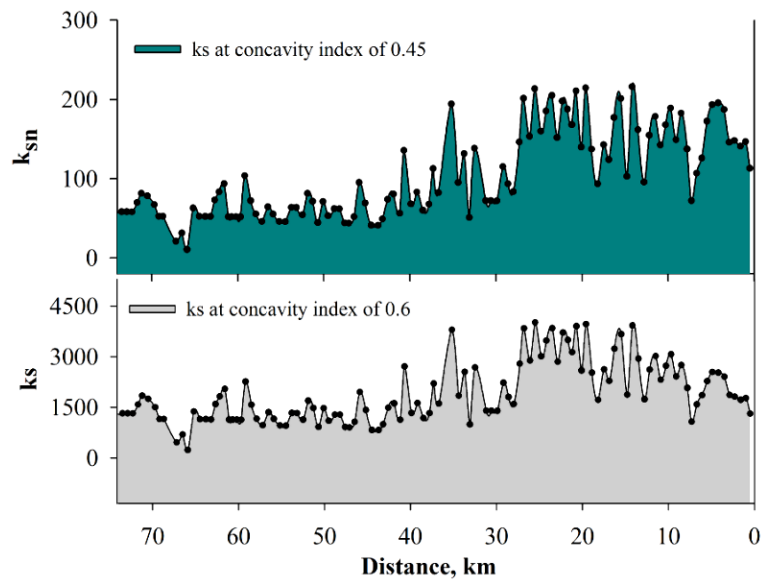


Fig. 4.4: Comparison of steepness index (k_s) at $\theta=0.45$ and $\theta=0.6$. k_{sn} refers to normalized steepness index

4.3.5. Valley floor width to valley height ratio

V_f values between Yamunotri and Wazri in the Higher Himalaya is consistently low ($V_f < 1$), ranging between 0.09 and 0.23 (Fig. 4.3). Further downstream from Wazri in the Lesser Himalaya, V_f values gradually increase from 0.23 to 2.12. V_f values as high as 1.68, 1.72, 1.86, 1.51, 1.80, 1.98, 2.12, 2.01, 1.81, 1.39, 1.33, 1.84, 1.96, 1.88, 1.82

and 1.84 consistently persist for a stretch of about 30 km between Gangani and Naugaon.

4.3.6. Rainfall and Normalized Difference Vegetation Index

The average annual rainfall is highest in the Higher Himalaya with 1798 ± 98 mm and lowest in the orographic front near the NAT (Gangani) with 1477 ± 88 mm (Fig. 4.5). At Damta (Lesser Himalaya), the average annual rainfall again increases to 1516 ± 87 mm. Following a similar pattern, the SW monsoon attains its highest in the Higher Himalaya with 1300 ± 62 mm, lowest near the NAT with 1123 ± 75 mm and moderate at Damta with 1190 ± 80 mm. The NDVI remains more or less same with values ranging between -0.1 to 0.42, implying vegetated hill slopes.

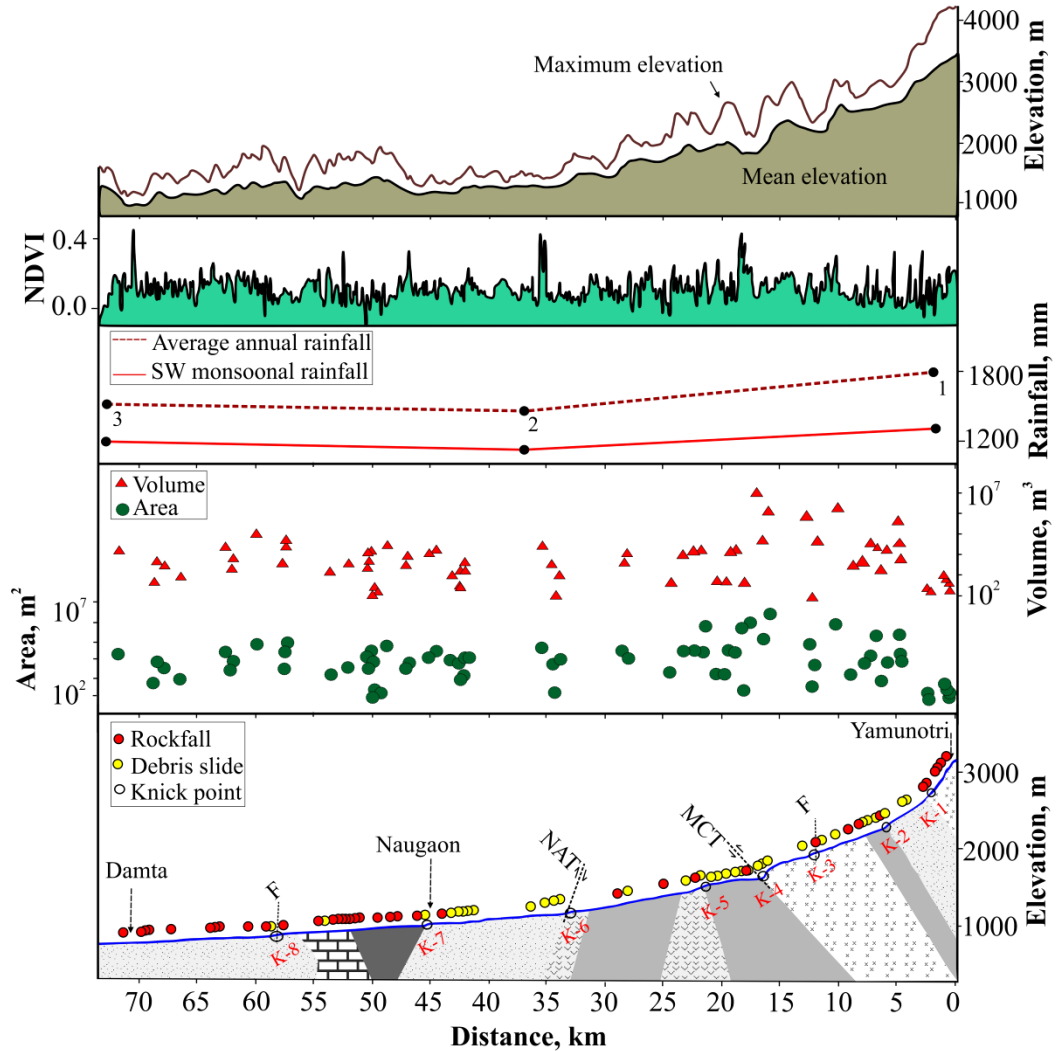


Fig.4.5: Precipitation regime of the Yamuna Valley. Spatial variability of topographic swath profile, normalized difference vegetative index (NDVI), annual rainfall, area and volume of individual landslides along the river longitudinal (L) profile. F-F denotes fault; MCT and NAT refer to the Main Central Thrust and the North Almora Thrust respectively

4.3.7. Rock mass strength

Results of SHR and GSI are presented in Fig. 4.6a. GSI values vary from 30 to 55, with an average of 45 in the Higher Himalaya and 38 in the Lesser Himalaya. The SHR, though not in strong correlation with GSI (Fig. 4.6b), follows a similar trend with values ranging between 14 and 62. An average value of 49 is noted in the Higher Himalaya and 41 in the Lesser Himalaya.

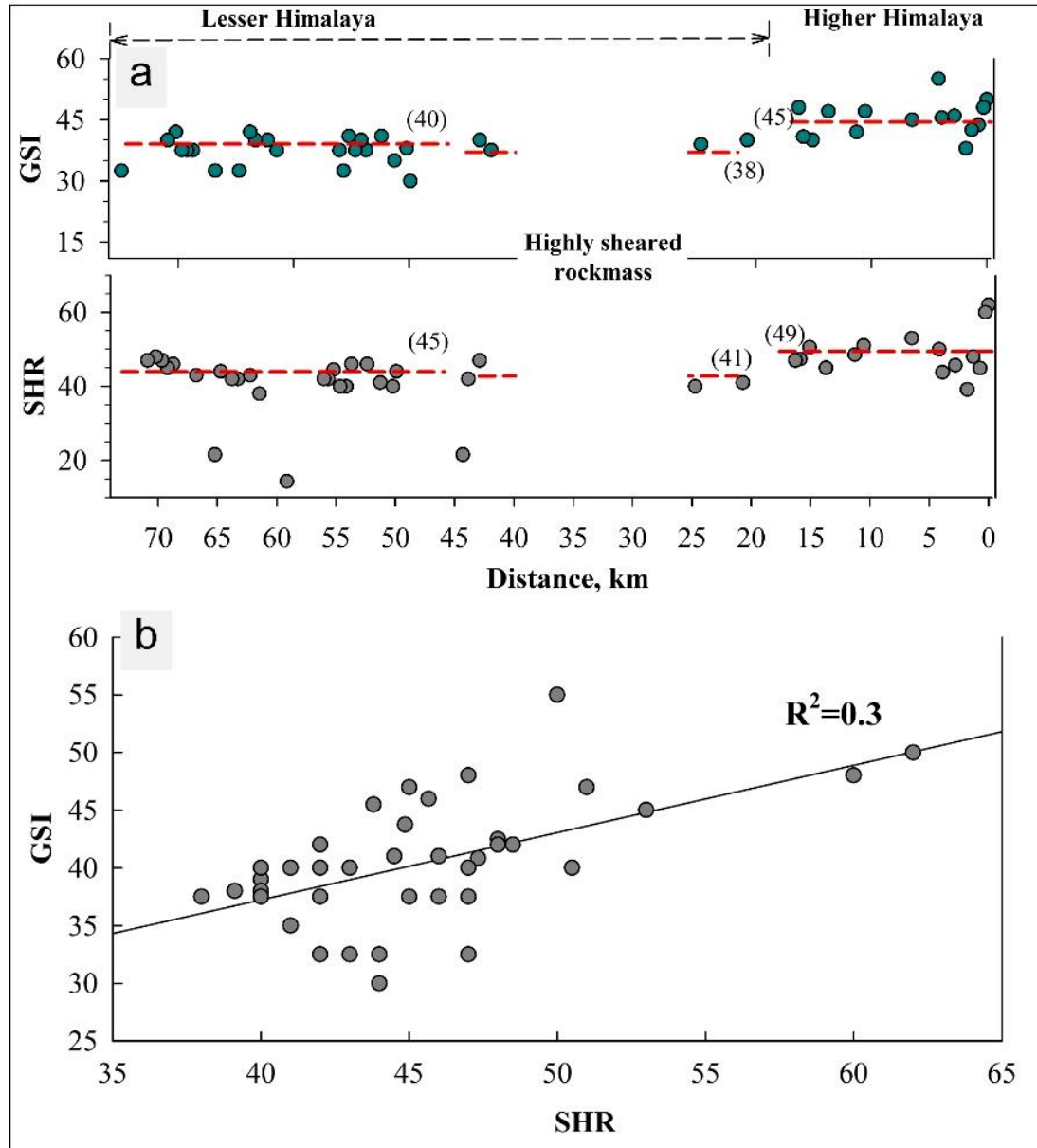


Fig. 4.6: Proxy for rock mass strength. GSI and SHR - Geological strength index and Schmidt hammer rebound. (a) Spatial variability of GSI and SHR. Red dashed line indicates average value; (b) correlation of SHR and GSI

4.4. Discussion

The study area comprises two main litho-tectonic divisions of the Himalaya, the Higher Himalaya and Lesser Himalaya. The interrelationship of landslides and other factors is discussed separately for these divisions.

4.4.1. Higher Himalaya

This region comprises 22 landslides (12 debris slides and 10 rockfalls) that constitute ~59% and ~75% of the total landslide area and volume respectively. With a maximum river channel gradient (~175 m/km), the Higher Himalaya in the study area also accommodates 3 knickpoints (K1, K2 and K3) where K1 and K2 correspond to lithological variation and K3 is due to a local fault (Fig. 4.3). Such high altitudinal changes (channel gradient) are also observed in topography that gains sudden rise in the north of the MCT. These observations indicate the influence of tectonics in this region. This notion of tectonic influence is further supplemented by the higher k_s and lower V_f in the region (Fig. 4.3). The rockfall-prone narrow, deep gorges in this region (Gupta et al., 2017) represent superficial imprints of tectonic uplift. Due to the high topography, which acts as an orographic barrier, the Higher Himalaya receives relatively higher rainfall than the Lesser Himalaya, which is situated to its south (Fig. 4.5). It is observed that k_s and SL are highest and V_f lowest at the MCT, signifying tectonic influence in this area. Despite vegetated hillslopes (NDVI=~0.35, Fig. 4.5) and strong rock mass ($GSI_{avg}=45$ and $SHR_{avg}=49$), large hillslope erosion, as evident from the high landslide volume (Fig. 4.5), further supports tectonic influence on mass wasting. Other studies too have pointed to tectonic implications in the Higher Himalaya (Seeber and Gornitz, 1983; Hodge et al., 2004; Harvey et al., 2015; Kumar et al., 2018a). Thus, based on the above observations it can be reasonably inferred that this tectonically active region is being vigorously uplifted, as a consequence of which landslides are an integral part of the system.

4.4.2. Lesser Himalaya

The Lesser Himalaya in the study area comprises 48 landslides (20 debris slides and 28 rockfalls) that make up 41% and 25% of the total landslide area and volume respectively. Based on distinct topographic variations (Fig. 4.3), this region can be subdivided into three parts, viz., (i) between Wazri and Gangani, (ii) Gangani to Naugaon, and (iii) Naugaon to Damta.

The first region that is in the immediate front of the orographic barrier comprises 12 landslides (8 debris slides and 4 rockfalls). Similar to its Higher Himalaya counterpart, this region also comprises voluminous landslides despite high vegetation (NDVI \approx 0.35, Fig. 4.5) and erosion-resistant rock masses (GSI \approx 40 and SHR \approx 41). The tectonic proxies' k_s , V_f and SL also reflect a similar regime as in the Higher Himalaya, which implies that the region is subject to tectonic influence. However, the region also witnessed relatively higher precipitation than the rest of the Lesser Himalaya (Fig. 4.5). Therefore, a process similar to that in the Higher Himalaya involving high precipitation, high uplift and high erosion (in the form of voluminous landslides) may also exist here. Further downstream, the valley attains a topographic depression between Gangani and Naugaon (Fig. 4.3) that has been described as a synclinal depression (Pachuari, 1972; Valdiya, 1980; Saklani et al., 1991). Lateral erosion prevails in this region as the channel has significantly widened and the majority of the landslides in this part of the region are debris slides. K_s and SL show minimum values while V_f attains a comparatively high value. In such regimes where lateral erosion of river channels is the norm and hillslopes are affected by debris slides, it is inferred that tectonic influence is less (Bull, 2009; Kumar et al., 2018a). Further south, the topography suddenly rises and the valley becomes narrow and deep with rockfalls as the dominant process of hillslope erosion (Fig. 4.3). K_s and SL also reflect higher values in this region. However, precipitation does not seem to play a significant role as NDVI and rainfall remains constant. Rock mass strength increases with relatively higher GSI (\sim 40) and SHR (\sim 45) in comparison to GSI (\sim 35) and SHR (\sim 20-40) of similar lithology between Gangani and Naugaon. Pachuari (1972), Valdiya (1980) and Saklani et al. (1991) have observed the influence of local faults in the sudden rise in the topography in this area.

4.4.3. Limitations

The following limitations are observed in inferring the inter-relationship of landslides; approximation of landslide thickness, temporal distribution of landslides and limited number of landslides. The approximation of landslide thickness is inevitable, considering the steep and inaccessible hillslopes. Moreover, landslide thickness values were used with the inclusion of uncertainty. The temporal distribution of landslides was not included since the present study attempts to explore the spatial

interrelationships only. Since the study was based on spatial interrelationships, only the main trunk and landslides along it were considered.

Chapter-5

SLOPE STABILITY EVALUATION

5.1 Introduction

Slope stability evaluation has been common practice in the Himalaya, Alps, Andes and Rocky mountain chains to understand the response of slope under various circumstances (Kalkani and Piteau, 1976; Eberhardt et al., 2004; Chang et al., 2010; Kanungo et al., 2013; Hetherington, 2014; Gupta et al., 2016a; Jamir et al., 2017). Such studies have been confined mostly to single landslide slopes owing to constraints posed due to lack of vast geotechnical data and time required for these. These limitations restrict regional slope stability evaluation; however if achieved, they can be vital for mitigation of socio-economic losses caused by frequent slope failures. Over the years, several techniques have been developed for assessing slopes. One such technique is the geomechanical characterization of slopes, which mainly incorporates field-based data of discontinuities, giving a precise quantitative idea about the strength of the rock mass and finally the overall credibility of the slope (Bieniawski 1979, 1989; Romana, 1985). Other methods, mostly GIS based, have been adopted to eradicate the problem of vast terrain evaluation, proving to be less time consuming and easily accessible through remotely sensed data (Lee et al., 1999; Baum et al., 2002; Miliareisis et al., 2005; Li et al., 2008; Carlton et al., 2017). Such methods however, are not effective in involving material inhomogeneity, spatial variation in rock mass condition and field stress conditions. Owing to this limitation, numerical modeling of individual landslide slopes proves to be more effective as it includes the above conditions (Griffiths and Lane, 1999; Zheng et al., 2005).

In this study, geomechanical characterisation of the slopes for assessment of rockfall hazards through various rock mass classifications, i.e., Rock Mass Rating (RMR), Slope Mass Rating (SMR), Geological Strength Index (GSI) and correlation among different classifications have been carried out to evaluate 92 rock mass exposures. The Finite Element Method (FEM), a numerical modeling technique, was used to evaluate 29 active debris slides in the study.

5.2 Methodology

5.2.1. Kinematic analyses of discontinuities

As the preliminary step to any rock slope assessment, kinematic analysis, which is purely geometric, helps to investigate the possible failure modes based on angular relationship of rock mass discontinuities and slope face failure (Markland, 1972; Goodman and Bray, 1976; Hocking, 1976; Cruden, 1978; Lucas, 1980; Hoek and Bray, 1981; Matheson, 1989; Kliche, 1999). The angular relationship between discontinuities and slope surfaces is used to determine the potential and likely modes of failure. Basically, it is concerned with the direction of the movement, and indicates which movement is allowable and which is constrained.

Kinematic slope stability analyses are traditionally carried out on stereonet, which is a convenient means of representing geological data. For the analyses, the lower hemisphere stereographical projection (equal angle) method described by Hoek and Bray (1981) and Goodman (1989) was used. This gives an overall general idea about the critical discontinuities that are responsible for the initiation of mass movements. Gupta and Tandon (2015) and Gupta et al. (2017) applied this analysis in the Higher Himalayan terrain to classify various rock exposures into different stability classes. This analysis is commonly used to evaluate the principle modes of failure like planar, wedge and toppling.

Planar failure occurs when the geological discontinuities strikes parallel to the slope face and dips downward at an inclination gentler than the overlying slope face (Hoek and Bray, 1981). For planar failure, the following geometrical conditions must be satisfied (Fig.5.1a):

1. The plane on which sliding occurs must strike parallel or nearly parallel (within $\pm 20^\circ$) to the slope face.
2. The failure plane must 'daylight' in the slope face. This means that its dip (β_j) must be smaller than the dip of the slope face (β_s).
3. The dip of the failure plane must be greater than the friction angle (ϕ) of the discontinuity plane.

Wedge failure is the sliding along a line of intersection of geological discontinuities, where the line of intersection plunges downwards at an inclination flatter than that of

the overlying slope face (Hoek and Bray, 1981); thus, the following geometrical conditions must be satisfied (Fig.5.1b):

1. The trend of the line of intersection (α_i) must be oriented within 90° of the dip direction of the slope face.
2. The plunge of the line of intersection (β_i) must be smaller than the dip of the slope face (β_s).
3. The plunge of the line of intersection must be greater than the friction angle (ϕ) of the discontinuity plane.

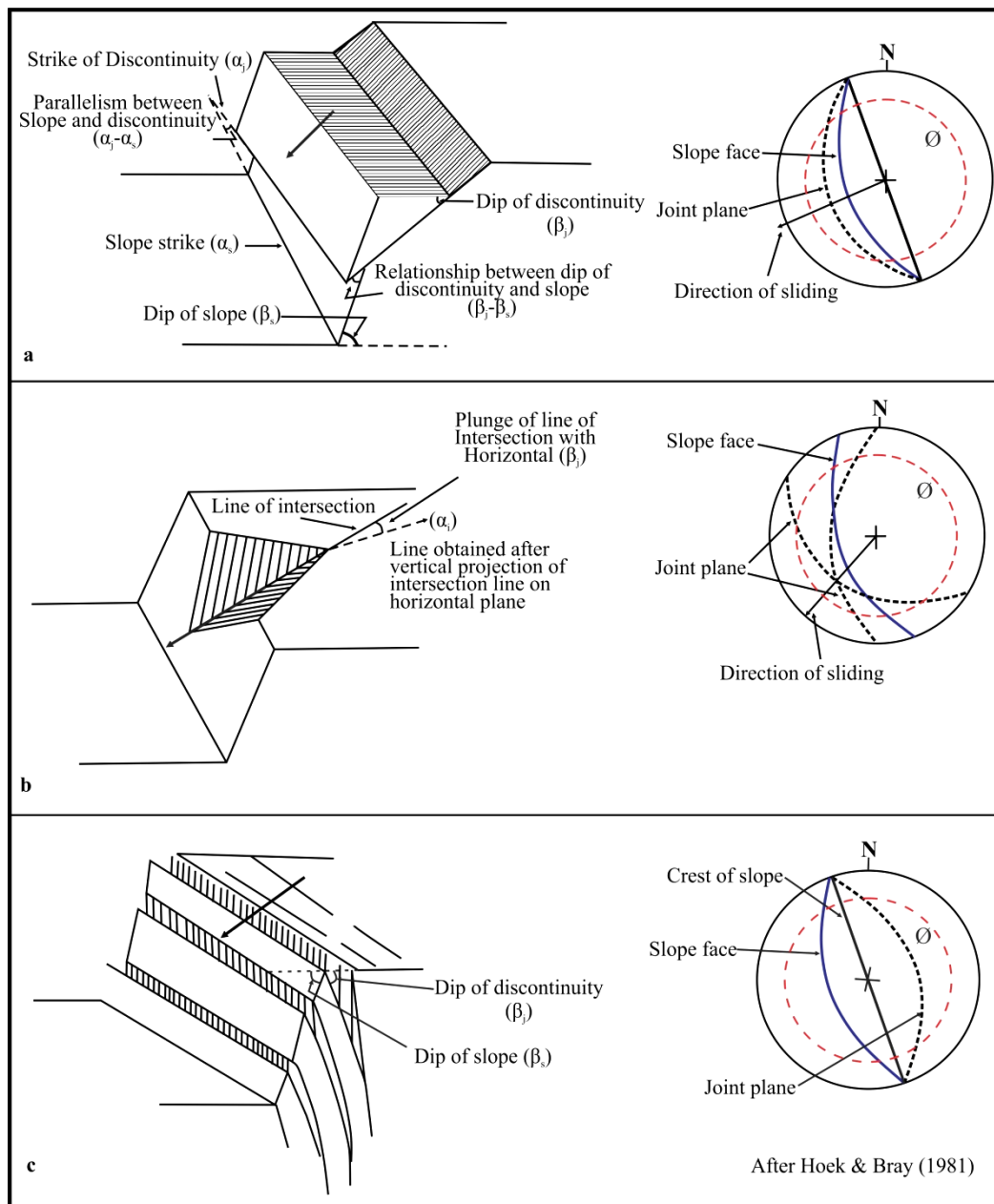


Fig. 5.1: Geometric representation and stereo-plots of structural discontinuities for (a) planar failure (b) wedge failure and (c) toppling failure. ϕ is the angle of internal friction

Toppling failure occurs when the centre of a block lies outside the outline of the base of the block, resulting in the development of overturning moments (Hoek and Bray, 1981). Figure 5.1c illustrates the geometry and stereographic representation of toppling failure. The geometric conditions similar to planar failure must be satisfied along with which, the discontinuities must satisfy the following equation:

$$90^\circ - \phi_p (\text{dip of plane}) \leq \phi_f (\text{dip of slope face}) - \phi_p (\text{friction angle along plane}) \quad (5.1)$$

The relative position of the planes representing joint sets, foliation planes, slope faces and possible wedge intersections were computed for each location to identify slopes prone to planar, wedge or toppling failure conditions. Slopes with three or more planes satisfying conditions for either planar or wedge failure, have been classified as “high hazard”, those with at least two planes satisfying conditions for failure, as “moderate hazard” and those with at least one plane satisfying conditions for failure, as “low hazard” and those with no plane for failure as “no hazard”.

However, kinematic analysis alone cannot be taken into consideration to understand possible rock failure. This limitation arises from the fact that kinematic analysis does not consider forces acting on slope-forming material. Therefore, the stability of slopes in engineering practice is usually analyzed by conventional methods (limit equilibrium analysis) and numerical modeling techniques, which provides a direct measure of stability in terms of the factor of safety (Kentli and Topal, 2004).

5.2.2. *Rock Mass Rating classification*

The RMR system classifies discontinuous rock masses using six parameters-(i) uniaxial compressive strength (UCS), (ii) rock quality designation (RQD), (iii) spacing of discontinuities (S_d), (iv) condition of discontinuities (C_d) (v) groundwater condition and (vi) orientation of discontinuities (Bieniawski, 1976). Since the sixth parameter related to orientation of the discontinuities involved a number of conditions, the RMR system was further modified by Romana (1985), which particularly considered the orientation of joints. Hence, only five parameters are calculated for the RMR system. These parameters are easily obtained from either borehole data or surface mapping. Table 5.1 lists the discontinuity conditions and their relative ratings that are used to determine the RMR value of the rock mass in the study area. Rating numbers are applied to each parameter from the published chart of Bieniawski (1979). Ratings are added to obtain a total of RMR value, the maximum

being 100. The final RMR value is classified into five rock-mass classes (Table 5.1). Higher rock mass rating indicates better rock-mass condition.

All the parameters are reasonably estimated with acceptable accuracy from a careful description of joints such as roughness, persistence, degree of weathering, type of infilling materials and signs of water seepages. Scanline surveys were conducted for generation of discontinuity data for the determination of RMR values. This involves stretching a measuring tape across the outcrop, then at the points where the tape intersects a discontinuity; the distance along the tape is recorded, as well as the conditions of the traversed discontinuities. The value of RQD is estimated from the number of discontinuities per unit volume (J_v). Palmstrom (1982) proposed the following equation to calculate RQD, using joint volume:

$$RQD = 115 - 3.3J_v \quad (5.2)$$

where J_v represents the total number of joints per cubic meter or volumetric joint count. The volumetric joint count is a measure of the number of joints within a unit volume of rock mass (Palmstrom, 1982; Sen and Eissa, 1992). It is defined as:

$$J_v = \sum_{i=1}^J \left(\frac{1}{S_i} \right) \quad (5.3)$$

where S_i is the average joint spacing in meters for the i^{th} joint set and J is the total number of joint sets.

The RMR for the rocks exposed is calculated using the following formula:

$$RMR = \sum RQD + UCS + S_d + C_d + \text{Water condition} + \text{Joint orientation} \quad (5.4)$$

5.2.3. Slope Mass Rating classification

The SMR system used to evaluate the stability of rock slopes (Romana, 1985) is a modification of the RMR and is obtained by adding the adjustment factors for the joints/slope relationship and adding a factor related to the method of excavation using the following equation:

$$SMR = RMR_{\text{basic}} - (F1 + F2 + F3 + F4) \quad (5.5)$$

where RMR_{basic} is rock mass rating according to Bienawski (1979, 1989). Table 5.1. lists the relative rating of the six parameters used to calculate the RMR.

$F1$, $F2$ and $F3$ are the adjustment factors related to joint orientation with respect to the slope. $F1$ indicates the degree of parallelism between the strike of the joint (α_j) and

the strike of the slope face (α_s). It ranges from 0.15 (when the angle between the two is $>30^\circ$ and the failure probability is very low) to 1.0 (when both are almost parallel and the failure probability is very high) (Romana 1985). Empirically, it was established that $F1 = (1 - \sin A)^2$, where A denotes the angle between the slope face and the strike of the joints.

F2 refers to the joint dip angle (β_j) in the planar failure mode and the plunge of the line of intersection of two joints (β_i) in the wedge failure mode. Its value also varies from 0.15 (when the dip of the critical joint or the plunge of the line of intersection of two joints is $<20^\circ$) to 1.0 (when the plunge is $>45^\circ$). For the toppling mode of failure, F2 remains equal to 1.0. Empirically, F2 is equal to $\tan \beta_j$ for planar failure and $\tan \beta_i$ for wedge failure.

F3 refers to the relationship between the declination of the slope face (β_s) and the joint (β_j). In planar failure, it is the probability of joints “day lighting” in the slope face. Its value varies from 0 to -60. It is zero (failure probability very low) when the dip of the joint (β_j) or the plunge of the line of intersection of two or more joints (β_i) is $>10^\circ$ lower than the dip of the slope (β_s) and is -60 (failure probability very high) when the dip of the slope (β_s) is $>10^\circ$ greater than the dip of the joint (β_j) or the plunge of the line of intersection of two or more joints (β_i). For the toppling failure, unfavorable conditions depend upon the sum of the dip of the joints and the slope ($\beta_j + \beta_s$) (Romana 1985). F4 is related to the method of excavation (Romana 1985).

The values of adjustment factors F1, F2, F3 and F4 for the different joint orientations are given in Table 5.2. The SMR classes are finally obtained by using the values of RMR_{basic} and adjustment factors in equation 5.5. SMR values ranges from 0-100; stability classes are assigned accordingly (Table 5.3).

5.2.4. Geological Strength Index classification

A detailed account of the GSI classification has been discussed in *Section 4.2.7.2* of Chapter 4.

Table 5.1: The relative weight of observational and laboratory-determined parameters used to calculate RMR_{basic} (Bieniawski, 1979)

1	Strength of Intact rock	Point load strength (MPa)	>10	10-4	4-2	2-1		
		Uniaxial compressive strength	>250	250-100	100-50	50-25	25-5	5-1 <1
	Rating		15	12	7	4	2	1 0
2	RQD (%)		100-90	90-75	75-50	50-25	<25	
	Rating		20	17	13	8	3	
3	Average spacing of discontinuity (m)		>2	2-0.6	0.6-0.2	0.2-0.06	<0.06	
	Rating		20	15	10	8	5	
4	Condition of discontinuity		Very rough, discontinuous, no separation, unweathered	Rough walls, separation <0.1 mm, slightly weathered	Slightly rough, separation <1 mm, highly weathered	Slickensides or gouge, <5 mm thick or separation 1-5 mm, continuous	Soft gouge, >5 mm thick or separation >5 mm continuous decomposed rock wall	
	Rating		30	25	20	10	0	
5	Groundwater condition		Completely dry	Damp	Wet	Dripping	Flowing	
	Rating		15	10	7	4	0	
Classification of rock mass			Very Good	Good	Fair	Poor	Very Poor	
RMR value			>80	61-80	41-60	21-40	<20	

Table 5.2: Values of adjustment factors for F1, F2, F3 and F4 (Romana, 1985)

Adjustment factors	Case of slope failure		Very favorable	Favorable	Fair	Unfavorable	Very unfavorable
F ₁	Planar (P) Toppling (T) Wedge (W)	$ \alpha_j - \alpha_s $ $ \alpha_j - \alpha_s - 180 $ $ \alpha_j - \alpha_s $	$>30^\circ$	30-20°	20-10°	10-5°	$<5^\circ$
	P/W/T	F ₁ rating	0.15	0.40	0.70	0.85	1.00
F ₂	Planar (P) Wedge (W)	$ \beta_j $ $ \beta_i $	$<20^\circ$	20-30°	30-35°	35-45°	$>45^\circ$
	P/W	F ₂ rating	0.15	0.40	0.70	0.85	1.00
	T	F ₂ rating	1.00	1.00	1.00	1.00	1.00
F ₃	Planar (P) Wedge (W)	$ \beta_j - \beta_s $ $ \beta_j - \beta_s $	$>10^\circ$	10-0°	0°	0-(-10°)	$<-10^\circ$
	T	$ \beta_j + \beta_s $	$<110^\circ$	110-120°	$>120^\circ$	---	---
	P/W/T	F ₃ rating	0	-6	-25	-50	-60
F ₄	Natural slope	Pre-splitting	Smooth blasting		Normal blasting		Poor blasting
	15	10	8		0		-8

Table 5.3: Values of stability classes as per SMR values (Romana, 1985)

Class No	V	IV	III	II	I
SMR value	0-20	21-40	41-60	61-80	81-100
Rock mass description	Very bad	Bad	Normal	Good	Very good
Stability	Completely unstable	Unstable	Partially stable	Stable	Completely stable
Failure	Big planar, soil like or circular	Planar or big wedges	Planar along some joints many wedges	Some block failure	No failure
Probability of failure	0.9	0.6	0.4	0.2	0

5.2.5. Finite Element Method

The FEM is a numerical technique to determine the field variance. It was initially developed for plane stress analysis in structural engineering to determine the approximate stress/strain/displacement on an object in response to applied force (Courant, 1943; Prager and Synge, 1947; Turner, 1956; Clough, 1980; Zienkiewicz et

al., 1977). It was later used for a wide range of applications including rock mechanics/slope stability problems (Owen and Hinton, 1980; Pande et al., 1990; Griffith and Lane, 1999; Griffiths and Marquez, 2007). FEM offers capability to not only design complex geometry but also to present distribution of stress and displacement pattern in the slope. In this technique, a complex region is divided into a finite number of internally contiguous elements of regular shape, which are defined by a fixed number of nodes (Fig. 5.2).

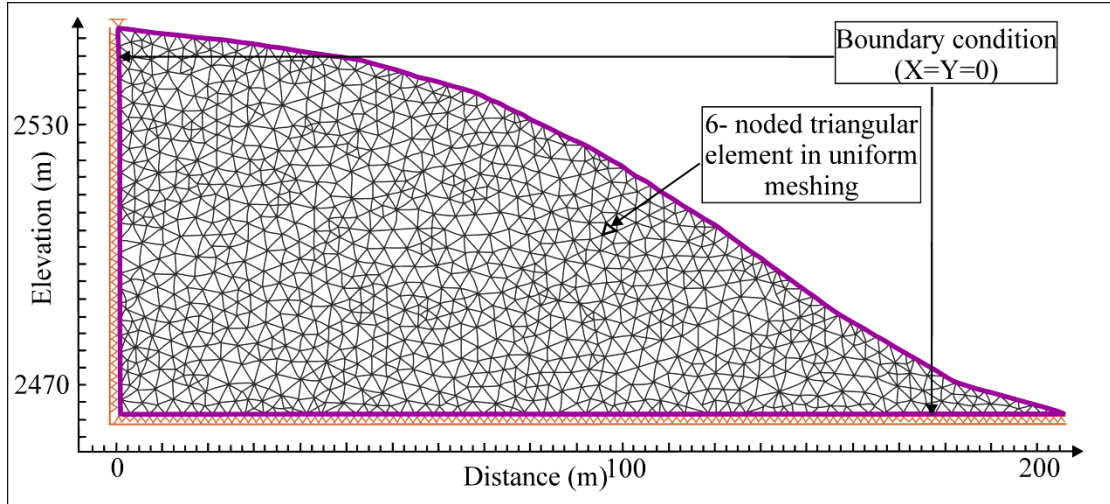


Fig 5.2: General finite element model configuration of slope using 6-noded triangular elements in uniform meshing

It is discretized into simple geometric shapes called finite elements. The various loads acting on the element along with constraints result in a set of equations. For static FEM analysis, the following equation is generally used:

$$K\Delta U = P - F \quad (5.6)$$

Where K is the stiffness (material property), ΔU is nodal displacement, P is applied load and F is the internal forces. In this study, analysis was performed using RS2 Phase2 (version 9.0) software. FEM was used along with the Shear Strength Reduction (SSR) technique to determine the Strength Reduction Factor (SRF).

The SRF represents the Factor of Safety (FoS) of the slope (Griffiths and Lane, 1999). The aim of the SSR approach is to determine reduced shear strength parameters notably C_r and ϕ_r that define critical state of the slope, beyond which (further decrease in C and ϕ) a slope fails. The approach is presented in the following equation:

$$C_r = C / \text{SRF}, \quad \tan \phi_r = \tan \phi / \text{SRF} \quad (5.7)$$

Here, C is cohesion and ϕ is angle of friction. In this process, SRF is increased and

decreased in an iterative manner until the slope fails (numerical non-convergence). The non-convergence criteria relating the slope failure was used to determine the critical SRF (Nian et al., 2012). The boundary condition with restraining movement was applied to the base and back of the slope sections, whereas the front face of the models was kept free for the movement (Fig. 5.2).

In order to quantify the deformation in the form of shear strain, total displacement and critical SRF, slope stability analyses were performed by plane strain (i.e., strain along Z direction=0) and FEM-SSR techniques. The SSR technique (Zienkiewicz et al., 1977; Matsui and San, 1992) was used to determine the FoS of the slope. The following flowchart (Fig. 5.3) shows the steps to a FEM analysis.

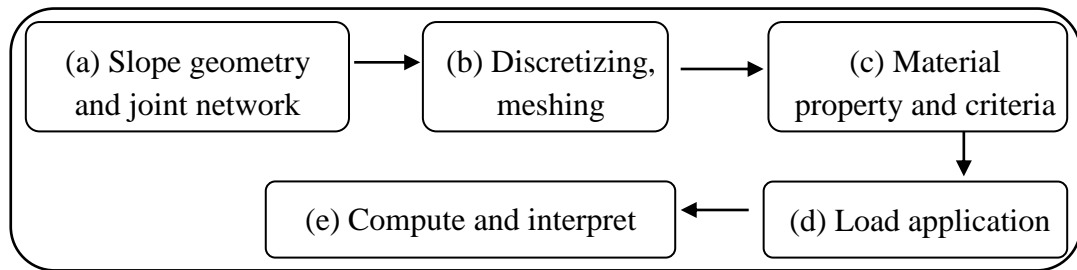


Fig 5.3: Flowchart in FEM used in the present study

(a) Slope geometry and joint network

LISS-IV and Cartosat DEM were used to extract slope geometry of the landslide. Joints mapped in the field were incorporated in the slope model for slope stability analysis. The joint properties were used in the Barton-Bandis (1990) criteria. The peak and residual GSI values were determined using the method proposed by Cai et al. (2007). The Joint Roughness Coefficient (JRC) values were determined using the chart proposed by Barton and Choubey (1977). The Joint Compressive Strength (JCS) value was determined using the empirical formula of Deere and Miller (1966) and Gupta and Tandon (2015) from the SHR values of the rock mass. Considering the influence of scale on JRC and JCS, scale-corrected JRC_n and JCS_n were calculated using the criteria of Barton and Bandis (1982). Joint stiffness (k_n and k_s) was determined using the stiffness criteria of Barton (1973) and rock mass modulus concept of Hoek et al. (2002). Details of the parameters used are presented in Table 5.4. Joints are considered as the interface in this continuum FEM modeling technique that has been used widely in rock slope stability studies (Pain et al., 2014; Xu et al., 2015).

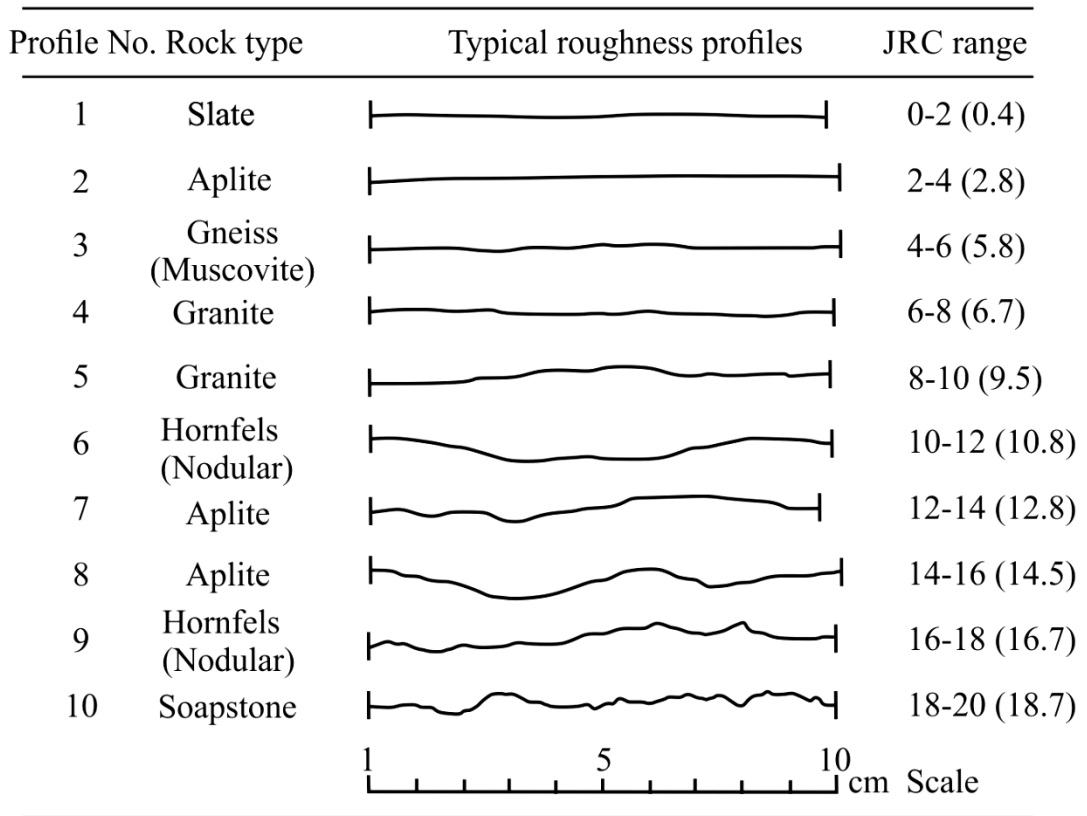


Fig.5.4: Standard roughness profile (after Jang et al., 2014)

(b) Mesh and boundary condition

Since FEM works on the principle of discretization of fixed number of elements, plane strain triangular elements with 6 nodes were used through graded mesh. The contiguity of mesh was checked to ensure that the mesh consists of a single continuous region. After several trials and errors, the quality of the elements was defined through the following conditions:

- (1) (Maximum side length)/(Minimum side length)>10.00
- (2) Minimum interior angle<20°
- (3) Maximum interior angle>120°

The boundary condition with restraining movement ($X=Y=0$) was applied to the base and back of the model, whereas the front face of the model was kept free for movement.

(c) *Material property and criteria*

For the soil samples, grain size analysis was carried out using the standard dry sieving method (Indian Standards [IS]: 2720, Part 4-1985). The grain size data was further analysed using GRADISTAT (v.8) software and the soil type classified as per Indian Standards (IS: 1498-1970). Cohesion (c) and angle of internal friction (ϕ) of the soils were determined by the direct shear test (IS: 2720-Part 13- 1986). The shear strengths were determined from the undrained direct shear test with water content close to the optimum limit as well as relative field conditions (IS: 2720, Part 13- 1986). The samples were sheared under constant normal stress of 50, 100 and 150 kN/m². The Young's modulus of soil was determined directly by Uniaxial Compressive Strength (UCS) tests, i.e., tests with constant (or zero) stress on the vertical surfaces. Three different rates of movements, i.e., 1.25 mm/min, 1.50 mm/min and 2.5 mm/min were used to determine the displacement (IS: 2720, Part 10-1991). The Unit Weight was determined subsequently with the UCS test by measuring the weight and volume of the moulded soil sample in the laboratory. Poisson's ratio for the different soil types was considered from the standard described by Bowles (1996). The soil properties thus obtained were used as input parameters in the stability analysis of each slope section. For rock samples, seismic velocities (P- and S-waves) were measured using CATS Ultrasonic (1.95) of Geotechnical Consulting & Testing Systems (GCTS) to determine the density, Young's modulus, and Poisson's ratio of rock sample. UCS of rock samples were determined as per IS: 9143-1979.

The properties of the soil and rock mass were used as input parameters in the modelling. Mohr-Coulomb (M-C) failure criterion (Coulomb, 1776; Mohr, 1914) and Generalized Hoek-Brown (GHB) criterion (Hoek et al., 1995) were used as the failure criteria for soil and rock respectively. The joints in the rock mass were applied using Barton-Bandis (B-B) slip criterion (Barton and Choubey, 1977; Barton and Bandis, 1990). The criteria are as follows:

$$\text{M-C criterion} \quad \tau = c + \sigma \tan \phi \quad (5.8)$$

Here, τ is shear stress along the shear plane at failure, C is the cohesion, σ is the normal stress on the shear plane and ϕ is the angle of friction. The M-C failure criteria can also be written as

$$\sigma_1 = \sigma_{ci} + (k) \sigma_3 \quad (5.9)$$

Here, σ_1 and σ_3 are the major and minor effective principal stresses at failure; σ_{ci} is compressive strength of material and k is the slope of the line relating σ_1 and σ_3 .

$$\text{GHB criterion} \quad \sigma_1 = \sigma_3 + \sigma_{ci} [m_b (\sigma_3 / \sigma_1) + s]^a \quad (5.10)$$

Here, σ_1 and σ_3 are the major and minor effective principal stresses at failure, σ_{ci} is the compressive strength of intact rock and m_b , s and a are material constants.

$$\text{B-B criterion} \quad \tau = \sigma_n \tan [\phi_r + \text{JRC} \log_{10} (\text{JCS} / \sigma_n)] \quad (5.11)$$

Here, τ is joint shear strength, σ_n is the normal stress across joints, ϕ_r is the reduced friction angle, JRC is the joint roughness coefficient and JCS is the joint compressive strength.

Both soil and rock mass were used as plastic type to account for plastic deformation. Soil was considered as elastic-perfect plastic material (Griffiths and Lane, 1999). Details of the criteria and related parameters used in the study are given in Table 5.4.

Table 5.4: Details of parameters used in FEM

Material Criteria		Parameters	Source
Rock mass	Generalized Hoek & Brown (GHB) Criteria (Hoek et al., 1995) $\sigma_1 = \sigma_3 + \sigma_{ci} [m_b (\sigma_3 / \sigma_{ci}) + s]^a$ $m_b = m_i e^{[(GSI-100)/(28-14D)]}$ $s = e^{[(GSI-100)/(9-3D)]}$ $a = \frac{1}{2} + \frac{1}{6} \left[e^{[-\frac{GSI}{15}]} - e^{[-\frac{20}{3}]} \right]$ Here, D is a factor which depends upon the degree of disturbance to which the rock mass has been subjected by blast damage and stress relaxation (Hoek et al., 2002). GSI (Geological Strength Index) is a rock mass characterization parameter (Hoek, 1994).	Unit Weight (MN/m ³)	Laboratory analysis (UCS) (IS: 9143-1979)
		Young's Modulus, E_i (MPa)	Laboratory analysis (Ultrasonic velocity test)
		Poisson's Ratio	Laboratory analysis (Ultrasonic velocity test)
		Uniaxial Compressive Strength, σ_{ci} (MPa)	Laboratory analysis (UCS) (IS: 9143-1979)
		Geological Strength Index	Field observation and empirical formulas from Cai et al. 2004; Cai et al. 2007
		Material Constant (m_i)	Standard values
		m_b	GSI was field dependent, m_i as per (Hoek and Brown, 1997) and D is used between 0-1 w.r.t. rock mass exposure and blasting
		s	
		a	
		D	

Joint	Barton-Bandis Criteria (Barton and Choubey, 1977; Barton and Bandis, 1990) $\tau = \sigma_n \tan [\phi_r + JRC \log_{10} (JCS/\sigma_n)]$ Here, τ is joint shear strength; σ_n is normal stress across joint; ϕ_r is reduced friction angle; JRC is joint roughness coefficient; JCS is joint compressive strength. The JRC and JCS were used as JRC_n and JCS_n following the scale corrections observed by Pratt (1974); Barton and Choubey, (1977) and proposed by Barton and Bandis, (1982).	Normal Stiffness, k_n (MPa/m)	E_i is lab dependent. L and GSI were field dependent. D is used between 0-1 in view of rock mass exposure and blasting
	Joint stiffness criteria (Goodman et al. 1968; Barton, 1972) $k_n = (E_i * E_m) / L * (E_i - E_m)$ Here, k_n is Normal stiffness; E_i is Intact rock modulus, E_m is Rock mass modulus; L is Mean joint spacing. $E_m = (E_i) * [0.02 + \{1 - D/2\} / \{1 + e^{(60 + 15 * D - GSI) / 11}\}]$ Here, E_m is based on Deere, (1968); Palmstrom and Singh, (2001); Hoek and Diederichs, (2006).	Shear Stiffness, k_s (MPa/m)	It is assumed as $k_n/10$. However, effect of denominator is also obtained from parametric studies
		Reduced friction angle, ϕ_r	Standard values from Barton, 1973; Barton and Choubey, 1977 and Jang et al., 2014
		Joint roughness coefficient, JRC	Field based data from profilometer and standard values
		Joint compressive strength, JCS (MPa)	Empirical equation of Deere and Miller (1966) relating Schmidt hammer rebound (SHR) values, σ_{ci} and unit weight of rock. SHR was field dependent.
		Scale corrected, JRC_n	Empirical equation of Barton and Bandis (1982)
		Scale corrected, JCS_n (MPa)	
	Material Criteria		Parameters
Soil	Mohr-Coulomb Criteria (Coulomb, 1776; Mohr, 1914) $\tau = C + \sigma_n \tan \phi$ Here, τ is Shear stress at failure; C is Cohesion; σ_n is normal strength; ϕ is angle of friction.	Unit Weight (MN/m ³)	Laboratory analysis (UCS) (IS: 2720-Part 10-1991)
		Young's Modulus, E_i (MPa)	Laboratory analysis (UCS); IS: 2720-Part 10-1991, Standard values from Kezdi, (1974); Obrzud and Truty, (2012)
		Poisson's Ratio	Standard values from Ohsaki and Iwasaki, (1973); Bowles, (1996); Das, (2002)
		Cohesion, C (MPa)	Laboratory analysis (Direct shear) (IS: 2720-Part 13- 1986)
		Friction angle, ϕ	

(d) Load

Field stress (load) was adjusted in view of the dominant forces, i.e., extensional or compressional (Eberhardt et al., 2004). The $k = \sigma_h / \sigma_v = 0.5$ was used in extensional regime, whereas $k = \sigma_h / \sigma_v = 1.5$ was used in compressional regime.

(e) *Compute and interpret*

The models were computed using RS2 software and later interpretations based on the total displacement and FoS determined.

5.3 Results

Stability analysis of any slope requires a comprehensive knowledge about the nature and geometry of the slope. In the present study the aim was to geomechanically characterize the rock slopes and numerically model the debris slopes.

Kinematic analysis relative to the orientation of the slope and discontinuities was carried out in order to determine the potential modes of failure. Table 5.5 gives the details of the type of failure at each of the 92 locations and the hazard class thereof. Based on the number of planes of failure, it has been observed that the Higher Himalaya region comprises mostly low hazard class (13 locations), eight locations of moderate hazard, eight locations of stable conditions and three sites of high hazard. In the Lesser Himalaya, twenty-four locations lie in the low hazard class, fourteen locations each in moderate and no hazard class and eight locations in the high hazard class.

Table 5.5: Details of rock mass exposures in the study area and results of kinematic analysis

Sl No	Location	Slope (dip amount/dip direction (°))	Joints (dip amount/dip direction (°))	Spacing of discontinuity (m)	Type of failure	Hazard class	Rock type	Litho-stratigraphic unit
1	30°59'59.2"N 78°27'46.9"E Elv. 3238±15m	~90/310 N	(J1)~88/295 N	0.3-0.4	PF/WF	Moderate Hazard	Quartzite	
			(J2) ~85/275 N	0.5-1				
			(J3) ~55/225 N	0.2-0.3				
			(J4) ~50/200 N	0.6-0.1				
			(F) 40/30 N	0.1-0.16				
2	30°59'56.9"N 78°27'45"E Elv. 3243±7m	~88/130 N	(J1) 72/60 N	0.5-1	PF	Low Hazard	Gneiss	
			(J2) 50/245 N	0.3-0.4				
			(F) 54/15 N	0.1-0.2				
3	30°59'55.7"N 78°27'43.3"E Elv. 3233±6m	~88/110 N	(J1) ~90/280 N	0.1-2	PF/WF	Moderate Hazard	Gneiss	
			(J2) ~28/5 N	0.5-1				
			(J3) ~38/190 N	0.5-1				
			(F) 50/200 N	0.1-0.2				
4	30°59'511.7"N 78°27'43.0"E Elv. 3226±6m	~88/75N	(J1) ~36/330 N	0.5-1	PF/WF	Low Hazard	Gneiss	
			(J2) ~45/150 N	0.5-1				
			(J3) ~85/60 N	0.5-1				

			(F) 36/330 N	0.05-0.1				H I G H E R H I M A L A Y A
5	30°59'50.7"N 78°27'43.3"E Elv. 3208±6m	~90/90N	(J1) ~55/190 N	0.5-1	PF	Low Hazard	Slate	
			(F) 40/170 N	0.1-0.2				
6	30°59'49.2"N 78°27'43.2"E Elv. 109±10m	>90/110 N	(J1) ~88/110 N	0.5-1	PF/WF	Low Hazard	Mica schist	
			(F) 54/0 N	0.1-0.2				
7	30°59'49.3"N 78°27'44.4"E Elv. 3119±2m	~90/70 N	(J1) ~82/105 N	0.3-0.4	PF/WF	Moderate Hazard	Mica schist	
			(J2) ~55/145 N	0.1-0.2				
			(J3) ~20/130 N	0.5-1				
			(F) 82/105 N	0.1-0.2				
8	30°59'49.6"N 78°27'74"E Elv. 3063±6m	~90/175 N	(J1) 67/65 N	0.1-0.15	TF	Low Hazard	Gneiss	
			(J2)30/160 N	0.1-0.2				
			(F) 30/160 N	0.05-0.1				
			(R)75/300 N					
9	30°59'39.9"N 78°27'36.9"E Elv. 3053±8m	~90/160 N	(J1) 65/210 N	0.5-1	PF/WF	Moderate Hazard	Mica schist	
			(F) 48/50 N	0.05-0.1				
			(R) 65/60 N					
10	30°59'39.9"N 78°27'36.3"E Elv. 3060±6m	>90/120 N	(J1) 35/320 N	0.1-0.15	PF/WF	High Hazard	Gneiss	
			(J2) ~90/50 N	0.1-0.2				
			(J3) ~50/100 N	0.1-0.2				
			(F) 50/100 N	0.2-0.3				
			(R) >90/140 N					
11	30°59'39.3"N 78°27'36.9"E Elv. 3033±8m	>90/13 N	(J1) 40/10 N	0.15-0.2	NF	No Hazard	Quartzite	
			(J2) 44/310 N	0.2-0.3				
			(F) 44/310 N	0.2-0.3				
			(R) 8/150 N					
12	30°59'35.7"N 78°27'32.14"E Elv. 3024±8m	~90/190 N	(J1) 40/220 N	0.4-0.5	PF/WF	Low Hazard	Mica schist	
			(F) 35/90 N	0.1-0.2				
			(R)70/65 N					
13	30°59'39.5"N 78°27'36.9"E Elv. 3022±5m	~90/100 N	(J1) 25/175 N	0.1-0.15	PF/WF	No Hazard	Quartzite	
			(J2) 85/30 N	0.2-0.3				
			(F) 65/30 N	0.1-0.2				
14	30°59'28.2"N 78°27'25.5"E Elv. 2928±8m	~60/200 N	(J1) 85/ 305 N	0.5-1	WF	Low Hazard	Gneiss	
			(F) 55/30 N	0.1-0.2				
			(R) 78/140 N					
15	30°59'22.9"N 78°27'20"E Elv. 2887±5m	~60/120 N	(J1) 55/195 N	0.15-2	NF	No Hazard	Gneiss	
			(F) 45/45 N	0.1-0.2				
			(R1) 74/120 N					
			(R2) 78/60 N					
16	30°59'21.7"N 78°27'16.6"E Elv. 2874±2m	60/160 N	(J1) 85/ 270 N	0.4-0.5	PF/WF	Moderate Hazard	Gneiss	
			(J2) 39/ 225 N	0.2-0.3				
			(F) 45/45 N	0.1-0.15				
			(R1) 90/140 N					

			(R2) 90/130 N					H I G H E R H I M A L A Y A
17	30°59'18.8"N 78°27'12.5"E Elv. 2864±6m	~90/290 N	(J1)26/35 N	0.5-1	PF	Low Hazard	Gneiss	
			(J2) 50/120 N	0.5-1				
			(J3) 65/310 N	0.2-0.25				
			(F) 26/35 N	0.1-0.15				
18	30°59'18.9"N 78°27'11.7"E Elv. 2861±7m	~90/210 N	(J1) 60/280 N	0.1-0.15	PF	No Hazard	Limestone	
			(J2) 35/345 N	0.1-0.15				
			(F) 35/345 N					
19	30°59'18.9"N 78°27'11.7"E Elv. 2860±7m	~90/200 N	(J1) 30/130 N	0.05-0.1	PF	Low Hazard	Limestone	
			(J2) 40/0 N	0.1-0.15				
			(F) 40/0 N	0.2-0.25				
			(R) 65/320 N					
20	30°59'18.8"N 78°27'12.7"E Elv. 2833±3m	>90/125 N	(J1) 72/220 N	0.2-0.25	PF/WF	Low Hazard	Quartzite	
			(J2)25/310 N	0.1-0.15				
			(F) 72/220 N	0.05-0.07				
			(R) 50/190 N					
21	30°59'11.1"N 78°27'14.3"E Elv. 2829±5m	>90/175 N	(J1)20/95 N	0.05-0.07	PF/WF	Low Hazard	Quartzite	
			(J2) 42/ 190 N	0.05-0.07				
			(R1) 40/200 N					
			(R2) 85/25 N					
22	30°59'2.8"N 78°26'49.1"E Elv. 2718±5m	90/180 N	(J1) 65/90 N	0.1-0.15	NF	No Hazard	Limestone	
			(F) 10/110 N	0.1-0.13				
23	30°58'44.5"N 78°26'25.6"E Elv. 2612±8m	>90/140 N	(J1) 77/230 N	0.05-0.07	PF/WF	Moderate Hazard	Limestone	
			(J2)65/10 N	0.1-0.14				
			(F) 25/20 N	0.1-0.2				
			(R) 76/130 N					
24	30°58'37.9"N 78°26'19.1"E Elv. 2425±5m	85/140 N	(J1) 75/135 N	0.1-0.15	PF/WF	Moderate Hazard	Gneiss	
			(J2)85/235 N	0.15-0.2				
			(F) 35/0 N	0.1-0.2				
			(R) 80/130 N					
25	30°57'30.7"N 78°25'24.9"E Elv. 2385±3m	60/355 N	(J1) 57/55 N	0.2-0.5	PF/WF	High Hazard	Quartzite	
			(J2) 60/280 N	0.1-0.15				
			(J3) 55/160 N	0.1-0.15				
			(F) 50/5 N	0.1-0.2				
26	30° 57' 12.2"N 78° 24' 50.4"E Elv. 2216±5m	80/350 N	(J1) 40/235 N	0.1-0.2	PF/WF	High Hazard	Gneiss	
			(J2) 50/355 N	0.2-0.3				
			(J3) 45/35 N	0.1-0.2				
			(F) 50/315 N	0.1-0.2				
27	30° 57' 0.5"N 78° 24'47.9"E Elv. 2213±5m	30/320 N	(J1) 85/175 N	0.2-0.4	WF	Low Hazard	Gneiss	
			(J2) 25/45 N	0.2-0.3				
28	30°55'57.2"N	75/240 N	(J1)80/155 N	0.1-0.2	WF/TF	Moderate	Gneiss	

	78°23'59.7"E Elv. 2060±5m		(J2)72/145 N	0.2-0.3		Hazard		H I G H E R
			(F) 50/75 N	0.1-0.15				
29	30°54'56.2"N 78°22'06.9"E Elv. 2024±5m	>90/290 N	(J1)75/25 N	0.05-0.1	WF	Low Hazard	Gneiss	H I M A L A Y A
			(J2)10/55 N	0.1-0.15				
			(J3)70/140 N	0.1-0.2				
30	30°54'46.8"N 78°21'54.5"E Elv. 1774±3m	>90/290 N	(J1)55/50 N	0.15-0.2	NF	No Hazard	Gneiss	
			(J2)25/90 N	0.1-0.15				
			(J3)0/90 N	0.2-0.25				
			(J4)75/110 N	0.15-0.3				
31	30°54'40.3"N 78°21'54.4"E Elv. 1770±3m	85/280 N	(J1)85/180 N	0.05-0.1	NF	No Hazard	Gneiss	
			(J2)26/120 N	0.2-0.25				
			(J3)15/330N	0.1-0.2				
32	30°54'23.1"N 78°20'46.9"E Elv. 1769±3m	60/185 N	(J1) 55/115N	0.1-0.2	NF	No Hazard	Gneiss	
			(J2) 15/280 N	0.05-0.1				
33	30°54'19.2"N 78°19'43.5"E Elv. 1765±6m	~75/55 N	(J1)45/70 N	0.25-0.3	WF	Low Hazard	Quartzite	
			(J2)70/220 N	0.5-1				
			(J3) 80/40 N	0.1-0.15				
			(J4)55/350 N	0.1-0.2				
34	30°51'44.6"N 78°17'32.3"E Elv. 1680±3m	70/40 N	(J1) 70/120 N	0.05-0.1	NF	No Hazard	Limestone	
			(J2) 84/50 N	0.1-0.15				
			(F) 25/225 N	0.1-0.2				
			(R) 84/120 N					
35	30°52'46.7"N 78°18'32.6"E Elv. 1546±3m	85/100 N	(J1) 65/50 N	0.05-0.1	NF	No Hazard	Limestone	
			(J2) 28/300 N	0.1-0.15				
			(F) 10/290 N	0.1-0.2				
36	30°51'21.4"N 78°17'11.9"E Elv. 1444±3m	85/125 N	(J1) 70/210 N	0.05-0.1	TF	No Hazard	Limestone	
			(J2) 85/305 N	0.15-0.3				
			(J3) 15/20 N	0.2-0.25				
			(J4) 65/50 N	0.1-0.2				
37	30°52'07.9"N 78°17'54.3"E Elv. 1470±4m	85/230 N	(J1) 40/60 N	0.1-0.15	WF	Low Hazard	Limestone	
			(J2) 45/210 N	0.15-0.2				
			(J3) 45/315 N	0.15-0.2				
38	30°51'13.1"N 78°16'59.9"E Elv. 1395±6m	80/310 N	(J1) 74/20 N	0.3-0.4	TF	No Hazard	Quartzite	
			(J2) 64/110 N	0.1-0.15				
			(J3) 20/25 N	0.1-0.2				
			(J4) 60/195 N	0.15-0.2				
39	30°49'06.7"N 78°13'59.1"E Elv. 1397±2m	70/20 N	(J1) 30/65 N	0.15-0.2	WF	Low Hazard	Slate	
			(J2) 70/320 N	0.1-0.15				
			(J3) 75/10 N	0.15-0.3				
			(J4) 80/240 N	0.4-0.5				
40	30°54'19.2"N 78°19'43.5"E Elv. 1765±6m	~70/200 N	(J1)40/45 N	0.1-0.3	WF	Low Hazard	Slate	
			(J2) 35/245 N	0.3-0.4				
			(J3)38/310 N	0.08-0.1				
41	30°54'19.2"N	85/5 N	(J1)30/35 N	0.3-0.5	WF	Low	Slate	

	78°19'43.5"E Elv. 1765±6m		(J2)85/4 N (F) 45/215 N	0.06-0.08 0.1-0.2		Hazard		L E S S E R H I M A L A Y A
42	30°54'19.2"N 78°19'43.5"E Elv. 1765±6m	60/315 N	(J1) 85/130 N (J2) 90/40 N (F) 65/290 N	0.08-0.1 0.1-0.2 0.1-0.15	PF	Low Hazard	Limestone	
43	30°54'19.2"N 78°19'43.5"E Elv. 1765±6m	70/340 N	(J1)70/35 N (J2)75/250 N (J3)13/168 N	0.2-0.24 0.1-0.15 0.15-0.18	WF	Low Hazard	Limestone	
44	30°47'48.9"N 78°10'51.5"E Elv. 1211±3m	85/20 N	(J1) 35/215 N (J2)69/30 N (J3)25/55 N (J4) 50/210 N (R1) 90/190 N	0.5-1 0.1-0.15 0.06-0.08 0.5-1 0.1-0.15	WF/TF	Moderate Hazard	Limestone	
45	30°47'44.8"N 78°10'6.4"E Elv. 1231±2m	85/30 N	(J1) 50/350 N (J2)30/175 N (J3)40/245 N (J4)30/75 N	0.1-0.15 0.1-0.15 0.2-0.5 0.15-2	WF	Low Hazard	Slate	
46	30°47'48.2"N 78°10'1.1"E Elv. 1220±6m	85/55 N	(J1) 65/275 N (J2) 35/210 N (J3) 65/25 N	0.1-0.3 0.1-0.15 0.08-0.1	WF	Moderate Hazard	Slate	
47	30°47'48.4"N 78°9'59.8"E Elv. 1218±7m	85/55 N	(J1) 60/275 N (J2) 45/95 N (J3)25/190 N (J4) 60/20 N	0.2-0.5 0.5-1 0.1-0.15 0.1-0.15	WF/TF	High Hazard	Limestone	
48	30°47'41.7"N 78°9'39.7"E Elv. 1227±6m	85/310 N	(J1) 57/240 N (J2) 40/65 N	0.5-1 0.1-0.15	NF	No Hazard	Limestone	
49	30°47'41.6"N 78°9'39.5"E Elv. 1227±2m	70/310 N	(J1) 30/355 N (J2) 35/175 N (J3) 50/75 N (J4) 45/275 N	0.1-0.15 0.25-0.3 0.5-1 0.04-0.06	WF	High Hazard	Quartzite	
50	30°46'54.3"N 78°7'7"E Elv. 1139±7m	70/300 N	(J1) 35/55 N (J2) 65/225 N (J3) 35/115 N	0.15-0.2 0.15-0.2 0.08-0.1	NF	No Hazard	Limestone	
51	30°46'52.7"N 78°7'8"E Elv. 1169±6m	80/350 N	(J1) 65/265 N (J2)55/75 N (J3)30/160 N (J4) 35/345 N	0.15-0.2 0.5-1 0.1-0.2 0.5-0.6	WF	Moderate Hazard	Limestone	
52	30°46'50.5"N 78°6'57.1"E Elv. 1163±6m	70/270 N	(J1)22/70 N (J2)50/335 N (F) 22/70 N (J3)38/175 N	0.2-0.3 0.1-0.15 0.1-0.15 0.5-1	NF	No Hazard	Slate	
53	30°46'25.27"N 78°6'43.06"E	85/94 N	(J1) 35/150 N (J2) 40/200 N	0.1-0.15 0.2-0.25	WF	Low Hazard	Slate	

	Elv. 1173±7m		(F) 35/150 N (R)85/155 N	0.1-0.15				L E S S E R H I M A L A Y A
54	30°46'18.6"N 78°6'39.3"E Elv. 1171±6m	85/230 N	(J1) 80/30 N (J2) 65/285 N (J3) 50/305 N (J4) 50/225 N	0.2-0.25 0.2-0.25 0.25-0.3 0.1-0.15	PF/WF	High Hazard	Limestone	
55	30°45'49"N 78°6'12"E Elv. 1136±9m	70/235 N	(J1) 45/75 N (J2) 85/20 N (J3) 60/340 N	0.25-0.3 0.1-0.15 0.1-0.15	PF/WF	Moderate Hazard	Slate	
56	30°45'49.2"N 78°6'12.6"E Elv. 1147±6m	80/320 N	(J1) 55/240 N (J2) 35/320 N (J3) 30/65 N	0.25-0.3 0.1-0.15 0.1-0.15	PF/WF	Low Hazard	Slate	
57	30°45'35.5"N 78°5'54.5"E Elv. 1128±2m	80/300 N	(J1) 55/20 N (J2) 90/10 N (J3) 40/300 N	0.8-1 0.5-0.6 0.21-0.25	PF/WF	Moderate Hazard	Slate	
58	30°45'27.1"N 78°5'43.4"E Elv. 1106±8m	60/345 N	(J1) 70/40 N (J2) 80/150 N (J3) 32/320 N	0.1-0.15 0.1-0.15 0.21-0.25	PF/WF	Low Hazard	Slate	
59	30°45'25"N 78°5'41.7"E Elv. 1106±6m	60/310 N	(J1)50/30 N (J2)45/180 N (J3) 40/290 N (F) 45/180 N	0.5-1 0.2-0.4 0.3-0.35 0.1-0.15	PF/WF	Moderate Hazard	Slate	
60	30°45'9"N 78°5'35.7"E Elv. 1078±7m	70/335 N	(J1) 55/265 N (J2) 30/225 N (J3) 60/75 N (R) 0/190 N	0.15-0.2 0.1-0.15 0.5-1 	NF	No Hazard	Quartzite	
61	30°45'1.6"N 78°5'18.5"E Elv. 1078±8m	60/320 N	(J1) 45/210 N (J2) 55/85 N (J3) 15/315 N	0.5-1 0.2-0.3 0.5-0.6	NF	No Hazard	Slate	
62	30°45'8.4"N 78°5'18.2"E Elv. 1069±5m	85/330 N	(J1)70/300 N (J2) 80/170 N (J3) 20/155 N (J4) 60/325 N	0.1-0.15 0.07-0.08 0.1-0.15 0.4-0.5	PF/WF	High Hazard	Slate	
63	30°45'2.6"N 78°5'9.4"E Elv. 1080±6m	85/320 N	(J1)32/190 N (J2)70/35 N (J3)50/300 N (J4)45/120 N (R1)35/120 N (R2)90/300 N	0.07-0.08 0.3-0.4 0.2-0.4 0.2-0.3 	PF/WF	Moderate Hazard	Slate	
64	30°44'54.3"N 78°5'5.1"E Elv. 1052±6m	80/280 N	(J1)72/175 N (J2) 40/350 N (J3)40/280 N (J4)30/105 N	0.5-1 0.1-0.15 0.5-1 0.4-0.5	PF/WF	Moderate Hazard	Slate	
65	30°44'51.1"N	85/285 N	(J1)80/335 N	0.1-0.15	PF/WF	High	Slate	

	78°5'5"E Elv. 1063±8m		(J2) 65/205 N (J3)35/300 N	0.2-0.4 0.1-0.15		Hazard		L E S S E R H I M A L A Y A
66	30°44'39.8"N 78°4'58.8"E Elv. 1090±8m	85/270 N	(J1) 65/185 N (J2)65/355 N (J3)60/100 N (J4)45/290 N	0.08-0.1 0.06-0.08 0.2-0.3 0.2-0.3	PF/WF	Moderate Hazard	Slate	
67	30°44'37.8"N 78°4'59"E Elv. 1063±6m	85/260 N	(J1) 35/140 N (J2)55/335 N (J3)40/260 N (J4)55/65 N	0.8-1 0.09-0.1 0.4-0.6 0.05-0.06	PF/WF	High Hazard	Limestone	
68	30°44'18.5"N 78°4'53.9"E Elv. 1027±6m	85/320 N	(J1) 45/235 N (J2)55/50 N (J3)30/320 N	0.5-0.6 0.04-0.06 0.2-0.3	PF/WF	Low Hazard	Limestone	
69	30°43'18.7"N 78°5'5.4"E Elv. 946±6m	60/255 N	(J1) 40/80 N (J2)60/340 N (J3)75/170 N (J4)35/260 N	0.1-0.2 0.05-0.07 0.2-0.4 0.4-0.5	PF/WF	Moderate Hazard	Slate	
70	30°43'15"N 78°5'5.9"E Elv. 952±7m	60/340 N	(J1) 65/125 N (J2)85/270 N (J3)55/20 N (J4)50/190 N	0.3-0.4 0.10-0.15 0.07-0.08 0.09-0.1	PF/WF	Low Hazard	Slate	
71	30°43'18.1"N 78°5'3.5"E Elv. 956.3±6m	60/335 N	(J1) 55/30 N (J2)80/70 N (J3)45/0 N (J4)80/285 N	0.2-0.3 0.3-0.4 0.15-0.2 0.4-0.5	WF	Moderate Hazard	Limestone	
72	30°43'13"N 78°5'4.4"E Elv. 951±8m	70/345 N	(J1) 45/55 N (J2)85/285 N (J3)35/200 N (J4)70/280 N	0.07-0.08 0.04-0.06 0.07-0.08 0.2-0.3	TF	Moderate Hazard	Limestone	
73	30°42'32.9"N 78°4'49.6"E Elv. 937.3±8m	60/340 N	(J1)30/45 N (J2) 48/210 N (J3)60/285 N	0.07-0.08 0.03-0.05 0.4-0.5	WF	Low Hazard	Slate	
74	30°42'21.3"N 78°4'29.9"E Elv. 930.6±6m	60/350 N	(J1)85/85 N (J2)45/95 N (J3)55/50 N (J4)60/225 N	0.1-0.15 0.4-0.6 0.5-1 0.4-0.5	WF	Low Hazard	Limestone	
75	30°42'17.2"N 78°4'22.8"E Elv. 950±5m	60/260 N	(J1)45/320 N (J2)90/160 N (J3)75/265 N (J4)55/80 N	0.08-0.1 0.4-0.5 0.5-1 0.07-0.08	TF	Low Hazard	Limestone	
76	30°42'5.7"N 78°4'27.1"E Elv. 972±6m	75/275 N	(J1)60/160 N (J2)65/205 N (J3)40/150 N	0.07-0.08 0.03-0.05 0.1-0.3	TF	Low Hazard	Limestone	
77	30°41'32.7"N	75/290 N	(J1) 25/215 N	0.1-0.15	TF	Low	Slate	

	78°4'18.3"E Elv. 984±7m		(J2)58/10 N (J3)75/170 N	0.4-0.6 0.2-0.3		Hazard		L E S S E R H I M A L A Y A
78	30°41'9.3"N 78°4'10.8"E Elv. 972.6±8m	60/290 N	(J1)75/220 N (J2)35/40 N (J3)40/170 N (F) 40/120 N	0.1-0.15 0.2-0.3 0.05-0.07 0.05-0.07	TF	Low Hazard	Slate	
79	30°40'56.2"N 78°4'3.9"E Elv. 970±7m	85/250 N	(J1) 50/130 N (J2) 45/10 N (J3) 20/150 N (J4)65/230 N	0.1-0.2 0.5-0.6 0.15-0.2 0.1-0.15	WF	Moderate Hazard	Slate	
80	30°40'37.9"N 78°4'14.8"E Elv. 1004±7m	60/5 N	(J1) 85/250 N (J2) 40/310 N (J3)50/25 N (J4)53/190 N	0.1-0.15 0.05-0.08 0.5-0.6 0.5-1	PF/WF	High Hazard	Slate	
81	30°40'35.7"N 78°4'7.4"E Elv. 1020±5m	65/280 N	(J1)50/105 N (J2)40/210 N (J3) 75/95 N	0.1-0.2 0.1-0.15 0.1-0.15	TF	Low Hazard	Slate	
82	30°40'24.4"N 78°4'6.5"E Elv. 1033±8m	85/245 N	(J1)85/175 N (J2)25/330 N (J3)90/240 N	0.15-0.2 0.15-0.2 0.25-0.3	NF	No Hazard	Slate	
83	30°39'43.6"N 78°3'36.2"E Elv. 1034±7m	80/290 N	(J1)65/325 N (J2)20/105 N (J3)80/245 N	0.2-0.4 0.15-0.2 0.15-0.2	WF	Low Hazard	Slate	
84	30°39'28.4"N 78°2'49.7"E Elv. 1019±7m	85/275 N	(J1)75/335 N (J2)75/240 N (J3) 25/125 N (R) 90/225 N	0.15-0.2 0.1-0.15 0.5-1 	WF	Low Hazard	Slate	
85	30°39'21.8"N 78°2'48.4"E Elv. 973±8m	70/10 N	(J1)55/305 N (J2)80/185 N (J3)25/20 N (R) 90/10 N	0.5-1 0.5-1 0.1-0.3 	TF	Low Hazard	Slate	
86	30°39'5.3"N 78°2'34.8"E Elv. 1003±5m	70/315 N	(J1)70/340 N (J2)80/260 N (J3)65/125 N (J4)65/300 N	0.1-0.15 0.05-0.08 0.5-0.6 0.5-1	PF/WF	High Hazard	Slate	
87	30°38'54.6"N 78°2'21.7"E Elv. 1005±3m	70/310 N	(J1) 30/55 N (J2)45/240 N	0.05-0.065 0.6-1	NF	No Hazard	Slate	
88	30°38'44.8"N 78°2'14.1"E Elv. 982±10m	60/315 N	(J1)245/90 N (J2)90/140 N (J3)30/320 N	0.04-0.06 0.4-0.5 0.3-0.4	TF	Low Hazard	Slate	
89	30°38'35.8"N 78°01'59.9"E Elv. 985±10m	60/315 N	(J1)35/130 N (J2)75/250 N (J3)75/320 N	0.2-0.25 0.2-0.25 0.1-0.15	NF	No Hazard	Slate	

90	30°38'38.1"N 78°1'39.6"E Elv. 986±8m	70/75 N	(J1)85/270 N	0.08-0.1	PF/WF	Moderate Hazard	Slate	
			(J2)85/180 N	0.5-0.6				
			(J3)28/210 N	0.1-0.15				
			(J4)60/30 N	0.5-1				
91	30°38'46.6"N 78°1'29.6"E Elv.955.5±6m	80/50 N	(J1) 25/340 N	0.1-0.15	NF	No Hazard	Slate	
			(J2)90/155 N	0.2-0.25				
			(J3)90/75 N	0.1-0.15				
92	30°38'58"N 78°1'24.5"E Elv. 967.6±7m	60/35 N	(J1) 45/320 N	0.05-0.1	NF	No Hazard	Slate	
			(J2)15/220 N	0.2-0.25				
			(J3)80/40 N	0.2-0.25				

NF: No Failure; PF: Planar Failure; WF: Wedge Failure; TF: Toppling Failure

To further assess the stability of slopes, GSI values of the rock mass were also obtained from field-based observation using the GSI chart of Marinos and Hoek (2000). The quantified approach, which is the modified GSI (Cai et al., 2007) was also used. GSI values assigned at various locations in the field, as well as the value calculated empirically are presented in Table 5.6. In the present study, the rock mass comprise highly weathered and fractured rocks. GSI values interpreted from the GSI chart range from 20-25 to 65-70, while the empirically quantified GSI values range from 21 to 57. The least and highest GSI value of 21 and 57 were both obtained from quartzite (location 21) in the Higher Himalaya Crystallines.

Slope stability assessment for debris slopes was carried out using FEM. FEM analyses of 29 slopes that were modelled show 11 slopes having FoS values between 1 and 2, whereas 18 slopes have $FoS \leq 1$ (Fig. 5.5). Results of FEM analysis are given in Table 5.7. Slopes with $FoS \leq 1$ are unstable (Matsui and San, 1992; Griffiths and Lane, 1999; Dawson et al., 1999; Jeremic, 2000; Zheng et al., 2005). Since the stability evaluation of the slopes was based on static analysis, slopes with FoS values between 1 and 2 are considered potentially unstable as they may become unstable during extreme rainfall or earthquake. Landslide dimensions (area and volume) and FoS were correlated to determine the relation between landslide dimension and slope instability. Though good correlation is not observed, landslide area and volume are noted to decrease with increasing FoS in the Higher Himalayan and Lesser Himalayan landslides (Fig. 5.6). However, area and volume in the Higher Himalayan landslides achieved better correlation ($R^2=0.13$ and $R^2=0.12$, respectively) with FoS than that in the Lesser Himalaya ($R^2=0.11$ for both area and volume). In the present study, the Higher Himalaya comprises 10 unstable and 3 potentially unstable landslide slopes, whereas the Lesser Himalayan comprises 8 unstable and 8 moderately stable landslide

slopes (Fig. 5.7). The total displacement in the Higher Himalayan landslide slopes varies between 0.005 ± 2.0 m and 4.35 ± 0.95 m, whereas in the Lesser Himalayan landslide slopes it varies from 0.01 ± 5.5 m to 3.35 ± 0.32 m. The landslide density, which is the ratio of number of landslides per length of the litho-tectonic division along the river, is highest in the Higher Himalaya ($L_d=2.64$). This includes the slopes of unstable and potentially unstable debris slides as well as rockfalls in the Higher Himalaya, whereas in the Lesser Himalaya, the landslide density is relatively low ($L_d=1.18$).

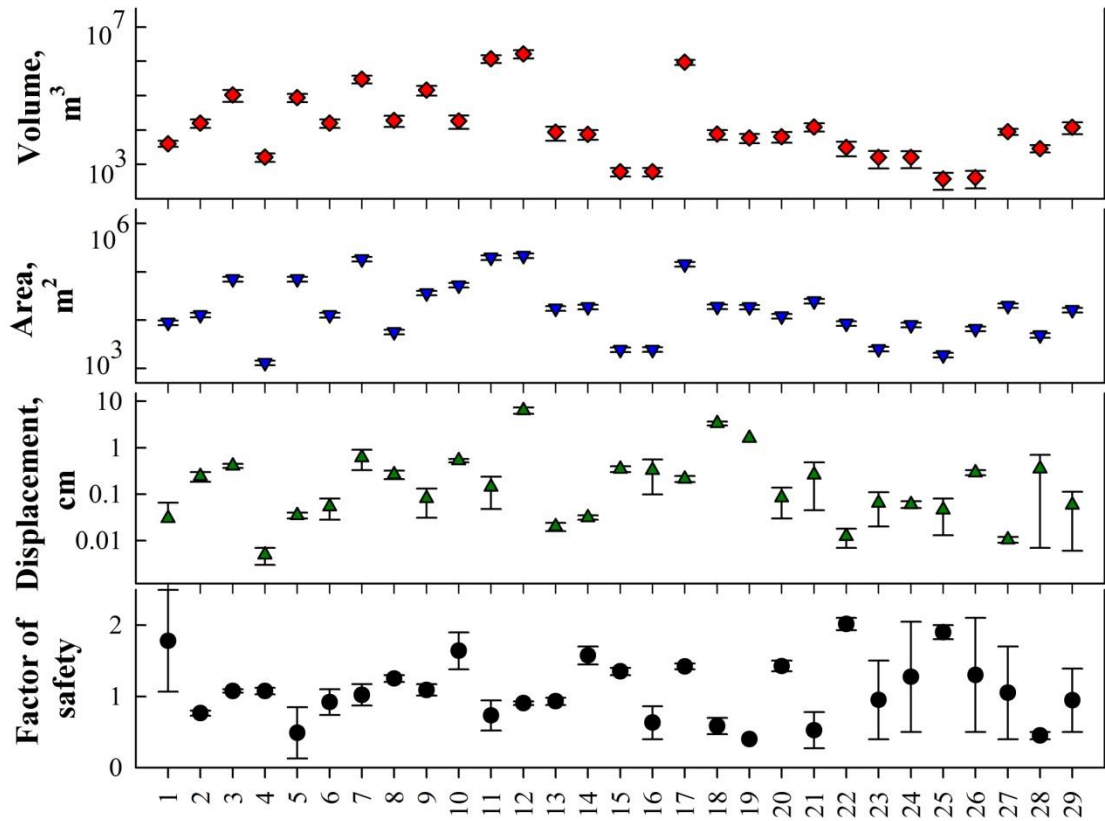


Fig. 5.5: Results of FEM analysis in terms of FoS and displacement (m)

Table 5.6: Geomechanical classification of the rock mass in the study area

Landslide No.	Rock type	RMR _{basic}	Class	Rock mass	SMR	Class	Stability	Category based on kinematic analysis	GSI value (field)	GSI, (empirical) (Cai et al., 2007)
1	Quartzite	57	III	Fair	49	III	Partially stable	Moderate Hazard	40-50	44
2	Gneiss	60	III	Fair	51	III	Partially stable	Low Hazard	60-65	50
3	Gneiss	42	III	Fair	33	IV	Unstable	Moderate Hazard	20-25	34
4	Gneiss	55	III	Fair	53	III	Partially stable	Low Hazard	45-50	45
5	Slate	55	III	Fair	46	III	Partially stable	Low Hazard	20-25	44
6	Mica schist	63	II	Good	54	III	Partially stable	Low Hazard	45-50	48
7	Mica schist	50	III	Fair	41	III	Partially stable	Moderate Hazard	45-50	40
8	Gneiss	42	III	Fair	38	IV	Unstable	Low Hazard	30-35	35
9	Mica schist	50	III	Fair	46	III	Partially stable	Moderate Hazard	30-35	39
10	Gneiss	40	IV	Poor	31	IV	Unstable	High Hazard	50-55	33
11	Quartzite	68	II	Good	60	III	Partially stable	No Hazard	45-50	57
12	Mica schist	55	III	Fair	47	III	Partially stable	Low Hazard	20-25	45
13	Quartzite	60	III	Fair	56	III	Partially stable	No Hazard	40-50	52
14	Gneiss	55	III	Fair	47	III	Partially stable	Low Hazard	35-40	42
15	Gneiss	47	III	Fair	38	IV	Unstable	No Hazard	40-45	36
16	Gneiss	55	III	Fair	47	III	Partially stable	Moderate Hazard	45-50	38
17	Gneiss	60	III	Fair	36	IV	Unstable	Low Hazard	35-40	35
18	Limestone	60	III	Fair	54	III	Partially stable	No Hazard	45-50	46
19	Limestone	40	IV	Poor	31	IV	Unstable	Low Hazard	45-50	34
20	Quartzite	42	III	Fair	34	IV	Unstable	Low Hazard	45-50	37
21	Quartzite	22	IV	Poor	14	V	Very unstable	Low Hazard	37-45	21
22	Limestone	59	III	Fair	50	III	Partially stable	No Hazard	35-40	41
23	Limestone	50	III	Fair	41	III	Partially stable	Moderate Hazard	30-35	38
24	Gneiss	60	III	Fair	56	III	Partially stable	Moderate Hazard	40-45	47
25	Quartzite	60	III	Fair	54	III	Partially stable	High Hazard	55-60	47
26	Gneiss	50	III	Fair	42	III	Partially stable	High Hazard	30-35	41
27	Gneiss	60	III	Fair	56	III	Partially stable	Low Hazard	30-35	49
28	Gneiss	55	III	Fair	46	III	Partially stable	Moderate Hazard	50-55	44
29	Gneiss	50	III	Fair	42	III	Partially stable	Low Hazard	55-60	42

30	Gneiss	55	III	Fair	46	III	Partially stable	No Hazard	40-45	41
31	Gneiss	55	III	Fair	54	III	Partially stable	No Hazard	40-45	51
32	Gneiss	47	III	Fair	46	III	Partially stable	No Hazard	35-30	45
33	Quartzite	55	III	Fair	47	III	Partially stable	Low Hazard	35-40	46
34	Limestone	42	III	Fair	33	IV	Unstable	No Hazard	35-40	36
35	Limestone	50	III	Fair	41	III	Partially stable	No Hazard	35-40	42
36	Limestone	50	III	Fair	41	III	Partially stable	No Hazard	40-45	42
37	Limestone	55	III	Fair	49	III	Partially stable	Low Hazard	40-45	47
38	Quartzite	55	III	Fair	51	III	Partially stable	No Hazard	40-45	51
39	Slate	45	III	Fair	41	III	Partially stable	Low Hazard	35-40	47
40	Slate	55	III	Fair	49	III	Partially stable	Low Hazard	40-45	49
41	Slate	47	III	Fair	38	IV	Unstable	Low Hazard	30-35	37
42	Slate	45	III	Fair	28	IV	Unstable	Low Hazard	40-45	27
43	Gneiss	60	III	Fair	52	III	Partially stable	Low Hazard	30-40	38
44	Limestone	55	III	fair	46	III	Partially stable	Moderate Hazard	25-30	44
45	Slate	55	III	fair	46	III	Partially stable	Low Hazard	35-40	44
46	Slate	55	III	fair	46	III	Partially stable	Moderate Hazard	45-50	42
47	Limestone	50	III	fair	41	III	Partially stable	High Hazard	25-30	37
48	Slate	55	III	fair	47	III	Partially stable	No Hazard	40-45	41
49	Quartzite	50	III	fair	46	III	Partially stable	High Hazard	40-45	43
50	Limestone	55	III	fair	47	III	Partially stable	No Hazard	25-30	43
51	Limestone	50	III	fair	44	III	Partially stable	Moderate Hazard	35-40	41
52	Slate	50	III	fair	41	III	Partially stable	No Hazard	20-25	39
53	Slate	55	III	fair	49	III	Partially stable	Low Hazard	40-45	43
54	Limestone	55	III	fair	47	III	Partially stable	High Hazard	30-35	41
55	Limestone	55	III	fair	46	III	Partially stable	Moderate Hazard	30-40	44
56	Limestone	60	III	fair	54	III	Partially stable	Low Hazard	25-30	50
57	Limestone	50	III	Fair	44	III	Partially stable	Moderate Hazard	45-50	42
58	Limestone	55	III	Fair	49	III	Partially stable	Low Hazard	30-40	48
59	Slate	60	II	Good	54	III	Partially stable	Moderate Hazard	30-40	43
60	Quartzite	55	III	Fair	46	III	Partially stable	No Hazard	45-50	41
61	Slate	60	III	Fair	51	III	Partially stable	No Hazard	30-40	45
62	Slate	50	III	Fair	41	III	Partially stable	High Hazard	35-40	38

63	Slate	55	III	Fair	46	III	Partially stable	Moderate Hazard	40-45	41
64	Slate	47	III	Fair	39	IV	Unstable	Moderate Hazard	40-50	38
65	Slate	60	III	Fair	51	III	Partially stable	High Hazard	30-40	46
66	Slate	55	III	Fair	47	III	Partially stable	Moderate Hazard	25-30	37
67	Limestone	50	III	Fair	40	III	Partially stable	High Hazard	30-40	41
68	Limestone	55	III	Fair	51	III	Partially stable	Low Hazard	25-29	45
69	Slate	50	III	Fair	44	III	Partially stable	Moderate Hazard	25-30	37
70	Slate	45	III	Fair	36	IV	Unstable	Low Hazard	40-45	36
71	Limestone	58	III	Fair	49	III	Partially stable	Moderate Hazard	40-50	44
72	Limestone	63	II	Good	57	III	Partially stable	Moderate Hazard	40-45	51
73	Slate	63	II	Good	59	III	Partially stable	Low Hazard	30-35	44
74	Limestone	43	III	Fair	34	IV	Unstable	Low Hazard	40-45	34
75	Limestone	55	III	Fair	46	III	Partially stable	Low Hazard	30-40	43
76	Limestone	40	IV	Poor	31	IV	Unstable	Low Hazard	40-50	22
77	Slate	58	III	Fair	49	III	Partially stable	Low Hazard	40-50	42
78	Slate	35	IV	Poor	26	IV	Unstable	Low Hazard	30-40	27
79	Slate	43	III	Fair	36	IV	Unstable	Moderate Hazard	30-40	39
80	Slate	40	IV	Poor	32	IV	Unstable	High Hazard	35-40	32
81	Slate	60	III	Fair	52	III	Partially stable	Low Hazard	40-50	46
82	Slate	50	III	Fair	41	III	Partially stable	No Hazard	30-40	40
83	Slate	63	II	Good	54	III	Partially stable	Low Hazard	35-40	48
84	Slate	55	III	Fair	46	III	Partially stable	Low Hazard	35-40	41
85	Slate	47	III	Fair	38	IV	Unstable	Low Hazard	40-50	35
86	Slate	60	III	Fair	51	III	Partially stable	High Hazard	35-40	39
87	Slate	60	III	Fair	51	III	Partially stable	No Hazard	30-35	45
88	Slate	50	III	Fair	41	III	Partially stable	Low Hazard	30-35	38
89	Slate	58	III	Fair	49	III	Partially stable	No Hazard	30-35	42
90	Slate	50	III	Fair	50	III	Partially stable	Moderate Hazard	30-35	47
91	Slate	50	III	Fair	41	III	Partially stable	No Hazard	30-35	40
92	Slate	55	III	Fair	46	III	Partially stable	No Hazard	35-40	41

Table 5.7: Details of debris slide and result of FEM analysis

LS No	Landslide	Landslide location	Type ^a	Area ^b (m ²)	Volume ^c (m ³)	Factor of Safety	Displacement (m)	Rock type	Stratigraphic Unit
1	Kharsali	78°26'21.84" 30°58'29.64"	Debris slide	8890±978	4001±803	1.78±0.71	0.03±0.04	Quartzite	H I G H E R H I M A L A Y A
2	Phulchatti-I	78°25'51.24" 30°57'57.24"	Debris slide	12762±1404	15953±4360	0.77±0.035	0.24±0.06	Gneiss	
3	Phulchatti-II	78°25'49.08" 30°57'45.00"	Debris slide	70515±7757	105773±40423	1.075±0.03	0.41±0.04	Gneiss	
4	Downstream of Asnaur Gad	78°25'11.86" 30°57'29.01"	Debris slide	1300±143	1625±444	1.08±0.05	0.005±2.0	Gneiss	
5	Sauri Gad-I	78°24'50.24" 30°57'12.23"	Debris slide	70600±7766	88250±24119	0.49±0.36	0.04±5.0	Limestone	
6	Sauri Gad-II	78°24'47.98" 30°57'00.52"	Debris slide	12700±1397	15875±4339	0.92±0.18	0.05±0.03	Limestone	
7	Hanuman Chatti-I 300m upstream	78°24'6.48" 30°56'0.60"	Debris slide	183468±20181	302722±78860	1.02±0.15	0.62±0.29	Gneiss	
8	Hanuman Chatti-II	78°23'55.43" 30°55'50.04"	Debris slide	5695±626	18983±6738	1.25±0.05	0.27±0.06	Limestone	
9	Wariya-I	78°23'38.76" 30°55'41.52"	Debris slide	36368±4000	145472±45696	1.09±0.08	0.08±0.05	Gneiss	
10	Wariya-II	78°23'48.84" 30°55'44.76"	Debris slide	52846±5813	18496±7743	1.64±0.26	0.53±0.04	Gneiss	
11	SynaChatti	78°21'33.23" 30°54'10.77"	Debris slide	198061±21787	1188366±292436	0.73±0.21	0.14±0.09	Gneiss	
12	Wazri-I	78°20'46.70" 30°54'23.05"	Debris slide	215480± 23703	1652013±450472	0.91±0.03	4.35±0.95	Gneiss	
13	Wazri-II 500m downstream	78°20'01.91" 30°54'28.02"	Debris slide	17440±1918	8720±3807	0.93±0.05	0.02±4.0	Quartzite	
14	Wazri-III	78°19'52.42" 30°54'38.70"	Debris slide	18700±2057	7480±2350	1.58±0.13	0.032±3.5	Quartzite	

15	Pali-I (Opp. Kupra vill.)	78°19'43.49" 30°54'19.14"	Debris slide	2450±270	613±167	1.35±0.05	0.35±0.05	Quartzite	L E S S E R H I M A L A Y A
16	Pali-II (Opp. Kupra vill.)	78°19'41.49" 30°54'08.27"	Debris slide	2460±271	615±168	0.63±0.23	0.33±0.23	Quartzite	
17	Silai Bend	78°19'30.37" 30°53'48.74"	Debris slide	144108±15852	936702±161869	1.42±0.04	0.22±0.03	Quartzite	
18	Upstream of Pujargaon	78°18'56.88" 30°53'23.64"	Debris slide	18959±2085	7584±2382	0.59±0.12	3.35±0.32	Quartzite	
19	Downstream of Yamuna Chatti	78°18'33.74" 30°52'47.37"	Debris slide	18673±2054	5913±1815	0.4±0	1.6±0	Limestone	
20	Kuthnaur	78°13'43.43" 30°47'07.09"	Debris slide	24747±2722	12374±3382	1.43±0.08	0.09±0.05	Slate	
21	Phooldhar	78°18'15.38" 30°52'26.91"	Debris slide	12085±1329	6445±2216	0.53±0.26	0.26±0.22	Limestone	
22	Chhatanga	78°10'13.21" 30°47'42.94"	Debris slide	8533±939	3129±1408	2.02±0.09	0.01±5.5	Limestone	
23	Kisna-I	78°10'07.42" 30°47'44.64"	Debris slide	2530±278	1602±840	0.95±0.55	0.07±0.05	Limestone	
24	Kisna-II	78°10'00.17" 30°47'48.46"	Debris slide	7929±872	1586±822	1.28±0.78	0.06±0.01	Limestone	
25	Tunalka-I	78°09'51.92" 30°47'49.39"	Debris slide	1884±207	377±195	1.9±0.1	0.05±0.03	Limestone	
26	Tunalka-II	78°09'52.18" 30°47'54.29"	Debris slide	6616±728	419±220	1.3±0.8	0.29±0.04	Limestone	
27	Tunalka-III	78°09'14.71" 30°47'36.14"	Debris slide	19926±2192	8967±1800	1.05±0.65	0.01±1.5	Slate	
28	Chhuri	78°05'33.71" 30°45'09.63"	Debris slide	4848±533	2909±716	0.45±0.05	0.35±0.35	Slate	
29	Barni Gad (300 m Downstream)	78°04'57.16" 30°42'57.89"	Debris slide	16198±1782	12149±4643	0.95±0.06	0.06±0.05	Limestone	

a: Classification based on Varnes (1978) and Hungr et al. (2012); b: Error (\pm) caused by GE measurement (1.11 %); c: Error (\pm) is the product of area \pm error and thickness \pm error. Thickness error (Std. dev.) corresponds to averaging of field based approximated thickness

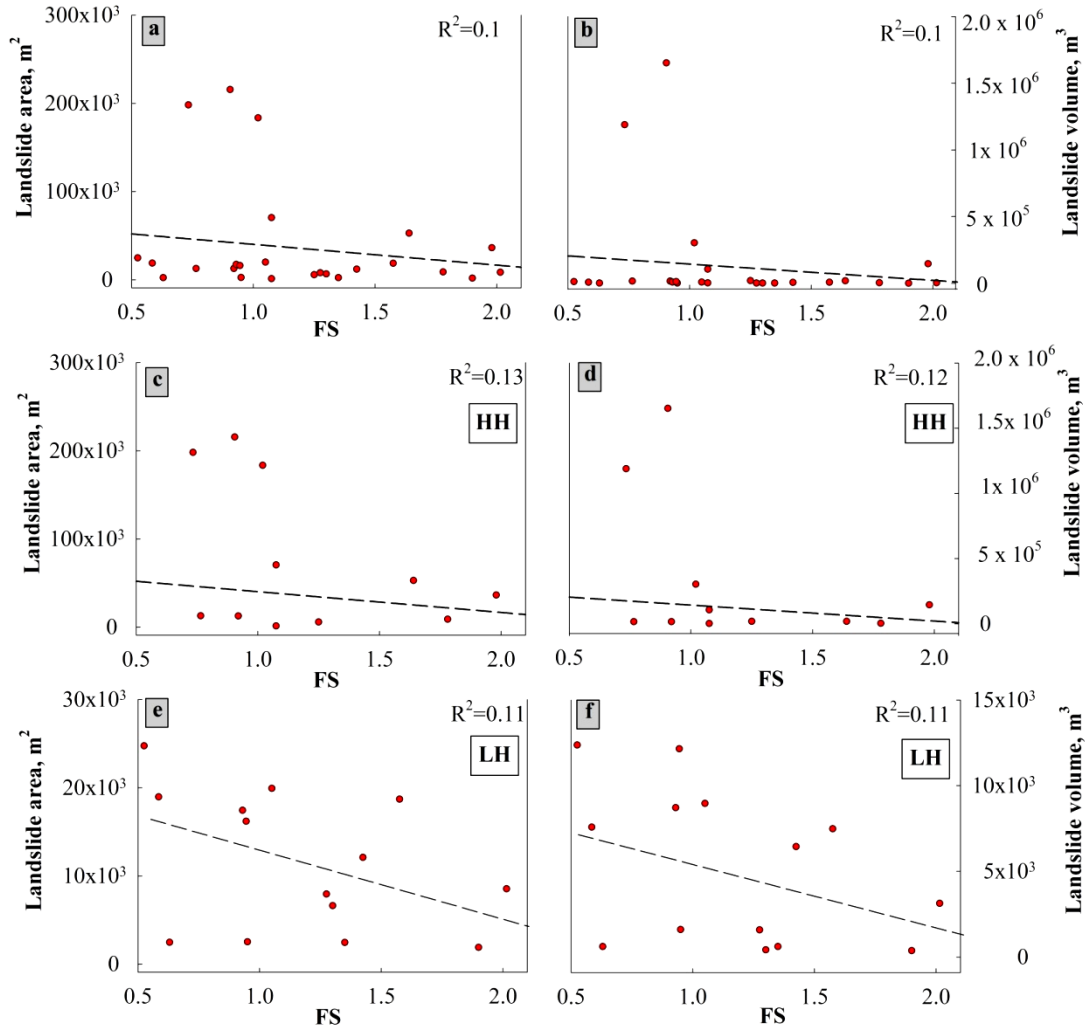


Fig. 5.6: Correlation between FoS, landslide area and volume. (a-b) FoS vs landslide area and FoS vs volume for 29 slopes. (c-d) FoS vs landslide area and FoS vs volume in the Higher Himalaya. (e-f) FoS vs landslide area and FoS vs volume in the Lesser Himalaya. The dashed line represents linear regression

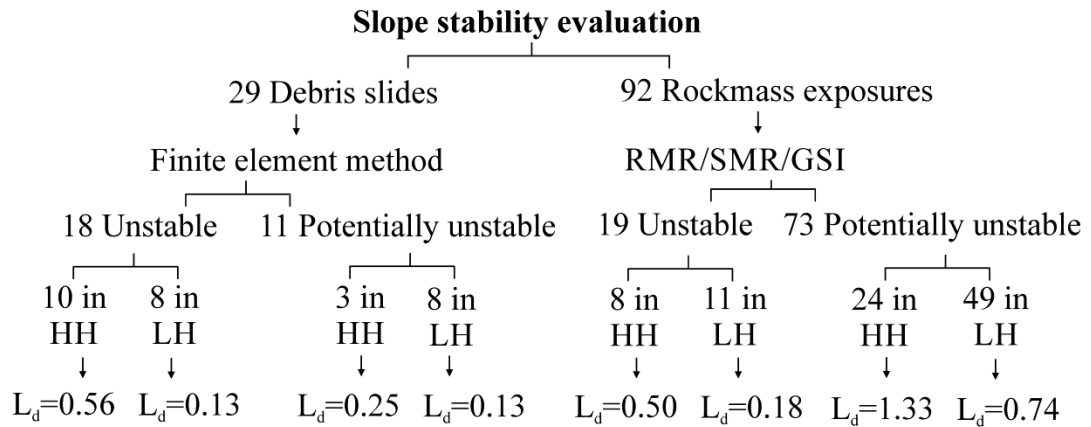


Fig 5.7: Results of slope stability evaluation. HH-Higher Himalaya; LH-Lesser Himalaya; L_d -Landslide density

5.4 Discussion

In the present study, kinematic analyses of 92 rock slopes were carried out based on the orientation of discontinuities with respect to slope angle and direction. Many slopes (59) in the study area fall under the category of ‘low hazard’ and ‘no hazard’ from kinematic analysis of discontinuities, but are ‘unstable’ by the other rock mass classifications (Table 5.5). Therefore, kinematic analysis of discontinuities gives a very conservative estimate of rock mass, on classification in terms of hazard potential. The geomechanical rock mass classification for all the 92 locations based on RMR, SMR and GSI values, which give an account of the condition of the rock mass and its stability, correspond relatively well with each other (Fig. 5.8). The highest and lowest values of GSI (59 and 21 respectively) are noted in the quartzitic rock of the Higher Himalayan Crystallines. Generally, quartzite is not weathered easily, and resistant to erosion. However, in the present scenario the two diverse values have a different story to tell. The low GSI value at location 21 could possibly be due to the highly fractured rock mass with continuous water flowing on the wall of the rock mass at its vicinity (Fig. 5.9a). Such a condition can lead to weathering, thereby making the rock mass weak and prone to slope instability. Hence, the highest potential to slope instability of ‘poor’ rock mass quality is observed here, with a very unstable slope and exceptionally low GSI value of 21. The GSI value empirically obtained (Cai et al., 2007) is near the field range (Marinos and Hoek, 2000).

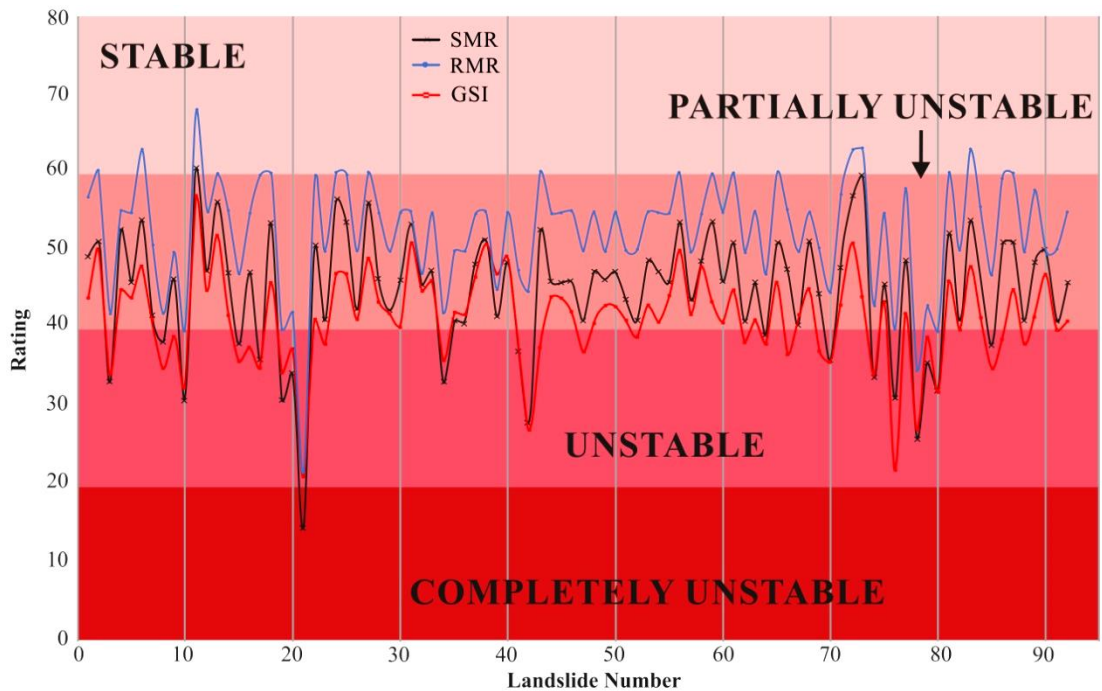


Fig 5.8: Results of rock mass classification using RMR, SMR and GSI

In the LH, a number of sites comprise highly fractured rock mass. Most of these slopes are located along road cuts, where blasting may have contributed to fracturing of the rock mass; the fractured surfaces do not extend for too long (~60 m) in certain locations (Fig. 5.9b). The influence of tectonically active faults in the region, discussed in Chapter 4, cannot be ruled out. The results of GSI has helped in estimating the Hoek and Brown criteria (m_b , a , s) (Table 5.6), which was used for numerical simulation of the rock mass strength parameter.

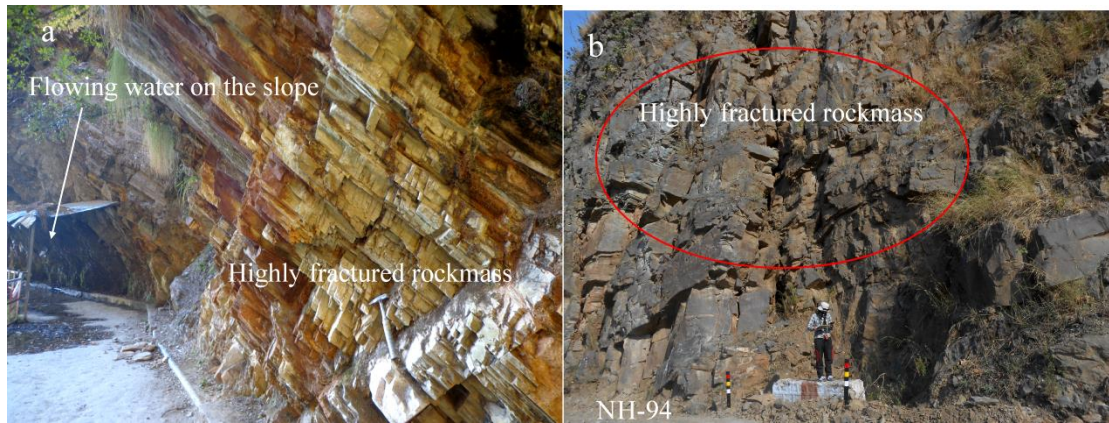


Fig. 5.9: Field exposures: (a) Highly fractured quartzite at location 21; (b) Highly fractured slate along NH-94

The numerical simulation of 29 debris slopes was carried out using FEM, of which, 18 were completely unstable and 11 were potentially unstable (Fig. 5.7). These are based on the SRF of the landslide slopes, which is the FoS of the slope (Griffith and Lane, 1999). Most of the unstable debris slides occur in the Higher Himalayan part of the study area (Fig. 5.7). This is mainly due to the steep gradients and relatively high shearing of the rocks. Gupta et al. (2016b), Jamir et al. (2017) and Kumar et al. (2019) have also observed high instability in other sections of the NW Higher Himalayan terrain. Similar to FEM-based stability evaluation, RMR, SMR and GSI also reveal that the Higher Himalayan slopes in the region, such as at location 21, are also highly unstable. Gupta et al. (2016b) have also observed dominance of rockfalls in the Higher Himalayan region.

Stability evaluation reveals that most of the unstable areas of debris slides and rockfalls lie in the Higher Himalaya. Jamir et al. (In Press) have observed relatively higher tectonic activity in the Higher Himalaya based on evaluation of geomorphic indices and hence, the unstable debris slides and rockfalls may owe their origin to tectonic uplift in the Higher Himalaya. Jaboyedoff et al. (2011) opine that active

tectonics influences slope stability and observed that the FoS is relatively low and displacement higher in the debris slides in the vicinity of the MCT. They ascribe this to tectonic uplift and counteracting gravity, which weakens slopes.

Further, there is a relatively higher volume of debris slides in the Higher Himalaya, where the unstable majority bears a transport-limited condition. Such transport-limited processes (Carson and Kirby, 1972; Arrowsmith et al., 1996) may result in higher sediment discharge from slopes during extreme rainfall or earthquake. The Higher Himalaya in the region constitutes an orographic barrier that receives relatively higher rainfall than the Lesser Himalaya (Jamir et al., In Press). Downstream of the NAT, the region accommodates debris slides with higher FoS and low displacement. It implies that slopes are relatively more stable than that of the Higher Himalaya, possibly due to tectonic and gravitational tranquility (Jaboyedoff et al. 2011).

Rainfall has been observed to affect the stability of slopes by changing the pore-water pressure, thereby promoting short-term failure during incessant rainfall and weathering in the long run (Dykes, 2002; Rahardjo et al., 2005). The NW Higher Himalaya hillslopes are subject to incessant rainfall of the SW monsoon, which results in high hill-slope erosion (Wulf et al., 2012; Kumar et al., 2019). Such hill-slope erosion may be responsible for the higher area and volume of debris slides in the Higher Himalaya.

5.4.1 Scope of the study

Landslides are often ignored and not much action is taken if they are confined to uninhabited areas. However, prior knowledge of susceptible zones and stability conditions would largely avert damage, particularly of portions of highways. Therefore, the ultimate purpose of geotechnical studies and modeling of some unstable slopes was to determine their FoS and propose preventive or mitigation measures to stabilize slopes. Therefore, the Wariya landslide was studied and mitigation measures were proposed, based on the geological and geotechnical conditions.

Slope stability evaluation helped to quantify instability along the weak slopes. The Wariya landslide slope that has a FoS of 1.09 is one of the most critical landslides in

the context of vulnerability. It poses a threat to the highway, residents of Wariya village and their agricultural tracts (Fig. 5.10a). This is a reactivated debris slide comprising a thick over-burden of slope-wash material of augen gneiss and mica schist. This retrogressive slide is subject to failure during intense rainfall (Singh et al., 2016). The possible causes of the slide are as follows:

- The rocks in the vicinity of the village are moderately fractured but highly affected by mechanical and chemical weathering. The northwest facing Wariya slope experiences heavy rainfall during the monsoon and snowfall during winter. The constant freezing and thawing fractures the rocks, which are highly susceptible to weathering during the monsoon and summer.
- Neotectonic activity in the rising Himalaya too has probably contributed to extensive rock fracturing.
- The upper Wariya slope is continuously charged with water from subsurface springs. Poor drainage in the area promotes the percolation of water into the slope material, causing the slope overburden to get oversaturated and prone to failure.
- Subsurface water currents are known to wash away finer sediments through pores, thereby reducing the cohesive nature of slope material. The cohesion of the slope material is 8.8 KPa, with an internal friction angle of 42.3° .
- Active toe erosion by the river has also contributed to slope instability.

In view of the characteristics of the slide and vulnerability it poses, the following remedial/mitigation measures are proposed (Fig. 5.10b).

1. Correcting drainage on the slope and its drainage area

- a. A surface ditch near the crown of the slide is necessary to control surface water. The surface ditch involves cutoff drains that cross the headwall of the slide and lateral drains to lead runoff around the edge of the slide zone. Surface ditches are useful in reducing the potential of surface slumping and preventing infiltration of water into the soil.
- b. Using lined channels to channelize spring waters. Lined channels have rigid boundaries which prevents surface runoff from percolating into the slopes.
- c. Drainage PVC (polyvinyl chloride) pipes can be used to channelize domestic discharge. This will eradicate infiltration into the slopes.

- d. Appropriately placed weep holes in the retaining walls will minimize pore-water pressure due to trapped subsurface water behind the walls.

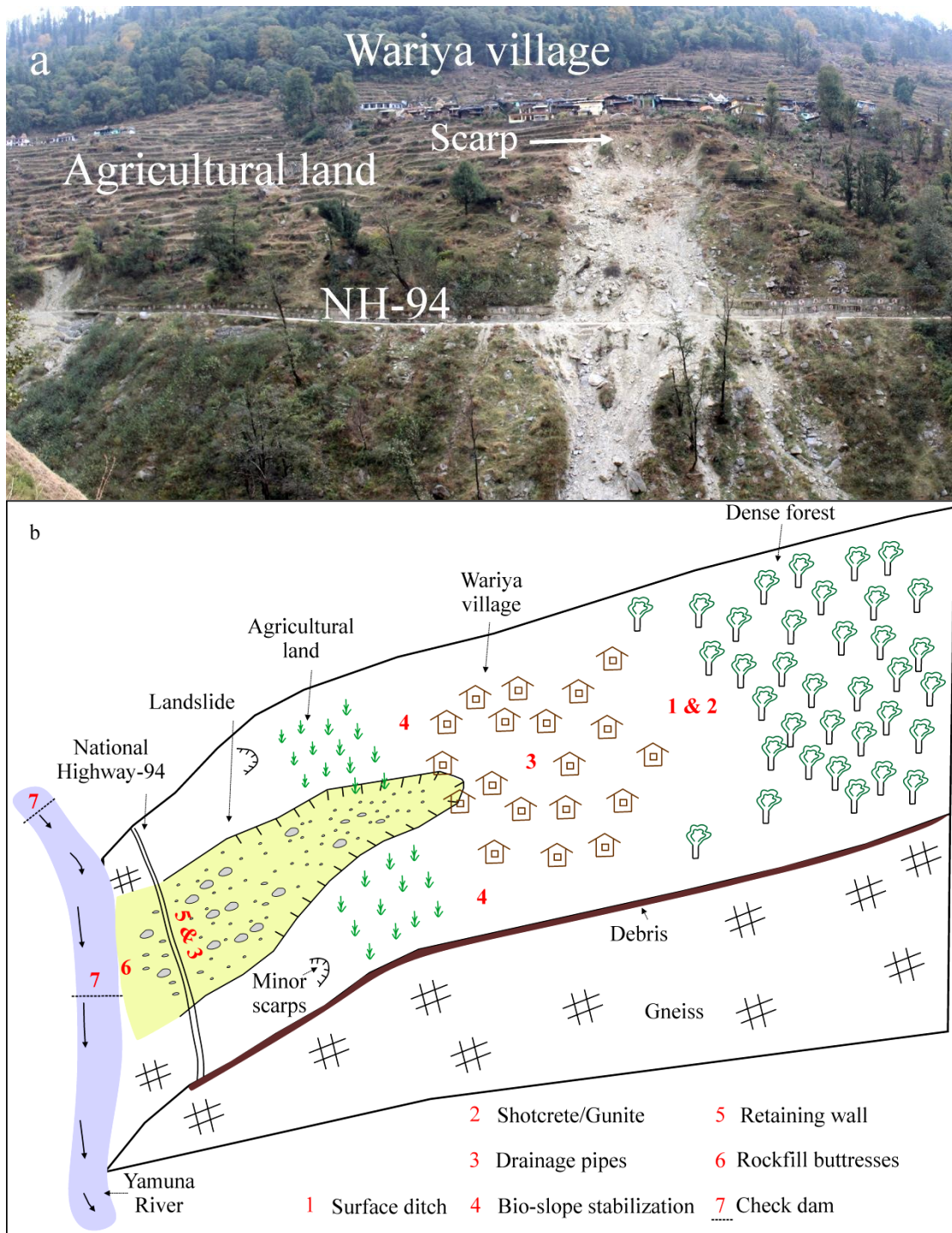


Fig. 5.10: (a) Present landslide at Wariya village; (b) Illustration for remedial/mitigation measures

2. Strengthening the slope, particularly at the crown of the landslide

- a. Shotcrete and/or Gunite into fractured rock masses near the landslide crown will reinforce potential rockfall areas. Shotcrete refers to spraying of concrete

by a dry or wet mix process, whereas gunite refers to dry mix process. While using gunite, water is injected immediately before application. Shotcrete contains aggregates of up to 2 cm in size, whereas gunite has smaller aggregates.

- b.* Wire meshing to hold the material along the crown and scarps. The wires can be nailed to the hillside at suitable places. This would prevent further over steepening of the slopes, which will help in stabilizing the existing slope.

3. Bio-stabilization

- a.* Rehabilitating the slope around the village and agricultural land by using root reinforcement to enhance soil resistance to erosion. In bio-stabilization, vegetation cover such as vetiver grass or other hedges is grown on the slope to enhance the shear strength of slope material. The type of vegetation can vary from locality to locality owing to varying climate and soil conditions.
- b.* Contour plowing to channelize the monsoon water away from the slope. Contour plowing involves planting across the slope along a specific contour line, which creates a water-break to slow down flow of water and prevent the formation of rills and gullies during incessant rainfall runoff.

4. Stabilizing the existing landslide debris

- a.* Retaining walls near the highway and along landslide slopes help protect against casualties and hold slope masses. Retaining walls are structures that are built to stop the progress of debris fall, rockfall or debris slide. Retaining walls can be made of timber, steel beams and reinforced earth material and rocks. The simplest type is the gabion wall that involves 10-20 cm rock blocks in a wired mesh.
- b.* Check dams across the river at strategic locations to reduce the flow velocity of the river. This would prevent further toe erosion of the slopes.
- c.* Rock-fill buttresses at the toe of slide zones restrict toe erosion by rivers. Higher frictional forces among rock fills keep them intact and decrease the shear force of the river on the slope toe.

5.4.2 Limitations

During the study, a few limitations associated with the methods, were observed for which counter measures/explanations are given below.

1. Debris thickness approximation: Though field-based landslide thickness approximation may not replace methods based on borehole and electrical resistivity (Perrone et al., 2014; Senthilkumar et al., 2017), field-based debris thickness approximation was the only viable method; this was also practiced by Larsen and Torres Sanchez (1998) and Guzzetti et al. (2009) considering steep and inaccessible hillslopes.
2. Slope geometry and material property:
 - a. Ideally, a 2D model may not represent the material and geometric variability, as well as stress and displacement in a landslide slope (Liu et al., 2018). However, in absence of subsurface data, mainly due to inaccessibility of the slopes and financial constraints, 3 slope sections were taken at each landslide. Further, material sampling was performed at more than 2 locations to minimize the uncertainty due to material and geometric variability.
 - b. The rock exposures were not large enough to model in view of the resolution of the DEM (10 m). Therefore, slope geometry and material inhomogeneity were not taken into consideration.
 - c. The geomechanical classification system of rock mass does not consider any force acting on the slopes. Hence, the rock masses were not modeled, and in the present study the FoS was not quantified.
3. Remedy and mitigation: Mitigation measures are based on field investigations and previous reports. Subsurface data could not be incorporated due to financial constraints.

Chapter 6

CONCLUSIONS

6.1. Conclusions

Landslides have become a major concern for the socio-economic health of the nation. Therefore, it is important to understand the nature of the landslides and their causes from a geological as well as geotechnical perspective. In the present study, in order to assess the spatial probability of landslide occurrence, a landslide susceptibility map was prepared using the bivariate Frequency Ratio method. The areal distribution of the study area is about 1440.22 km², out of which an area of 4.11 km² is occupied by active landslides. A total of 154 landslides were mapped in the study area. About 55% (789.11 km²) of the total area falls in the Very Low Susceptible zone, followed by 15% (214.62 km²) in the Low Susceptible zone and 10% each in the Very High Susceptible zone (143.08 km²), High Susceptible zone (143.14 km²) and Moderate Susceptible zone (143.89 km²). A major portion of the study area along the southerly and westerly facing slopes, with slope angles ranging from 30°-45°, have a high probability of landslide occurrence. Such slopes are generally observed at high elevations of 1500-2000 m. Landslide incidences are also observed in some low-angle slopes (20°-25°) at relatively lower elevations, which could possibly be due to river erosion of the hillslopes. This is further supported by the presence of high frequency of landslides in the close proximity of drainage. Proximity to lineaments and roads was also noted to play a dominant role in contributing to instability of slopes. This is evident from the highly pulverised rock masses in the regions near faults/thrusts and highly fractured rocks along roads.

The landslide susceptibility map prepared was validated using three approaches. The first approach included partitioning of the landslide database. Here, a high proportion of the sample landslides (21 landslides) occur in the Very High Susceptibility zone and 4 landslides lie in the High Susceptibility zone, which is an indication of the reliability of the procedure. The second approach was the evaluation of the map using the success rate curve, which accounted for 74% accuracy. The susceptibility map generated was successfully validated in the field, which testifies to its accuracy.

The LSM helped demarcate zones that are highly prone to landslides, which indicates the dominant influencing factors in the region. Therefore, in order to ascertain the major causes of landslide in the area, the spatial interrelationship of the causative factors with landslide incidences were analysed in a GIS platform using geomorphic indices as proxies and followed by physical verification in the field. Analytical results indicate that the Higher Himalaya and a part of the Lesser Himalaya, between Wazri (MCT) and Gangani (NAT), are affected by higher uplift and high rainfall. Therefore, landslides constitute the dominant mass wasting process in the area. The occurrence of voluminous landslides ($\sim 10^6 \text{ m}^3$) in this region implies high hillslope erosion. In the Lesser Himalaya, downstream of the Gangani, distinct patterns are observed between Gangani and Naugaon and between Naugaon and Damta. A topographic depression is observed in the former, where the weak rocks in the synclinal structure are considered the primary factor for landslide initiation. A topographic rise (anticlinal structure) is observed in the latter. The local Barni Gad Fault and relatively higher tectonic activity are potential causes for landslides in this area. The upper part of the Higher Himalaya and lower part of the Lesser Himalaya show signs of tectonic uplift that coincide with an abundance of rockfall, whereas dominance of debris slides coincide with regional thrust faults, i.e., MCT and NAT. At the MCT, a possible feedback process involving high precipitation and tectonic uplift is considered to be the main reason of debris slides, whereas at the NAT, rock shearing is the main factor for debris slides.

The delineation of landslides and the identification of possible causative factors for slope failure would not be complete if the slopes were not evaluated for stability. Hence, 29 debris slides and 92 rock exposures were analysed in order to evaluate slope stability. For the debris slides, FEM-based static analysis was performed to determine the FoS of the slopes and for the rocks slopes, kinematic analysis and rock mass classification were carried out. Out of the 29 debris slides, 18 slides are highly unstable ($\text{FoS} \leq 1$) and 11 are potentially unstable ($1 \leq \text{FoS} \leq 2$), with debris volumes of $3.36 \pm 0.9 \times 10^6 \text{ m}^3$ and $1.14 \pm 0.2 \times 10^6 \text{ m}^3$ respectively. Of the 92 rock exposures studied in this study, 19 slopes represent highly unstable conditions with SMR values ranging from 0-20, whereas 73 slopes are potentially unstable with SMR values ranging from 41-60. In the study area, the tectonically active Higher Himalaya portion comprises the highest landslide density ($L_d = 2.64$) as compared to that of the Lesser Himalaya

($L_d=1.18$). The relatively low FoS (0.91 ± 0.03) and higher displacement (4.35 ± 0.95 m) in the debris slides in the MCT region may be the result of interaction between tectonic uplift and counteracting gravity that weakened the slopes.

6.2. Prospects of the work

The ever increasing developmental activities in this part of the Himalayan terrain have grown manifold and hence, identification of landslide prone areas is of utmost importance for any future land use planning and developmental programs. The findings of this study will help the planners and stakeholders to strategize further activities in the area.

Since the study area is still in the initial stages of development, further slope changes by human interference is evident, which will make the weak slopes of the terrain more susceptible to mass wasting. Hence, monitoring the susceptible slopes of this study can help avert major disasters.

The Char Dham Yatra corridor is of strategic importance. However, the rocks, particularly in the Higher Himalaya, dangerously hang over parts of the road (Fig. 5.9). Gupta et al. (2017) have also discussed the vulnerability of the slopes in Higher Himalaya. The rocks of such slopes are therefore, under intense stress, which is compounded by the stresses due to ongoing tectonism. The rocks are further subjected to mechanical and chemical weathering and may disintegrate in the long run. Hence, detailed geotechnical investigations need to be taken up to develop prevention and/or mitigation measures.

This study has future prospects, considering the regional instability regime and their relation with landslide (debris slide) dimensions. These include the evaluation of influence of changing climate on the hill slopes (Ballantyne, 2002; Korup et al., 2010), evaluation of potential landslide damming sites (Kumar et al., 2018b) and evaluation of regional sediment discharge (Hovius et al. 1997).

Remedial/mitigation measures

Landslides are inevitable, and recurring in nature. However, some extent of the impact of the landslide can be reduced by initiating appropriate mitigation measures.

Based on the slope stability analysis and the present scenario of the study area, the following precautionary measures may be taken up.



Fig. 6.1: Overhanging slope along part of the Char Dham Yatra route

Monitoring and forecasting

The areas categorized as landslide susceptible zones must be prioritized and monitored by adopting various methods such as real-time GPS monitoring of the landslides, setting up stations for precipitation monitoring, earthquakes and early warning systems. In the present study area, rainfall is the major trigger for landslides. However, only one station at Barkot monitors rainfall. Given the vast expanse of the region and the highly mountainous terrain, where orographic control of rainfall is the norm, a single monitoring station serves no justifiable purpose. Satellite-based systems provide rainfall data on regional scales, which may not be helpful locally. Hence, a number of rain gauges spread strategically over the region, are the dire need of the hour. Taking the socio-economy into consideration, monitoring should include areas that have suffered landslides in the past, slopes that are highly fractured and/or weathered, slopes under excessive land use, such as dams, quarries, road cuts,

agricultural land, etc. and areas of intense fluvial erosion, besides the active landslides.

Environmental measures

Landslide occurrences are high in barren land and sparsely vegetated regions, particularly along steep slopes. This calls for proper land use planning and effective measures to promote afforestation. Vegetation stabilises the soil surface by the intertwining of the roots, which thereby obstructs the seepage of surface runoff. Depending on the type of slope condition and environment, the type of vegetation adaptable to local conditions may be used. Such bio-slope stabilization is cost-efficient and effective.

Engineering measures

In the areas identified as unstable and partially stable, removal of the overburden / loose rock from potentially unstable slopes is important. Water logging in slopes is one of the most common causes of slope failure. Therefore, it is necessary to have proper drainage systems in place to channelize subsurface water and surface runoff. Surface runoff must be prevented from entering tension cracks or open joints. Subsurface water should not be allowed to saturate the slope material. This may be prevented by properly installing subsurface drains to channelize water safely out, thereby reducing undesirable pore pressure.

The slopes in the proximity of streams are most prone to toe cutting. This may be prevented by constructing grip walls or rock-filled buttresses at the toe of susceptible slopes. In the exposed rock masses, particularly at the crowns of slides where tension cracks and fractures are common, shotcreting, involving spraying of impermeable material such as mortar or asphalt into the fractures, is useful. Retaining walls have been successfully used in areas with sufficient space at the toes of slopes. Such restraining structures are particularly useful where slopes are rendered unstable due to slope cuts for roads. They help increase the shearing resistance in the uphill slope material and thus, prevent further sliding. Weep-holes through retaining walls are a must. These consist of drainage pipes slightly tilted toward the road, through which excess subsurface water from the uphill sides are drained out. This helps in reducing pore pressure in the slope material, which suitably increases their shearing strength.

Lined drains should be constructed all along the roads, which will channelize water to safe areas. Appropriately placed culverts along road sections is very important. All surface waters should be trained into the culverts.

Social awareness

Social awareness is of utmost importance, as lives and property are at stake during landslides. People should be made aware of the dangers posed by erecting structures in vulnerable areas. Proper construction and maintenance of drainage is an important area of awareness. Knowledge on proper land use practice for site specific slopes, depending on the nature of the slopes, should be shared with the people.

BIBLIOGRAPHY

- Agarwal, N.C., Kumar, G., 1973. Geology of the upper Bhagirathi and Yamuna Valleys, Uttarkashi district, Kumaun Himalaya. *Himalayan Geology* 3, 2-23.
- Aier, I., Singh, M.P., Thong, G.T., Ibotombi, S., 2012. Instability analyses of Merhülietsa slide, Kohima, Nagaland. *Natural hazards* 60(3), 1347-1363.
- Akgun, A., 2012. A comparison of landslide susceptibility maps produced by logistic regression, multi-criteria decision, and likelihood ratio methods: a case study at İzmir, Turkey. *Landslides* 9, 93–106.
- Aleotti, P., Chowdhury, R., 1999. Landslide hazard assessment: summary review and new perspectives. *Bull. Eng. Geol. Environ.* 58, 21–44.
- Alexander, D., Formichi, R., 1993. Tectonic causes of landslides. *Earth Surf. Process. Landforms* 18, 311–338.
- Anantharaman, M.S., 1980. Landslides, The tragedy of Garhwal Himalaya. *The Himachal XXXII*, 19.
- Anbalagan, R., 1992. Landslide hazard evaluation and zonation mapping in mountainous terrain. *Engineering Geology* 32(4), 269-277.
- Anbalagan, R., Kumar, R., Lakshmanan, K., Parida, S., Neethu, S., 2015. Landslide hazard zonation mapping using frequency ratio and fuzzy logic approach, a case study of Lachung Valley, Sikkim. *Geoenvironmental Disasters* 2(1), 6.
- Anbalagan, R., Singh, B., 1996. Landslide hazard and risk assessment mapping of mountainous terrains - a case study from Kumaun Himalaya, India. *Engineering Geology* 43, 237–246.
- Arita, K., 1983. Origin of the inverted metamorphism of the Lower Himalayas, central Nepal. *Tectonophysics* 95(1-2), 43-60.
- Arrowsmith, J.R., Pollard, D.D., Rhodes, D.D., 1996. Hillslope development in areas of active tectonics. *Journal of Geophysical Research: Solid Earth* 101(B3), 6255-6275.
- Ashby, J., 1971. Sliding and toppling modes of failure in models and jointed rock slopes. Imperial College, University of London.
- Auden, J.B., 1934. The geology of the Krol belt. *Rec. Geol. Surv. India* 67(4), 357-454.
- Auden, J.B., 1935. Traverses in the Himalaya. *Records of Geological survey of India* 69, 123-167.

- Auden, J.B., 1936. Dehra Dun district and Tehri-Garhwal state, United Provinces. Records Geol. Surv. India 71(1), 73-75.
- Auden, J.B., 1949. A geological discussion on the Satpura hypothesis and Garo-Rajmahal gap. Proceedings, National Institute of Science of India, Geological Survey of India, Bangalore, Karnataka, 315-340.
- Ayalew, L., Yamagishi, H., 2005. The application of GIS-based logistic regression for landslide susceptibility mapping in the Kakuda-Yahiko Mountains, Central Japan. *Geomorphology* 65(1-2), 15-31.
- Aydin, A., 2008. ISRM Suggested Method for Determination of the Schmidt Hammer Rebound Hardness: Revised Version, in: *The ISRM Suggested Methods for Rock Characterization, Testing and Monitoring: 2007-2014*. Springer International Publishing, Cham, 25–33.
- Aydin, A., Basu, A., 2005. The Schmidt hammer in rock material characterization. *Engineering Geology* 81(1), 1-14.
- Ballantyne, C.K., 2002. Paraglacial geomorphology. *Quat. Sci. Rev.* 21, 1935–2017.
- Barton, N., 1973. Review of a new shear-strength criterion for rock joints. *Engineering Geology* 7(4), 287-332.
- Barton, N., Bandis, S., 1982. Effects of block size on the shear behavior of jointed rock. In *The 23rd US symposium on rock mechanics (USRMS)*. American Rock Mechanics Association.
- Barton, N., Bandis, S.C., 1990. Review of predictive capabilities of JRC-JCS model in engineering practice. In *Rock Joints, Proc int symp on rock joints, Loen, Norway* (eds N. Barton and O. Stephenson) 603-610.
- Barton, N., Choubey, V., 1977. The shear strength of rock joints in theory and practice. *Rock Mechanics and Rock Engineering* 10 (1-2), 1–54.
- Barton, N., Lien, R. and Lunde, J., 1974. Engineering classification of rock masses for the design of tunnel support. *Rock mechanics* 6(4), 189-236.
- Barton, N., Stephansson, O., 1990. Rock joints: proceedings of the International Symposium on Rock Joints, Loen, Norway, 4-6 June, 1990. A.A. Balkema.
- Barton, N.R., 1972, September. A model study of rock-joint deformation. In *International Journal of Rock Mechanics and Mining Sciences & Geomechanics Abstracts* 9 (5), 579-582. Pergamon.

- Baum, R. L., Savage, W. Z., Godt, J. W., 2002. TRIGRS – a FORTRAN program for transient rainfall infiltration and grid-based regional slope stability analysis, US Geological Survey Open-File Report 2002-424, 38.
- Beggs, J.S., 1983. Kinematics. Hemisphere Pub. Corp, Washington, New York, London.
- Bernardi De León, R., 2009. Road development in Podocarpus National Park: an assessment of threats and opportunities. *Journal of sustainable forestry* 28(6-7), 735-754.
- Bhargava, O.N., 1972. A reinterpretation of the Krol Belt. *Himalayan Geology* 2, 47-81.
- Bhasin, R., Kaynia, A.M., 2004. Static and dynamic simulation of a 700-m high rock slope in western Norway. *Engineering Geology* 71, 213–226.
- Bhattacharya, A.R., Weber, K., 2004. Fabric development during shear deformation in the Main Central Thrust zone, NW-Himalaya, India. *Tectonophysics* 387(1-4), 23-46.
- Bieniawski, Z.T., 1976. Rock mass classification in rock engineering applications. In *Proceedings of a Symposium on Exploration for Rock Engineering* 12, 97-106.
- Bieniawski, Z.T., 1979. The geomechanics classification in rock engineering applications. In *4th ISRM Congress. International Society for Rock Mechanics*.
- Bieniawski, Z.T., 1989. *Engineering rock mass classifications: a complete manual for engineers and geologists in mining, civil, and petroleum engineering*. John Wiley & Sons.
- Bin, Chen, A., Jiang, W., Chen, Z., 2017. The response of vegetation growth to shifts in trend of temperature in China. *J. Geogr. Sci.* 27, 801–816.
- Biyani, A. K., 1995. Structural and metamorphic history of Higher Himalayan Zone of Phulchatti to Yamunotri area, with special reference to Main Central Thrust in Garhwal Himalaya. Unpublished D. Phil, thesis, HNB Garhwal University, Srinagar.
- Blöthe, J.H., Korup, O., Schwanghart, W., 2015. Large landslides lie low: Excess topography in the Himalaya-Karakoram ranges. *Geology* 43, 523–526.
- Borgatti, L., Soldati, M., 2010. Landslides as a geomorphological proxy for climate change: A record from the Dolomites (northern Italy). *Geomorphology* 120, 56–64.

- Bouchez, J.L., Pecher, A., 1981. The Himalayan Main Central Thrust pile and its quartz-rich tectonites in central Nepal. *Tectonophysics* 78(1-4), 23-50.
- Bowles, L.E., 1996. *Foundation analysis and design*. McGraw-hill.
- Brabb, E.E., 1993. Proposal for worldwide landslide hazard maps. In *Seventh International Conference and Field Workshop on Landslides in Czech and Slovak Republics*, 15-27.
- Brabb, E.E., Pampeyan, E.H., Bonilla, M.G., 1972. Landslide susceptibility in San Mateo County, California (No. 360).
- Brand, E.W., 1988. Landslide risk assessment in Hong Kong. In *Proceedings 5th International Symposium on Landslides, Lausanne*, 1, 1059-1074.
- Brookfield, M.E., 1998. The evolution of the great river systems of southern Asia during the Cenozoic India-Asia collision: rivers draining southwards. *Geomorphology* 22 (3-4), 285-312.
- Bull, W.B., 2009. *Tectonically active landscapes* (1st Edn.). West Sussex, UK: John Wiley and Sons.
- Bull, W.B., 2011. *Tectonically active landscapes*. John Wiley & Sons.
- Bull, W.B., McFadden, L.D., 1977. Tectonic geomorphology north and south of the Garlock Fault, California. *Geomorphol. Arid Reg.*, 115–138.
- Burbank, D.W., 2002. Rates of erosion and their implications for exhumation. *Mineral. Mag.* 66, 25–52.
- Burbank, D.W., Anderson, R.S, 2011. *Tectonic geomorphology*. John Wiley & Sons, 460.
- Burbank, D.W., Leland, J., Fielding, E., Anderson, R.S., Brozovic, N., Reid, M.R., Duncan, C., 1996. Bedrock incision, rock uplift and threshold hillslopes in the northwestern Himalayas. *Nature* 379, 505–510.
- Burchfiel, B.C., Zhiliang, C., Hodges, K. V, Yuping, L., Royden, L.H., Changrong, D., Jiene, X., 1992. The South Tibetan Detachment System, Himalayan Orogen: Extension Contemporaneous With and Parallel to Shortening in a Collisional Mountain Belt, in: *Geological Society of America Special Papers* 1–41.
- Cai, M., Kaiser, P.K., Tasaka, Y., Minami, M., 2007. Determination of residual strength parameters of jointed rock masses using the GSI system. *International Journal of Rock Mechanics and Mining Sciences* 44(2), 247-265.
- Cai, M., Kaiser, P.K., Uno, H., Tasaka, Y., Minami, M., 2004. Estimation of rock mass deformation modulus and strength of jointed hard rock masses using the

- GSI system. *International Journal of Rock Mechanics and Mining Sciences* 41(1), 3-19.
- Can, T., Nefeslioglu, H.A., Gokceoglu, C., Sonmez, H., Duman, T.Y., 2005. Susceptibility assessments of shallow earthflows triggered by heavy rainfall at three catchments by logistic regression analyses. *Geomorphology* 72(1-4), 250-271.
- Carlton, B.D., Price, K., Vanneste, M., Forsberg, C.F., 2017. Development and application of a regional slope stability assessment screening tool, in: *Advances in Natural and Technological Hazards Research*. Springer, Cham, 267–276.
- Carrara, A., 1983. Multivariate models for landslide hazard evaluation. *Journal of the International Association for Mathematical Geology* 15(3), 403-426.
- Carrara, A., Cardinali, M., Detti, R., Guzzetti, F., Pasqui, V., Reichenbach, P., 1991. GIS techniques and statistical models in evaluating landslide hazard. *Earth surface processes and landforms* 16(5), 427-445.
- Carrara, A., Pike, R.J., 2008. GIS technology and models for assessing landslide hazard and risk. *Geomorphology* 94 (3-4), 257-260.
- Cascini, L., 2008. Applicability of landslide susceptibility and hazard zoning at different scales. *Engineering Geology* 102, 164–177.
- Cascini, L., Ciurleo, M., Di Nocera, S., Gullà, G., 2015. A new–old approach for shallow landslide analysis and susceptibility zoning in fine-grained weathered soils of southern Italy. *Geomorphology* 241, 371–381.
- Chang, K.T., Wan, S., Lei, T.C., 2010. Development of a spatial decision support system for monitoring earthquake-induced landslides based on aerial photographs and the finite element method. *International journal of applied earth observation and geoinformation* 12(6), 448-456.
- Chen, M., Xie, P., Janowiak, J.E., Arkin, P.A., 2002. Global land precipitation: A 50-yr monthly analysis based on gauge observations. *Journal of Hydrometeorology* 3(3), 249-266.
- Chen, W., Chai, H., Sun, X., Wang, Q., Ding, X., Hong, H., 2016. A GIS-based comparative study of frequency ratio, statistical index and weights-of-evidence models in landslide susceptibility mapping. *Arabian Journal of Geosciences* 9(3), 204.

- Cheng, Y.M., Lansivaara, T., Wei, W.B., 2007. Two-dimensional slope stability analysis by limit equilibrium and strength reduction methods. *Computers and Geotechnics* 34(3), 137-150.
- Choubey, V.D., Litoria, P.K., 1990, August. Landslide hazard zonation in the Garhwal Himalaya, a terrain evaluation approach. In 6th IAEG Congress, 1, 65-72. Balkema Rotterdam.
- Chung, C.J.F., Fabbri, A.G., 1999. Probabilistic prediction models for landslide hazard mapping. *Photogrammetric engineering and remote sensing* 65(12), 1389-1399.
- Chung, C.-J.F., Fabbri, A.G., 2003. Validation of Spatial Prediction Models for Landslide Hazard Mapping *Nat. Hazards* 30, 451–472.
- Clarke, B.A., Burbank, D.W., 2010. Bedrock fracturing, threshold hillslopes, and limits to the magnitude of bedrock landslides. *Earth Planet. Sci. Lett.* 297, 577–586.
- Clough, R.W., 1980. The finite element method after twenty-five years: A personal view. *Comput. Struct.* 12, 361–370.
- Coulomb, C.A., 1776. An attempt to apply the rules of maxima and minima to several problems of stability related to architecture. *Mémoires de l'Académie Royale des Sciences*, 7, 343-382.
- Courant, R., 1943. Variational methods for the solution of problems of equilibrium and vibrations, *Bulletin of the American Mathematical Society*. Washington.
- Crozier, M.J., 2010. Deciphering the effect of climate change on landslide activity: A review. *Geomorphology* 124, 260–267.
- Cruden, D.M., 1978. A method of distinguishing between single and double plane sliding of tetrahedral wedges. In *International Journal of Rock Mechanics and Mining Sciences and Geomechanics Abstracts* 15(4), 217-217. Elsevier Science.
- Cruden, D.M., 1991. A simple definition of a landslide." *Bulletin of Engineering Geology and the Environment* 43(1), 27-29.
- Cruden, D.M., Varnes, D.J., 1996. Landslides: investigation and mitigation. Chapter 3-Landslide types and processes. *Spec. Rep. - Natl. Res. Counc. Transp. Res. Board*.
- Dai, F.C., Lee, C.F., 2002. Landslide characteristics and slope instability modeling using GIS, Lantau Island, Hong Kong. *Geomorphology* 42(3-4), 213-228.

- Dai, F.C., Lee, C.F., Li, J.X.Z.W., Xu, Z.W., 2001. Assessment of landslide susceptibility on the natural terrain of Lantau Island, Hong Kong. *Environmental Geology* 40(3), 381-391.
- Dai, F.C., Lee, C.F., Ngai, Y.Y., 2002. Landslide risk assessment and management: an overview. *Engineering Geology* 64(1), 65-87.
- Das, B.M., 2002. Soil mechanics laboratory manual, 35-44. New York, USA: Oxford university press.
- Das, I., Sahoo, S., van Westen, C., Stein, A., Hack, R., 2010. Landslide susceptibility assessment using logistic regression and its comparison with a rock mass classification system, along a road section in the northern Himalayas (India). *Geomorphology* 114, 627–637.
- Dawson, E.M., Roth, W.H., Drescher, A., 1999. Slope stability analysis by strength reduction. *Geotechnique* 49(6), 835-840.
- Day, M.J., Goudie, A.S., 1977. Field assessment of rock hardness using the Schmidt test hammer. *British Geomorphology Research Group Technical Bulletin* 18, 19-29.
- Deere, D.U., 1968. Geological consideration. *Rock mechanics in engineering practice*.
- Deere, D.U., Miller, R.P., 1966. Engineering classification and index properties for intact rock. *Illinois Univ At Urbana Dept Of Civil Engineering*.
- Deering, D.W., 1978. Rangeland reflectance characteristics measured by aircraft and spacecraft sensors. *Texas A&M Univ. Texas A & M University*.
- Dhakal, A.S., Amada, T., Aniya, M., 2000. Landslide hazard mapping and its evaluation using GIS: an investigation of sampling schemes for a grid-cell based quantitative method. *Photogrammetric Engineering and Remote Sensing* 66(8), 981-989.
- Dhondial, D.P., Ali, K.N., 1967. General Report of GSI for 1964-65. *Rec. Geol. Surv. Ind*, 99(1), 35-36.
- Ding, Q., Chen, W., Hong, H., 2017. Application of frequency ratio, weights of evidence and evidential belief function models in landslide susceptibility mapping. *Geocarto international* 32(6), 619-639.
- Dobhal, D.P., Gupta, A.K., Mehta, M., Khandelwal, D.D., 2013. Kedarnath disaster: facts and plausible causes. *Current Science* 105(2), 171-174.

- Duman, T.Y., Can, T., Gokceoglu, C., Nefeslioglu, H.A., Sonmez, H., 2006. Application of logistic regression for landslide susceptibility zoning of Cekmece Area, Istanbul, Turkey. *Environmental Geology* 51(2), 241-256.
- Duncan, J.M., 1996. State of the art: limit equilibrium and finite-element analysis of slopes. *Journal of Geotechnical engineering* 122(7), 577-596.
- Dykes, A.P., 2002. Weathering-limited rainfall-triggered shallow mass movements in undisturbed steepland tropical rainforest. *Geomorphology* 46(1-2), 73-93.
- Eberhardt, E., Stead, D., Coggan, J.S., 2004. Numerical analysis of initiation and progressive failure in natural rock slopes—the 1991 Randa rockslide. *Int. J. Rock Mech. Min. Sci.* 41, 69–87.
- Ercanoglu, M., Gokceoglu, C., 2004. Use of fuzzy relations to produce landslide susceptibility map of a landslide prone area (West Black Sea Region, Turkey). *Engineering Geology* 75(3-4), 229-250.
- Erener, A., Lacasse, S., Kaynia, A.M., 2007. Hazard Mapping by Frequency Ratio Approach using GIS. In *Proceedings of CIG/ISPRS Conference on Geomatics for Disaster and Risk Mitigation*, Toronto, Canada, 23-25.
- Fabbri, A.G., Chung, C.J.F., Cendrero, A., Remondo, J., 2003. Is prediction of future landslides possible with a GIS?. *Natural Hazards* 30(3), 487-503.
- Fell, R., Whitt, G., Miner, T., Flentje, P., 2008. Guidelines for landslide susceptibility, hazard and risk zoning for land use planning. *Engineering Geology* 102, 83–84.
- Fernandes, N.F., Guimarães, R.F., Gomes, R.A., Vieira, B.C., Montgomery, D.R., Greenberg, H., 2004. Topographic controls of landslides in Rio de Janeiro: field evidence and modeling. *Catena* 55(2), 163-181.
- Fisher, G.B., Amos, C.B., Bookhagen, B., Burbank, D.W., Godard, V., 2012. Channel widths, landslides, faults, and beyond: The new world order of high-spatial resolution Google Earth imagery in the study of earth surface processes 1–22.
- Flint, J.J., 1974. Stream gradient as a function of order, magnitude, and discharge. *Water Resour. Res.* 10(5), 969-973.
- Fredlund, D.G., Krahn, J., 1977. Comparison of slope stability methods of analysis. *Can. Geotech. J.* 14, 429–439.
- Gadgil, S., 2003. The Indian monsoon and its variability. *Annu. Rev. Earth Planet. Sci.* 31, 429–467.
- Gansser, A., 1964. *Geologic History of the Himalaya*. Interscience Publishers, London, 235–245.

- Gariano, S.L., Guzzetti, F., 2016. Landslides in a changing climate. *Earth-Science Rev.* 162, 227-252.
- Garzanti, E., Baud, A., Mascle, G., 1987. Sedimentary record of the northward flight of India and its collision with Eurasia (Ladakh Himalaya, India). *Geodinamica Acta*, 1(4-5), 297-312.
- Ghosh, S., Van Westen, C.J., Carranza, E.J.M., Ghoshal, T.B., Sarkar, N.K., Surendranath, M., 2009. A quantitative approach for improving the BIS (Indian) method of medium-scale landslide susceptibility. *Journal of the Geological Society of India* 74(5), 625.
- Glade, T., Crozier, M. J., 2005. A review of scale dependency in landslide hazard and risk analysis. *Landslide hazard and risk* 75, 138.
- Gökceoglu, C., Aksoy, H., 1996. Landslide susceptibility mapping of the slopes in the residual soils of the Mengen region (Turkey) by deterministic stability analyses and image processing techniques. *Engineering Geology* 44(1-4), 147-161.
- Goodman, R.E., 1989. *Introduction to rock mechanics* (Vol. 2). New York: Wiley.
- Goodman, R.E., Bray, J.W., 1976. *Toppling of Rock Slopes*. Toppling rock slopes.
- Goodman, R.E., Taylor, R.L., Brekke, T.L., 1968. A model for the mechanics of jointed rock. *Journal of Soil Mechanics & Foundations Div.*
- Gorum, T., Fan, X., van Westen, C.J., Huang, R.Q., Xu, Q., Tang, C., Wang, G., 2011. Distribution pattern of earthquake-induced landslides triggered by the 12 May 2008 Wenchuan earthquake. *Geomorphology* 133(3-4), 152-167.
- Goudie, A.S., 2016. Quantification of rock control in geomorphology. *Earth-science reviews* 159, 374-387.
- Gregory, D.I., Schumm, S.A., 1987. The effect of active tectonics on alluvial river morphology. In *River Channels: Environment and Process* 18, 41-68. Blackwell Oxford.
- Griesbach, C.L., 1880. Palaeontological notes on the Lower Trias of the Himalayas. *Records of the Geological Survey of India* 13(2), 94-113.
- Griesbach, C.L., 1891. *Geology of the central Himalayas*. Office of the Geological Survey.
- Griffiths, D. V., Fenton, G.A., 2004. Probabilistic Slope Stability Analysis by Finite Elements. *J. Geotech. Geoenvironmental Eng.* 130, 507–518
- Griffiths, D. V., Lane, P.A., 1999. Slope stability analysis by finite elements. *Géotechnique* 49, 387–403.

- Griffiths, D. V., Marquez, R.M., 2007. Three-dimensional slope stability analysis by elasto-plastic finite elements. *Géotechnique* 57, 537–546.
- Grohmann, C.H., Smith, M.J., Riccomini, C., 2011. Multiscale analysis of topographic surface roughness in the Midland Valley, Scotland. *IEEE Transactions on Geoscience and Remote Sensing* 49(4), 1200-1213.
- Gupta V., Jamir I., Kumar V., Devi M., 2017. Geomechanical characterization of slopes for assessing rockfall hazards between Janki Chatti and Yamunotri Temple, Yamuna valley, Higher Himalaya, India. *Himalayan Geology* 38 (2), 156-170.
- Gupta, R.P., Joshi, B.C., 1990. Landslide hazard zoning using the GIS approach—a case study from the Ramganga catchment, Himalayas. *Engineering Geology* 28(1-2), 119-131.
- Gupta, V. 1998. Structure and geomorphology of the Upper Satluj Valley, District Kinnaur, Himachal Pradesh with special reference to landslides. Unpublished D. Phil. thesis, HNB Garhwal University, Srinagar, India.
- Gupta, V., 2005. The relationship between tectonic stresses, joint patterns and landslides in the higher Indian Himalaya. *J. Nepal Geol. Soc.* 31, 51-58.
- Gupta, V., 2009. Non-destructive testing of some Higher Himalayan Rocks in the Satluj Valley. *Bull. Eng. Geol. Environ.* 68(3), 409-416.
- Gupta, V., Bhasin, R.K., Kaynia, A.M., Kumar, V., Saini, A.S., Tandon, R.S., Pabst, T., 2016a. Finite element analysis of failed slope by shear strength reduction technique: a case study for Surabhi Resort Landslide, Mussoorie township, Garhwal Himalaya. *Geomatics, Nat. Hazards Risk* 7, 1677–1690.
- Gupta, V., Mahajan, A.K., Thakur, V.C., 2015. A study on landslides triggered during Sikkim earthquake of September 18, 2011. *Himalayan Geology* 36, 81-90.
- Gupta, V., Nautiyal, H., Kumar, V., Jamir, I., Tandon, R.S., 2016b. Landslide hazards around Uttarkashi township, Garhwal Himalaya, after the tragic flash flood in June 2013. *Nat. Hazards* 80, 1689–1707.
- Gupta, V., Sah, M.P., 2008a. The relationship between Main Central Thrust (MCT) and the spatial distribution of mass movement in the Satluj valley, northwestern Higher Himalaya, India. *Zeitschrift für Geomorphol.* 52, 169–179.
- Gupta, V., Sah, M.P., 2008b. Spatial variability of mass movements in the Satluj Valley, Himachal Pradesh during 1990 ~ 2006. *J. Mt. Sci.* 5, 38–51.

- Gupta, V., Tandon, R.S., 2015. Kinematic rockfall hazard assessment along a transportation corridor in the Upper Alaknanda valley, Garhwal Himalaya, India. *Bulletin of Engineering Geology and the Environment* 74(2), 315-326.
- Guzzetti, F., Ardizzone, F., Cardinali, M., Rossi, M., Valigi, D., 2009. Landslide volumes and landslide mobilization rates in Umbria, central Italy. *Earth Planet. Sci. Lett.* 279, 222–229.
- Guzzetti, F., Cardinali, M., Reichenbach, P., Carrara, A., 2000. Comparing landslide maps: A case study in the upper Tiber River Basin, central Italy. *Environmental management* 25(3), 247-263.
- Guzzetti, F., Carrara, A., Cardinali, M., Reichenbach, P., 1999. Landslide hazard evaluation: a review of current techniques and their application in a multi-scale study, Central Italy. *Geomorphology* 31, 181–216.
- Guzzetti, F., Reichenbach, P., Cardinali, M., Galli, M., Ardizzone, F., 2005. Probabilistic landslide hazard assessment at the basin scale. *Geomorphology* 72(1-4), 272-299.
- Hack, J.T., 1973. Stream-profile analysis and stream-gradient index. *Journal of Research of the US Geological Survey* 1(4), 421-429.
- Harmon, R.S., Doe III, W.W., Doe, W.W. eds., 2001. *Landscape erosion and evolution modeling*. Springer Science & Business Media.
- Harrison, T.M., Grove, M., Lovera, O.M., Catlos, E.J., D'Andrea, J., 1999. The origin of Himalayan anatexis and inverted metamorphism: models and constraints. *Journal of Asian Earth Sciences* 17(5-6), 755-772.
- Harvey, J.E., Burbank, D.W., Bookhagen, B., 2015. Along-strike changes in Himalayan thrust geometry: Topographic and tectonic discontinuities in western Nepal. *Lithosphere* 7, 511–518.
- Hayden, H.H., 1904. The geology of Spiti, with part of Burshar and Rupshu. *Mem. Geol. Surv. India* 36, 1-129.
- Hazarika, D., Wadhawan, M., Paul, A., Kumar, N., Borah, K., 2017. Geometry of the Main Himalayan Thrust and Moho beneath Satluj valley, northwest Himalaya: Constraints from receiver function analysis. *J. Geophys. Res. Solid Earth* 122, 2929–2945.
- Heim, A. and Gansser, A., 1939. Central Himalaya, Geological observation of Swiss Expedition in 1936. *Mem. Soc. Helv. Sci. Nat.* 73, 1-245

- Henriques, C., Zêzere, J.L., Marques, F., 2015. The role of the lithological setting on the landslide pattern and distribution. *Engineering Geology* 189, 17–31.
- Hetherington, R.M., 2014. Slope stability analysis of Mount Meager, south-western British Columbia, Canada.
- Hocking, G., 1976. A method for distinguishing between single and double plane sliding of tetrahedral wedges. In *International Journal of Rock Mechanics and Mining Sciences & Geomechanics Abstracts* Vol. 13 (7), 225-226. Pergamon.
- Hodges, K.V., 2000. Tectonics of the Himalaya and southern Tibet from two perspectives. *Geological Society of America Bulletin* 112(3), 324-350.
- Hodges, K.V., Wobus, C., Ruhl, K., Schildgen, T., Whipple, K., 2004. Quaternary deformation, river steepening, and heavy precipitation at the front of the Higher Himalayan ranges. *Earth and Planetary science letters* 220(3-4), 379-389.
- Hoek E., Bray, J W., 1981. *Rock Slope engineering*, Institute of Mining and Metallurgy. Institution of Mining and Metallurgy. London
- Hoek, E., 1988. The Hoek-Brown failure criterion-a 1988 update. In *Proc. 15th Canadian Rock Mech. Symp.* 31-38. Toronto, Dept. Civil Engineering, University of Toronto.
- Hoek, E., 1994. Strength of rock and rock masses. *ISRM News Journal* 2(2), 4-16.
- Hoek, E., 1998. Tunnel support in weak rock. In *Keynote address, Symposium of Sedimentary Rock Engineering*, Taipei, Taiwan 12.
- Hoek, E., Brown, E.T., 1980. Empirical strength criterion for rock masses. *Journal of Geotechnical and Geoenvironmental Engineering* 106(ASCE 15715).
- Hoek, E., Brown, E.T., 1997. Practical estimates of rock mass strength. *International journal of rock mechanics and mining sciences* 34(8), 1165-1186.
- Hoek, E., Carranza-Torres, C., Corkum, B., 2002. Hoek-Brown failure criterion-2002 edition. *Proceedings of NARMS-Tac*, 1, 267-273.
- Hoek, E., Diederichs, M.S., 2006. Empirical estimation of rock mass modulus. *International journal of rock mechanics and mining sciences* 43(2), 203-215.
- Hoek, E., Kaiser, P.K., Bawden, W.F., 1995. *Support of Underground Excavations in Hard Rock* AA Balkema. Rotterdam/Brookfield.
- Holland, T.H., 1908. On the occurrence of striated boulders in the Blaini Formation of Simla, with a discussion of the geological age of the beds. *Records of the Geological Survey of India* 37(3), 129-135.

- Hoover Mackin, J., 1948. Concept of the graded river. Geological Society of America Bulletin 59(5), 463-512.
- Hovius, N., Stark, C.P., Allen, P.A., 1997. Sediment flux from a mountain belt derived by landslide mapping. *Geology* 25, 231.
- Howard, A.D., Kerby, G., 1983. Channel changes in badlands. *Geol. Soc. Am. Bull.* 94, 739.
- Hungr, O., Leroueil, S., Picarelli, L., 2012. Varnes classification of landslide types, an update. In 11th International Symposium on Landslides 1,47-58. CRC Press Taylor&Francis Group.
- Hungr, O., Leroueil, S., Picarelli, L., 2014. The Varnes classification of landslide types, an update. *Landslides* 11 (2), 167-194.
- Hutchinson, J.N., 1995. Landslide hazard assessment. *Landslides* 1805-1841.
- Islam, R., Gururajan, N.S., 2003. Geochemistry, petrogenesis and tectonic setting of Akpa-Rakcham granites of Sutlej valley, Himachal Pradesh, India. *Himal. Geol.* 24, 63–76.
- Ives, J.D., Messerli, B., 1981. Mountain hazards mapping in Nepal introduction to an applied mountain research project. *Mountain Research and Development* 223-230.
- Jaboyedoff, M., Crosta, G.B., Stead, D., 2011. Slope tectonics: a short introduction. Geological Society, London, Special Publications, 351(1), 1-10.
- Jackson, R.D., Huete, A.R., 1991. Interpreting vegetation indices. *Prev. Vet. Med.* 11, 185–200.
- Jain, A.K., 1971. Stratigraphy and tectonics of lesser Himalayan region of Uttarkashi, Garhwal Himalaya. *Himalayan Geology* 1, 25-58.
- Jamir, I., Gupta, V., Kumar, V., Thong, G.T., 2017. Evaluation of potential surface instability using finite element method in Kharsali Village, Yamuna Valley, Northwest Himalaya. *J. Mt. Sci.* 14, 1666–1676.
- Jamir, I., Gupta, V., Kumar, V., Thong, G.T., Inter- and intra-relationship of landslides; Case study of Yamuna valley, Northwest Himalaya. *Physical Geography* (In press)
- Jang, H.S., Kang, S.S., Jang, B.A., 2014. Determination of joint roughness coefficients using roughness parameters. *Rock mechanics and rock engineering* 47(6), 2061-2073.

- Jang, H.S., Kang, S.S., Jang, B.A., 2014. Determination of joint roughness coefficients using roughness parameters. *Rock mechanics and rock engineering* 47(6), 2061-2073.
- Jayangondaperumal, R., Thakur, V.C., Joevivek, V., Rao, P.S., Gupta, A.K., 2018. *Active Tectonics of Kumaun and Garhwal Himalaya*. Berlin (in press): Springer.
- Jeremić, B., 2000. Finite element methods for 3D slope stability analysis. In *Slope Stability*, 224-238.
- Jing, L., 2003. A review of techniques, advances and outstanding issues in numerical modelling for rock mechanics and rock engineering. *Int. J. Rock Mech. Min. Sci.* 40, 283–353.
- Kalkani, E.C., Piteau, D.R., 1976. Finite element analysis of toppling failure at Hell's Gate Bluffs, British Columbia. *Bulletin of the Association of Engineering Geologists* 13(4), 315-327.
- Kanungo, D. P., 2006. GIS-Based Landslide Susceptibility Studies Using Neural and Fuzzy approaches. Unpublished D. Phil. Thesis, IIT, Roorkee, India.
- Kanungo, D.P., Arora, M.K., Sarkar, S., Gupta, R.P., 2006. A comparative study of conventional, ANN black box, fuzzy and combined neural and fuzzy weighting procedures for landslide susceptibility zonation in Darjeeling Himalayas. *Engineering Geology* 85, 347–366.
- Kanungo, D.P., Arora, M.K., Sarkar, S., Gupta, R.P., 2009. Landslide Susceptibility Zonation (LSZ) Mapping – A Review. *J. South Asia Disaster Stud.* 2, 81–105.
- Kanungo, D.P., Pain, A., Sharma, S., 2013. Finite element modeling approach to assess the stability of debris and rock slopes: a case study from the Indian Himalayas. *Nat. Hazards* 69, 1–24.
- Kanungo, D.P., Sarkar, S., 2003. Landslides and terrain parameters in Darjeeling Himalaya. *Himalayan Geol* 24(2), 55-62.
- Kayastha, P., Dhital, M.R., De Smedt, F., 2013. Evaluation and comparison of GIS based landslide susceptibility mapping procedures in Kulekhani watershed, Nepal. *Journal of the Geological Society of India* 81(2), 219-231.
- Kaynia, A.M., Papathoma-Köhle, M., Neuhäuser, B., Ratzinger, K., Wenzel, H., Medina-Cetina, Z., 2008. Probabilistic assessment of vulnerability to landslide: Application to the village of Lichtenstein, Baden-Württemberg, Germany. *Eng. Geol.* 101(1-2), 33-48.

- Keller, E.A., Pinter, N., 1996. Active tectonics. Upper Seddle River, NJ, USA: Prentice Hall, 19, 359.
- Kentli, B., Topal, T., 2004. Assessment of rock slope stability for a segment of the Ankara–Pozantı motorway, Turkey. *Engineering Geology* 74(1-2), 73-90.
- Kézdi, Á., 1974. Soil physics (Vol. 1). Elsevier Science & Technology.
- Khatttri, K.N., Chander, R., Gaur, V.K., Sarkar, I., 1989. New seismological results on the tectonics of the Garhwal Himalaya. *Proceedings of the Indian Academy of Sciences-Earth and Planetary Sciences* 98(1), 91-109.
- Kirby, E., Whipple, K., 2001. Quantifying differential rock-uplift rates via stream profile analysis. *Geology* 29(5), 415-418.
- Kirkby, M., 1988. Hillslope runoff processes and models. *J. Hydrol.* 100, 315–339.
- Kliche, C., 1999. Rock slope stability. Society for Mining, Metallurgy, and Exploration. Inc (SME), Litleton.
- Kohn, M.J., 2014. Himalayan metamorphism and its tectonic implications. *Annual Review of Earth and Planetary Sciences* 42, 381-419.
- Korup, O., 2006. Rock-slope failure and the river long profile. *Geology* 34(1), 45-48.
- Korup, O., Densmore, A.L., Schlunegger, F., 2010. The role of landslides in mountain range evolution. *Geomorphology* 120, 77–90.
- Koukis, G., Sabatakakis, N., Ferentinou, M., Lainas, S., Alexiadou, X., Panagopoulos, A., 2009. Landslide phenomena related to major fault tectonics: rift zone of Corinth Gulf, Greece. *Bulletin of engineering geology and the environment* 68(2), 215-229.
- Koukis, G., Ziourkas, C., 1991. Slope instability phenomena in Greece: a statistical analysis. *Bulletin of the International Association of Engineering Geology-Bulletin de l'Association Internationale de Géologie de l'Ingénieur* 43(1), 47-60.
- Kumar, G., 1970. Geology and sulphide mineralization in the Pokhri area, Chamoli district, UP. *Geol. Surv. India, Calcutta. Base metals, Misc. Publication* 16(1), 92-98.
- Kumar, G., 2005. Geology of Uttar Pradesh & Uttaranchal. GSI Publications, 2(1).
- Kumar, R., Anbalagan, R., 2015. Landslide susceptibility zonation in part of Tehri reservoir region using frequency ratio, fuzzy logic and GIS. *J. Earth Syst. Sci.* 124(2), 431-448.

- Kumar, V., Gupta, V., Jamir, I., 2018a. Hazard evaluation of progressive Pawari landslide zone, Satluj valley, Himachal Pradesh, India. *Nat. Hazards* 93, 1029–1047.
- Kumar, V., Gupta, V., Jamir, I., Chatteraj, S.L., 2018b. Evaluation of potential landslide damming: Case study of Urni landslide, Kinnaur, Satluj valley, India. *Geosci. Front.*
- Kumar, V., Gupta, V., Sundriyal, Y.P., 2019. Spatial interrelationship of landslides, litho-tectonics, and climate regime, Satluj valley, Northwest Himalaya. *Geol. J.* 54, 537–551.
- Kummerow, C., Barnes, W., Kozu, T., Shiue, J., Simpson, J., 1998. The tropical rainfall measuring mission (TRMM) sensor package. *Journal of atmospheric and oceanic technology* 15(3), 809-817.
- Lan, H.X., Zhou, C.H., Wang, L.J., Zhang, H.Y., Li, R.H., 2004. Landslide hazard spatial analysis and prediction using GIS in the Xiaojiang watershed, Yunnan, China. *Engineering Geology* 76(1-2), 109-128.
- Lang, A., Moya, J., Corominas, J., Schrott, L., Dikau, R., 1999. Classic and new dating methods for assessing the temporal occurrence of mass movements. *Geomorphology* 30, 33–52.
- Larsen, M.C., Torres-Sánchez, A.J., 1998. The frequency and distribution of recent landslides in three montane tropical regions of Puerto Rico. *Geomorphology* 24, 309–331.
- Lee, H., Locat, J., Dartnell, P., Israel, K., Florence Wong, W., 1999. Regional variability of slope stability: application to the Eel margin, California. *Mar. Geol.* 154, 305–321.
- Lee, H.J., Edwards, B.D., 1986. Regional Method to Assess Offshore Slope Stability. *J. Geotech. Eng.* 112, 489–509.
- Lee, S., 2005. Application of logistic regression model and its validation for landslide susceptibility mapping using GIS and remote sensing data. *International Journal of Remote Sensing* 26(7), 1477-1491.
- Lee, S., 2007. Application and verification of fuzzy algebraic operators to landslide susceptibility mapping. *Environmental Geology* 52(4), 615-623.
- Lee, S., Chwae, U., Min, K., 2002. Landslide susceptibility mapping by correlation between topography and geological structure: the Janghung area, Korea. *Geomorphology* 46(3-4), 149-162.

- Lee, S., Min, K., 2001. Statistical analysis of landslide susceptibility at Yongin, Korea. *Environmental Geology* 40(9), 1095-1113.
- Lee, S., Pradhan, B., 2006. Probabilistic landslide hazards and risk mapping on Penang Island, Malaysia. *Journal of Earth System Science* 115(6), 661-672.
- Lee, S., Pradhan, B., 2007. Landslide hazard mapping at Selangor, Malaysia using frequency ratio and logistic regression models. *Landslides* 4, 33–41.
- Lee, S., Talib, J.A., 2005. Probabilistic landslide susceptibility and factor effect analysis. *Environ. Geol.* 47, 982–990.
- LeFort, P., 1975. Himalayas—Collided range—Present knowledge of continental arc: *American Journal of Science*, v.
- Li, L., Lan, H., Guo, C., Zhang, Y., Li, Q., Wu, Y., 2017. A modified frequency ratio method for landslide susceptibility assessment. *Landslides* 14(2), 727-741.
- Li, S., Gu, S., Liu, W., Han, H., Zhang, Q., 2008. Water quality in relation to land use and land cover in the upper Han River Basin, China. *Catena* 75(2), 216-222.
- Lifton, N.A., Chase, C.G., 1992. Tectonic, climatic and lithologic influences on landscape fractal dimension and hypsometry: implications for landscape evolution in the San Gabriel Mountains, California. *Geomorphology* 5(1-2), 77-114.
- Lifton, Z.M., Thackray, G.D., Van Kirk, R., Glenn, N.F., 2009. Influence of rock strength on the valley morphometry of Big Creek, central Idaho, USA. *Geomorphology* 111(3-4), 173-181.
- Liu, C.C., Luo, W., Chung, H.W., Yin, H.Y., Yan, K.W., 2018. Influences of the Shadow Inventory on a Landslide Susceptibility Model. *ISPRS International Journal of Geo-Information* 7(9), 374.
- Lucas, J.M., 1980. A general stereographic method for determining the possible mode of failure of any tetrahedral rock wedge. In *International Journal of Rock Mechanics and Mining Sciences & Geomechanics Abstracts* 17(1), 57-61. Pergamon.
- Luirei, K., Bhakuni, S.S., Kothiyari, G.C., 2018. Geomorphologic study of the valley floor in different tectonic segments along Kosi River valley between South Almora Thrust and Himalayan Frontal Thrust: Kumaun Himalaya, India. *Geol. J.* 53, 1500–1515.

- Mach, K., Mastrandrea, M., 2014. In C. B. Field, & V. R. Barros (Eds.), *Climate change 2014: Impacts, adaptation, and vulnerability* (Vol. 1). Cambridge and New York: Cambridge University Press.
- Magliulo, P., Di Lisio, A., Russo, F., 2009. Comparison of GIS-based methodologies for the landslide susceptibility assessment. *Geoinformatica* 13(3), 253-265.
- Mahesh, P., Gupta, S., Saikia, U., Rai, S.S., 2015. Seismotectonics and crustal stress field in the Kumaon–Garhwal Himalaya. *Tectonophysics* 655,124-138.
- Malamud, B.D., Turcotte, D.L., Guzzetti, F., Reichenbach, P., 2004. Landslide inventories and their statistical properties. *Earth Surf. Process. Landforms* 29, 687–711.
- Malik, J.N., Mohanty, C., 2007. Active tectonic influence on the evolution of drainage and landscape: geomorphic signatures from frontal and hinterland areas along the Northwestern Himalaya, India. *Journal of Asian Earth Sciences* 29(5-6), 604-618.
- Marinos, P., Hoek, E., 2000. GSI: a geologically friendly tool for rock mass strength estimation. In *ISRM international symposium*. International Society for Rock Mechanics.
- Marinos, V.I., Marinos, P., Hoek, E., 2005. The geological strength index: applications and limitations. *Bulletin of Engineering Geology and the Environment* 64(1), 55-65.
- Markland, J.T., 1972. A useful technique for estimating the stability of rock slopes when the rigid wedge slide type of failure is expected, Imperial College Rock Mechanics Research Imprints. London.
- Marquer, D., Chawla, H.S., Challandes, N., 2000. Pre-alpine high-grade metamorphism in High Himalaya crystalline sequences: Evidence from Lower palaeozoic Kinnauer Kailas granite and surrounding rocks in the Sutlej Valley (Himachal Pradesh, India). *Eclogae Geologicae Helvetiae* 93(2), 207-220.
- Marston, R.A., Miller, M.M., Devkota, L.P., 1998. Geocology and mass movement in the Manaslu-Ganesh and Langtang-Jugal himals, Nepal. *Geomorphology* 26(1-3), 139-150.
- Martha, T.R., Kerle, N., Jetten, V., Van Westen, C.J., Vinod Kumar, K., 2010. Landslide Volumetric Analysis Using Cartosat-1-Derived DEMs. *IEEE Geosci. Remote Sens. Lett.* 7, 582–586.

- Martha, T.R., Roy, P., Govindharaj, K.B., Kumar, K.V., Diwakar, P.G., Dadhwal, V.K., 2015. Landslides triggered by the June 2013 extreme rainfall event in parts of Uttarakhand state, India. *Landslides* 12, 135–146.
- Matheson, G.D., 1989. The collection and use of field discontinuity data in rock slope design. *Quarterly Journal of Engineering Geology and Hydrogeology* 22(1), 19–30.
- Matsui, T., San, K. C., 1992. Finite element slope stability analysis by shear strength reduction technique. *Soils Found* 32 (1), 59–70.
- Medlicott, H.B., 1864. On the geological Structure and relations of the Himalayan ranges, between the rivers Ganges and Ravee. *Mem. Geol. Surv. India* 3, 102.
- Mehrotra, G.S., Dharmaraju, R., Prakash, S., 1994. Morphometric appraisal of slope instability of Chilla landslide, Garhwal. *J. Geol. Soc. India* 44, 203–211.
- Mehta, P.N., 1971. Some observations on the Tons thrust and their significance. *Indian Minerals* 25(1). 66-68.
- Merritts, D., Vincent, K.R., 1989. Geomorphic response of coastal streams to low, intermediate, and high rates of uplift, Medocino triple junction region, northern California. *Geological Society of America Bulletin* 101(11), 1373-1388.
- Metcalf, R.P., 1993. Pressure, temperature and time constraints on metamorphism across the Main Central Thrust zone and High Himalayan Slab in the Garhwal Himalaya. *Geological Society, London, Special Publications* 74(1), 485-509.
- Middlemiss, C.S., 1885. A fossiliferous series in the Lower Himalaya, Garhwal. *Rec. Geol. Surv. India* 18(2), 73-77.
- Middlemiss, C.S., 1887. Crystalline and metamorphic rocks of the Lower Himalaya, Garhwal and Kumaun. *Rec. Geol. Surv. India* 20(3), 134-143.
- Miliareisis, G., Sabatakakis, N., Koukis, G., 2005. Terrain pattern recognition and spatial decision making for regional slope stability studies. *Natural Resources Research* 14(2), 91-100.
- Misra, R.C., Sharma, R.P., 1967. Geology of Devidhura area, Almora, UP. *Geological Society of India* 8, 110-118.
- Mohammed, N.Z., Ghazi, A., Mustafa, H.E., 2013. Positional accuracy testing of Google Earth. *International Journal of Multidisciplinary Sciences and Engineering* 4(6), 6-9.
- Mohr, H., 1914. Geologie der Wechselbahn (insbesondere des grossen Hartbergtunnels)... Vienna-Kais. Akad. d. Wissensch. (German)

- Molin, P., Fubelli, G.I., 2005. Morphometric evidence of the topographic growth of the Central Apennines. *Geografia Fisica e Dinamica Quaternaria* 28(3), 47-61.
- Myneni, R.B., Hall, F.G., Sellers, P.J., Marshak, A.L., 1995. The interpretation of spectral vegetation indexes. *IEEE Trans. Geosci. Remote Sens.* 33, 481–486.
- Najman, Y., Garzanti, E., 2000. Reconstructing early Himalayan tectonic evolution and paleogeography from Tertiary foreland basin sedimentary rocks, northern India. *Geological Society of America Bulletin* 112(3), 435-449.
- Nandi, A., Shakoor, A., 2010. A GIS-based landslide susceptibility evaluation using bivariate and multivariate statistical analyses. *Engineering Geology* 110(1-2), 11-20.
- Nian, T.-K., Huang, R.-Q., Wan, S.-S., Chen, G.-Q., 2012. Three-dimensional strength-reduction finite element analysis of slopes: geometric effects. *Can. Geotech. J.* 49, 574–588.
- Nilsen, T.H., 1979. Relative slope stability and land-use planning in the San Francisco Bay region, California (Vol. 944). US Govt. Print. Off.
- Obrzud, R., Truty, A., 2012. The hardening soil model-a practical guidebook z soil. PC100701 Report.
- Oh, H.J., Lee, S., Soedradjat, G.M., 2010. Quantitative landslide susceptibility mapping at Pemalang area, Indonesia. *Environmental Earth Sciences* 60(6), 1317-1328.
- Ohsaki, Y., Iwasaki, R., 1973. On dynamic shear moduli and Poisson's ratios of soil deposits. *Soils and Foundations*, 13(4), 61-73.
- Oldham, R.D., 1883. Note on the geology of Jaunsar and the Lower Himalayas. *Rec. GSI*, 16(4), 193-198.
- Online GSI portal: www.gsi.gov.in (Accessed December 2016).
- Online Submission and Monitoring of Environmental Clearance, Ministry of Environment, Forest and Climate Change, Government of India. Available online:
http://environmentclearance.nic.in/writereaddata/modification/PreviousTOR/0_0_29092014ZM36AAnnexure-ANNEXUREIandII.pdf (Accessed on 20 December 2016)
- Owen, D.R.J., Hinton, E., 1980. A simple guide to finite elements. Pineridge Press Limited.

- Pachauri, A.K., 1972. Stratigraphy, correlation and tectonics of the area around Purola, Uttarkashi and Dehra Dun Districts (UP). *Himalayan Geology* 2, 370-387.
- Pachauri, A.K., Gupta, P.V., Chander, R., 1998. Landslide zoning in a part of the Garhwal Himalayas. *Environmental Geology* 36(3-4), 325-334.
- Pachauri, A.K., Pant, M., 1992. Landslide hazard mapping based on geological attributes. *Engineering Geology* 32(1-2), 81-100.
- Pain, A., Kanungo, D.P., Sarkar, S., 2014. Rock slope stability assessment using finite element based modelling – examples from the Indian Himalayas. *Geomech. Geoengin.* 9, 215–230.
- Palmström, A., 1982. The volumetric joint count-a useful and simple measure of the degree of rock jointing. In 41st International Congress. Assoc. Eng. Geol. Delphi 5, 221-228.
- Palmström, A., Singh, R., 2001. The deformation modulus of rock masses—comparisons between in situ tests and indirect estimates. *Tunnelling and Underground Space Technology* 16(2), 115-131.
- Pande, G.N., Beer, G., Wiley, J., 1990. *Numerical Methods in Rock Mechanics*.
- Pandey, V.K., Pourghasemi, H.R., Sharma, M.C., 2018. Landslide susceptibility mapping using maximum entropy and support vector machine models along the Highway Corridor, Garhwal Himalaya. *Geocarto International* 1-20.
- Pardeshi, S.D., Autade, S.E., Pardeshi, S.S., 2013. Landslide hazard assessment: recent trends and techniques. *Springer plus* 2(1) 1-23.
- Parkash, S., 2011. Historical records of socio-economically significant landslides in India. *J South Asia Disaster Studies* 4(2), 177-204.
- Parkash, S., Kathait, A., 2014. A selected annotated bibliography and bibliography on landslides in India. National Institute of Disaster Management, Ministry of Home Affairs, Govt. of India, New Delhi, 172.
- Pathak, S., Nilsen, B., 2004. Probabilistic rock slope stability analysis for Himalayan conditions. *Bull. Eng. Geol. Environ.* 63, 25–32.
- Pati, U.C., Rao, P.N., 1983. Geotectonics of the Main Central Thrust of UP Himalaya. *Himalayan shears*.
- Paul, S.K., Bartarya, S.K., Rautela, P., Mahajan, A.K., 2000. Catastrophic mass movement of 1998 monsoons at Malpa in Kali Valley, Kumaun Himalaya (India). *Geomorphology* 35(3-4), 169-180.

- Perrone, A., Lapenna, V., Piscitelli, S., 2014. Electrical resistivity tomography technique for landslide investigation: A review. *Earth-Science Reviews* 135, 65-82.
- Peruccacci, S., Brunetti, M.T., Luciani, S., Vennari, C., Guzzetti, F., 2012. Lithological and seasonal control on rainfall thresholds for the possible initiation of landslides in central Italy. *Geomorphology* 139, 79-90.
- Petley, D.N., 2010. On the impact of climate change and population growth on the occurrence of fatal landslides in South, East and SE Asia. *Quarterly Journal of Engineering Geology and Hydrogeology* 43(4), 487-496.
- Pettifer, G.S., Fookes, P.G., 1994. A revision of the graphical method for assessing the excavatability of rock. *Quarterly Journal of Engineering Geology and Hydrogeology* 27(2), 145-164.
- Pilgrim, G.E., 1906. Notes on the geology of a portion of Bhutan. *Records of Geological Survey of India* 34, 22-30.
- Pilgrim, G.E., West, W.D., 1928. The structure and correlation of the Simla rocks. *Mere. Geol. Surv. India* 53(140).
- Pilgrim, G.E., 1910. Preliminary note on a revised classification of the Tertiary freshwater deposits of India. *Records of the Geological Survey of India* 40, 185-205.
- Pourghasemi, H.R., Mohammady, M., Pradhan, B., 2012. Landslide susceptibility mapping using index of entropy and conditional probability models in GIS: Safarood Basin, Iran. *Catena* 97, 71-84.
- Pradhan, B., Lee, S., 2010. Delineation of landslide hazard areas on Penang Island, Malaysia, by using frequency ratio, logistic regression, and artificial neural network models. *Environmental Earth Sciences* 60(5), 1037-1054.
- Pradhan, B., Oh, H.J., Buchroithner, M., 2010. Weights-of-evidence model applied to landslide susceptibility mapping in a tropical hilly area. *Geomatics, Natural Hazards and Risk* 1(3), 199-223.
- Prager, W., Synge, J.L., 1947. Approximation in elasticity based on the concept of function space., *Q J Appl Math.*
- Prakash, P., 2018. Study the 2013 Flood Damages and Risk Assessment in Kedarnath, Himalaya Area Using Geoinformatic Techniques. *J Geogr Nat Disast* 8(1): 1000216.

- Pratt, H.R., 1974. Friction and deformation of jointed quartz diorite. In Proc. Of 3rd ISRM Congress, Denver, 306-310.
- Radbruch-Hall, D.H., Crowther, K.C., 1973. Map showing areas of estimated relative amounts of landslides in California (747).
- Rahardjo, H., Lee, T.T., Leong, E.C., Rezaur, R.B., 2005. Response of a residual soil slope to rainfall. *Can. Geotech. J.* 42, 340–351.
- Rahman, A.A., Boguslawski, P., Anton, F., Said, M.N., Omar, K.M., (Eds.) 2014. *Geoinformation for informed decisions*. Switzerland: Springer International Publishing
- Raina, B.N., 1978. A review of the stratigraphy and structure of Lesser Himalaya of Uttar Pradesh and Himachal Pradesh. *Tectonic Geology of the Himalaya, Today and Tomorrow's Printers and Publishers, New Delhi*, 79-112.
- Rao, P.N., Dungrakoti, B.D., Verma, R.N., 1981. Tectonic framework of Wazri area with special reference to the main central thrust in Yamuna valley, Uttarkashi district, Uttar Pradesh. *Records of the Geological Survey of India* 112(2), 74-83.
- Rautela, P., Lakhera, R.C., 2000. Landslide risk analysis between Giri and Tons Rivers in Himachal Himalaya (India). *Int. J. Appl. Earth Obs. Geoinf.* 2, 153–160.
- Rautela, P., Thakur, V.C., 1999. Landslide hazard Zonation in Kaliganga and Madhyamaheshwar valleys of Garhwal Himalaya: A GIS based approach. *Himalayan Geology* 20(2):31-44.
- Ray, P.C., Parvaiz, I., Jayangondaperumal, R., Thakur, V.C., Dadhwal, V.K., Bhat, F.A., 2009. Analysis of seismicity-induced landslides due to the 8 October 2005 earthquake in Kashmir Himalaya. *Current Science* 1742-1751.
- Regmi, A.D., Devkota, K.C., Yoshida, K., Pradhan, B., Pourghasemi, H.R., Kumamoto, T., Akgun, A., 2014. Application of frequency ratio, statistical index, and weights-of-evidence models and their comparison in landslide susceptibility mapping in Central Nepal Himalaya. *Arabian Journal of Geosciences* 7(2), 725-742.
- Reichenbach, P., Galli, M., Cardinali, M., Guzzetti, F., Ardizzone, F., 2004. Geomorphological mapping to assess landslide risk: Concepts, methods and applications in the Umbria region of central Italy. *Landslide Hazard Risk* 429-468.

- Reichenbach, P., Rossi, M., Malamud, B.D., Mihir, M., Guzzetti, F., 2018. A review of statistically-based landslide susceptibility models. *Earth-Science Rev.* 180, 60–91.
- Remondo, J., González, A., De Terán, J.R.D., Cendrero, A., Fabbri, A., Chung, C.J.F., 2003. Validation of landslide susceptibility maps; examples and applications from a case study in Northern Spain. *Natural Hazards* 30(3), 437-449.
- Rhea, S., 1993. Geomorphic observations of rivers in the Oregon Coast Range from a regional reconnaissance perspective. *Geomorphology* 6(2), 135-150.
- Roe, G.H., Montgomery, D.R., Hallet, B., 2002. Effects of orographic precipitation variations on the concavity of steady-state river profiles. *Geology* 30(2), 143-146.
- Romana, M., 1985. New adjustment ratings for application of Bieniawski classification to slopes. In *Proceedings of the international symposium on role of rock mechanics, Zacatecas, Mexico* 49-53.
- Romana, M.R., 1993. A geomechanical classification for slopes: slope mass rating. In *Rock testing and site characterization* 575-600. Pergamon.
- Rouse Junior, J. W., Haas, R. H., Schell, J. A., Deering, D. W., Harlan, J. C.. 1974. Monitoring the vernal advancement and retrogradation (greenwave effect) of natural vegetation. Greenbelt, MD, USA: NASA/GSFC, Final Report, n. September 1972, 1-137.
- Rupke, J., 1974. Stratigraphic and structural evolution of the Kumaon Lesser Himalaya. *Sedimentary Geology* 11(2-4), 81-265.
- Saha, A.K., Gupta, R.P., Sarkar, I., Arora, M.K., Csaplovics, E., 2005. An approach for GIS-based statistical landslide susceptibility zonation—with a case study in the Himalayas. *Landslides* 2(1), 61-69.
- Saklani, P.S., 1971. Structure and tectonics of the Pratapnagar area, Garhwal Himalaya. *Himalayan Geology* 1, 75-91.
- Saklani, P.S., Nainwal, D.C., Singh, V.K., 1991. Geometry of the composite Main Central Thrust (MCT) in the Yamuna valley, Garhwal Himalaya, India. *N. Jb. Geol. Paläont. Mh* 1991, 364-380.
- Saklani, P.S., Pande, I.C., 1970. Geology of the Pratapnagar area Tehri-Garhwal Uttar Pradesh. *Bulletin of Indian Geological Association* 3, 13-18.
- Santacana, N., Baeza, B., Corominas, J., De Paz, A., Marturiá, J., 2003. A GIS-based multivariate statistical analysis for shallow landslide susceptibility mapping in

- La Pobla de Lillet area (Eastern Pyrenees, Spain). *Natural hazards* 30(3), 281-295.
- Sanwal, R., Jaiswal, P., Baruah, Manoj, K., 2005. Landslide zonation mapping in Yamuna basin, Dehradun, Uttarkashi Tehri – Garhwal and Chamoli districts, Uttaranchal (phase- 2) (field season: 2003-04 and 2004-05). (Unpublished report)
- Sarkar, K., Buragohain, B., Singh, T.N., 2016. Rock slope stability analysis along NH-44 in Sonapur area, Jaintia hills district, Meghalaya. *Journal of the Geological Society of India* 87(3), 317-322.
- Sarkar, S., Gupta, P.K., 2005. Techniques for landslide hazard zonation–Application to Srinagar-Rudraprayag area of Garhwal Himalaya. *rn*, 79, 0.
- Sarkar, S., Kanungo, D.P., 2004. An integrated approach for landslide susceptibility mapping using remote sensing and GIS. *Photogrammetric Engineering & Remote Sensing* 70(5), 617-625.
- Sarkar, S., Kanungo, D.P., Mehrotra, G.S., 1995. Landslide hazard zonation: a case study in Garhwal Himalaya, India. *Mountain Research and Development* 301-309.
- Sarkar, S., Kanungo, D.P., Mehrotra, G.S., 1995. Landslide hazard zonation: a case study in Garhwal Himalaya, India. *Mountain Research and Development* 301-309.
- Sarkar, S., Kanungo, D.P., Patra, A.K., Kumar, P., 2008. GIS based spatial data analysis for landslide susceptibility mapping. *Journal of Mountain Science* 5(1), 52-62.
- Sarkar, S., Roy, A.K., Martha, T.R., 2013. Landslide susceptibility assessment using information value method in parts of the Darjeeling Himalayas. *Journal of the Geological Society of India* 82(4), 351-362.
- Saxena, M.N., 1971. The crystalline axis of the Himalaya: the Indian shield and continental drift. *Tectonophysics* 12(6), 433-447.
- Scherler, D., Bookhagen, B., Strecker, M.R., 2014. Tectonic control on ¹⁰Be-derived erosion rates in the Garhwal Himalaya, India. *Journal of Geophysical Research: Earth Surface* 119(2), 83-105.
- Schmidt, E., 1951. A non-destructive concrete tester. *Concrete* 59(8), 34-35.

- Searle, M.P., Metcalfe, R.P., Rex, A.J., Norry, M.J., 1993. Field relations, petrogenesis and emplacement of the Bhagirathi leucogranite, Garhwal Himalaya. *Geological Society, London, Special Publications* 74(1), 429-444.
- Searle, M.P., Simpson, R.L., Law, R.D., Parrish, R.R., Waters, D.J., 2003. The structural geometry, metamorphic and magmatic evolution of the Everest massif, High Himalaya of Nepal–South Tibet. *Journal of the Geological Society* 160(3), 345-366.
- Seeber, L., Gornitz, V., 1983. River profiles along the Himalayan arc as indicators of active tectonics. *Tectonophysics* 92(4), 335-367.
- Şen, Z., Eissa, E.A., 1992. Rock quality charts for log-normally distributed block sizes. In *International journal of rock mechanics and mining sciences & geomechanics abstracts* 29(1), 1-12. Pergamon.
- Senthilkumar, V., Chandrasekaran, S.S., Maji, V.B., 2017. Geotechnical characterization and analysis of rainfall—induced 2009 landslide at Marappalam area of Nilgiris district, Tamil Nadu state, India. *Landslides* 14(5), 1803-1814.
- Shao, Y., 2009. 1. Wind Erosion and Wind-Erosion Research, in: *Physics and Modelling of Wind Erosion*. Springer Netherlands, Dordrecht, 1–11.
- Sharma, V. K., Kandpal, G. C., 1996. Landslide hazard zonation mapping [LZM] - an input for Geo-environmental assessment of a part of Garhwal Himalaya. *Proc. Symp. NW Himalaya and Foredeep. Geol. Surv. Ind. Spl. Pub.* 21 (2):81-84
- Shroder, J.F., Bishop, M.P., 1998. Mass movement in the Himalaya: new insights and research directions. *Geomorphology* 26, 13–35.
- Siddique, T., Alam, M.M., Mondal, M.E.A., Vishal, V., 2015. Slope mass rating and kinematic analysis of slopes along the national highway-58 near Jonk, Rishikesh, India. *Journal of Rock Mechanics and Geotechnical Engineering* 7(5), 600-606.
- Siddique, T., Pradhan, S.P., 2018. Stability and sensitivity analysis of Himalayan road cut debris slopes: an investigation along NH-58, India. *Nat. Hazards* 93, 577–600.
- Silva, P.G., Goy, J.L., Zazo, C., Bardají, T., 2003. Fault-generated mountain fronts in southeast Spain: geomorphologic assessment of tectonic and seismic activity. *Geomorphology* 50(1-3), 203-225.

- Simpson, J., Kummerow, C., Tao, W.K., Adler, R.F., 1996. On the tropical rainfall measuring mission (TRMM). *Meteorology and Atmospheric physics* 60(1-3), 19-36.
- Singh, B., Das, S., Singh, P., 2016. Detailed geological investigation of subsidence/slide affected areas near Wariya village (NH-134), Yamuna Valley and Bandarkot village in Bhagirathi valley, Uttarkashi district in Uttarakhand. (FS 2015-2016) (GSI unpublished report)
- Singh, K., Thakur, V.C., 2001. Microstructures and strain variation across the footwall of the Main Central Thrust Zone, Garhwal Himalaya, India. *Journal of Asian Earth Sciences* 19(1-2), 17-29.
- Singh, P.K., Kainthola, A., Singh, T.N., 2015. Rock mass assessment along the right bank of river Sutlej, Luhri, Himachal Pradesh, India. *Geomatics, Natural Hazards and Risk* 6(3), 212-223.
- Singh, T.N., Verma, A.K., Sarkar, K., 2010. Static and dynamic analysis of a landslide. *Geomatics, Nat. Hazards Risk* 1, 323–338.
- Sinha, B.N., 1975. Landslides in Darjeeling district (WB) and adjacent areas. *Bul. GSI B* 36, 1-45.
- Skempton, A.W., Hutchinson, J.N., 1969. Stability of natural slopes and embankment foundations, state-of-the-art report. *Proc. 7th Int. Conf. Soil Mech. Found. Eng.* 291-340.
- Snyder, N.P., Whipple, K.X., Tucker, G.E., Merritts, D.J., 2000. Landscape response to tectonic forcing: Digital elevation model analysis of stream profiles in the Mendocino triple junction region, northern California. *Geological Society of America Bulletin* 112(8), 1250-1263.
- Snyder, N.P., Whipple, K.X., Tucker, G.E., Merritts, D.J., 2003. Channel response to tectonic forcing: field analysis of stream morphology and hydrology in the Mendocino triple junction region, northern California. *Geomorphology* 53(1-2), 97-127.
- Soeters, R., Van Westen, C.J., 1996. Slope instability recognition, analysis and zonation. *Landslides: investigation and mitigation* 247, 129-177.
- Solaimani, K., Mousavi, S.Z., Kaviani, A., 2013. Landslide susceptibility mapping based on frequency ratio and logistic regression models. *Arabian Journal of Geosciences* 6(7), 2557-2569.

- Sorkhabi, R.B., Stump, E., Foland, K., Jain, A.K., 1999. Tectonic and cooling history of the Garhwal Higher Himalaya (Bhagirathi Valley): constraints from thermochronological data. *Geodynamics of the NW Himalaya*. Gondwana Research Group Memoir 6, 217-235.
- Srikantia, S.V., Bhargava, O.N., 1998. *Geology of Himachal Pradesh*. GSI Publications, 2(1).
- Srivastava, H.B., Tripathy, N.R., 2007. Geometrical analysis of mesoscopic shear zones in the crystalline rocks of MCT Zone of Garhwal Higher Himalaya. *Journal of Asian Earth Sciences* 30(5-6), 599-612.
- Srivastava, P., Mitra, G., 1994. Thrust geometries and deep structure of the outer and lesser Himalaya, Kumaon and Garhwal (India): Implications for evolution of the Himalayan fold-and-thrust belt. *Tectonics* 13(1), 89-109.
- Srivastava, V. K., 1974. Progress report for field season 1973-74 GSI unpublished report
- Standard-IS: 2720 (Part 4)–1985. Methods of test for soils: Determination of grain size analysis of soil, New Delhi, India.
- Standard-IS: 1498–1970 (Reaffirmed 2007). Classification and identification of soils for general engineering purposes. New Delhi, India.
- Standard-IS: 2720 (Part 10)–1991. Method of test for soils: Unconfined Compressive Strength, New Delhi, India.
- Standard-IS: 2720 (Part 13)–1986. Method of test for soils: Direct shear test, New Delhi, India.
- Standard-IS: 9143-1979. Method for the determination of unconfined compressive strength of rock materials, New Delhi, India.
- Sujatha, E.R., Rajamanickam, G.V., Kumaravel, P., 2012. Landslide susceptibility analysis using Probabilistic Certainty Factor Approach: A case study on Tevankarai stream watershed, India. *Journal of earth system science* 121(5), 1337-1350.
- Telbisz, T., Kovács, G., Székely, B., Szabó, J., 2013. Topographic swath profile analysis: a generalization and sensitivity evaluation of a digital terrain analysis tool. *Zeitschrift für Geomorphol* 57(4), 485-513.
- Thakur, V.C., 1992. *Geology of western Himalaya* 19, 366. Pergamon.

- Thakur, V.C., Misra, D.K., 1984. Tectonic framework of the Indus and Shyok suture zones in eastern Ladakh, northwest Himalaya. *Tectonophysics* 101(3-4), 207-220.
- Thomas, G., J. C. Michael., 2004. A review of scale dependency in landslide hazard and risk analysis. *Landslide Hazard and Risk*. John Wiley & Sons, Ltd: 102-114.
- Tucker, C.J., 1979. Red and photographic infrared linear combinations for monitoring vegetation. *Remote sensing of Environment* 8(2), 127-150.
- Tucker, C.J., Justice, C.O., Prince, S.D., 1986. Monitoring the grasslands of the Sahel 1984-1985. *International Journal of Remote Sensing* 7(11), 1571-1581.
- Tucker, G.E., Bras, R.L., 1998. Hillslope processes, drainage density, and landscape morphology. *Water Resour. Res.* 34, 2751–2764.
- Turner, M.J., 1956. Stiffness and Deflection Analysis of Complex Structures. *J. Aeronaut. Sci.* 23, 805–823.
- Valdiya, K.S., 1962. An outline of the stratigraphy and structure of the southern part of Pithoragarh district, Uttar Pradesh. *Geological Society of India* 3, 27-48.
- Valdiya, K.S., 1965. Petrography and sedimentation of the sedimentary zone of southern Pithoragarh, UP Himalaya. *DN Wadia Commemorative Volume. Min. Met. Inst. India Calcutta*, 521-544.
- Valdiya, K.S., 1975. Lithology and age of the Tal Formation in Garhwal, and implication on stratigraphic scheme of Krol Belt in Kumaun Himalaya. *Geological Society of India* 16(2), 119-134.
- Valdiya, K.S., 1980. *Geology of kumaun lesser Himalaya*. Wadia Institute of Himalayan Geology.
- Valdiya, K.S., 1995. Proterozoic sedimentation and Pan-African geodynamic development in the Himalaya. *Precambrian Research* 74(1-2), 35-55.
- Valdiya, K.S., 1998. *Dynamic Himalaya*. Universities press. 178
- Van Westen, C.J., 1993. Application of geographic information systems to landslide hazard zonation.
- Van Westen, C.J., 1994. GIS in landslide hazard zonation: a review, with examples from the Andes of Colombia. In *Mountain environments & geographic information systems*, 135-166, Taylor & Francis.
- Van Westen, C.J., Castellanos, E., Kuriakose, S.L., 2008. Spatial data for landslide susceptibility, hazard, and vulnerability assessment: an overview. *Engineering Geology* 102(3-4), 112-131.

- Van Westen, C.J., Rengers, N., Soeters, R., 2003. Use of geomorphological information in indirect landslide susceptibility assessment. *Natural hazards* 30(3), 399-419.
- Van Westen, C.J., Van Asch, T.W., Soeters, R., 2006. Landslide hazard and risk zonation—why is it still so difficult?. *Bulletin of Engineering geology and the Environment* 65(2), 167-184.
- Vannay, J.C., Grasemann, B., 2001. Himalayan inverted metamorphism and syn-convergence extension as a consequence of a general shear extrusion. *Geol. Mag.* 138, 253–276.
- Varnes, D.J., 1978. Slope movement types and processes. *Special report* 176, 11-33.
- Varnes, D.J., 1984. Landslide hazard zonation: a review of principles and practice (No. 3).
- Wadia, D.N., 1931. The syntaxis of the northwest Himalaya: its rocks, tectonics and orogeny. *Rec. Geol. Surv. India* 65(2), 189-220.
- Wadia, D.N., 1953. *Geology of India*, third edition. MacMillan and Co. Limited, London. 553.
- Wang, Y., Lin, Q., Shi, P., 2018. Spatial pattern and influencing factors of landslide casualty events. *Journal of Geographical Sciences* 28(3), 259-274.
- Wells, S.G., Bullard, T.F., Menges, C.M., Drake, P.G., Karas, P.A., Kelson, K.I., Ritter, J.B., Wesling, J.R., 1988. Regional variations in tectonic geomorphology along a segmented convergent plate boundary pacific coast of Costa Rica. *Geomorphology* 1(3), 239-265.
- Wessels, K.J., van den Bergh, F., Scholes, R.J., 2012. Limits to detectability of land degradation by trend analysis of vegetation index data. *Remote Sens. Environ.* 125, 10–22.
- Whipple, K.X., Tucker, G.E., 1999. Dynamics of the stream-power river incision model: Implications for height limits of mountain ranges, landscape response timescales, and research needs. *Journal of Geophysical Research: Solid Earth* 104(B8), 17661-17674.
- Whittaker, A.C., Cowie, P.A., Attal, M., Tucker, G.E., Roberts, G.P., 2007. Bedrock channel adjustment to tectonic forcing: Implications for predicting river incision rates. *Geology* 35(2), 103-106.

- Wieczorek, G.F., 1984. Preparing a detailed landslide-inventory map for hazard evaluation and reduction. *Bulletin of the Association of Engineering Geologists* 21(3), 337-342.
- Wobus, C., Whipple, K.X., Kirby, E., Snyder, N., Johnson, J., Spyropolou, K., Crosby, B., Sheehan, D., 2006. Tectonics from topography: Procedures, promise, and pitfalls, in: *Special Paper 398: Tectonics, Climate, and Landscape Evolution*. Geological Society of America 55–74.
- Wolff, D.B., Marks, D.A., Amitai, E., Silberstein, D.S., Fisher, B.L., Tokay, A., Wang, J., Pippitt, J.L., 2005. Ground validation for the tropical rainfall measuring mission (TRMM). *Journal of Atmospheric and Oceanic Technology* 22(4), 365-380.
- Wong, F.S., 1984. Uncertainties in FE modeling of slope stability. *Comput. Struct.* 19, 777–791.
- Wright, R.H., Campbell, R.H., Nilsen, T.H., 1974. Preparation and use of isopleth maps of landslide deposits. *Geology* 2(10), 483-485.
- Wulf, H., Bookhagen, B., Scherler, D., 2012. Climatic and geologic controls on suspended sediment flux in the Sutlej River Valley, western Himalaya. *Hydrol. Earth Syst. Sci.* 16, 2193–2217.
- Xie, P., Arkin, P.A., 1997. Global precipitation: A 17-year monthly analysis based on gauge observations, satellite estimates, and numerical model outputs. *Bulletin of the American Meteorological Society* 78(11), 2539-2558.
- Xu, C., Dai, F., Xu, X., Lee, Y.H., 2012. GIS-based support vector machine modeling of earthquake-triggered landslide susceptibility in the Jianjiang River watershed, China. *Geomorphology* 145, 70-80.
- Xu, C., Xu, X., Shyu, J.B.H., Zheng, W., Min, W., 2014. Landslides triggered by the 22 July 2013 Minxian–Zhangxian, China, Mw 5.9 earthquake: inventory compiling and spatial distribution analysis. *Journal of Asian Earth Sciences* 92, 125-142.
- Xu, Q., Chen, J., Li, J., Zhao, C., Yuan, C., 2015. Study on the Constitutive Model for Jointed Rock Mass. *PLoS One* 10, e0121850.
- Yalcin, A., 2008. GIS-based landslide susceptibility mapping using analytical hierarchy process and bivariate statistics in Ardesen (Turkey): comparisons of results and confirmations. *Catena* 72(1), 1-12.

- Yalcin, A., Reis, S., Aydinoglu, A.C., Yomralioglu, T., 2011. A GIS-based comparative study of frequency ratio, analytical hierarchy process, bivariate statistics and logistics regression methods for landslide susceptibility mapping in Trabzon, NE Turkey. *Catena* 85(3), 274-287.
- Yang, L., Wylie, B.K., Tieszen, L.L., Reed, B.C., 1998. An Analysis of Relationships among Climate Forcing and Time-Integrated NDVI of Grasslands over the U.S. Northern and Central Great Plains. *Remote Sens. Environ.* 65, 25–37.
- Yatagai, A., Kamiguchi, K., Hamada, A., Arakawa, O. and Yasutomi, N., 2010. Daily precipitation analysis of using a dense network of rain gauges and satellite estimates over South Asia: quality control. In *Remote Sensing and Modeling of the Atmosphere, Oceans, and Interactions III* (7856), 785604. International Society for Optics and Photonics.
- Yilmaz, I., 2009. Landslide susceptibility mapping using frequency ratio, logistic regression, artificial neural networks and their comparison: a case study from Kat landslides (Tokat—Turkey). *Computers & Geosciences* 35(6), 1125-1138.
- Yin, A., 2006. Cenozoic tectonic evolution of the Himalayan orogen as constrained by along-strike variation of structural geometry, exhumation history, and foreland sedimentation. *Earth-Science Reviews* 76(1-2), 1-131.
- Zhao, Y., Huang, Y., Liu, H., Wei, Y., Lin, Q., Lu, Y., 2018. Use of the Normalized Difference Road Landside Index (NDRLI)-based method for the quick delineation of road-induced landslides, *Sci. Rep.* 8, 17815.
- Zheng, H., Liu, D.F., Li, C., 2005. Slope stability analysis based on elasto-plastic finite element method. *International Journal for Numerical Methods in Engineering* 64(14), 1871-1888.
- Zienkiewicz, O.C., Kelly, D.W., Bettess, P., 1977. The coupling of the finite element method and boundary solution procedures. *Int. J. Numer. Methods Eng.* 11, 355–375.

APPENDIX 1

Landslide details: HH, Higher Himalaya; LH, Lesser Himalaya. The classification of landslide type is based on Varnes, (1978)

Sl. No	Landslide location	Type ^a	Area ^b (m ²)	Volume ^c (m ³)	Stratigraphic Unit
1	78°27'43.1" 30°59'51.7"	Rockfall	320±35	288±162	H I G H E R H I M A L A Y A
2	78°27'36.46" 30°59'40.11"	Rockfall	610±67	549±309	
3	78°27'25.40" 30°59'28.38"	Rockfall	850±94	765±431	
4	78°27'25.04" 30°59'28.09"	Rockfall	1050±116	1050±544	
5	78°27'10.64" 30°59'18.04"	Rockfall	300±33	270±152	
6	78°26'51.61" 30°59'03.53"	Rockfall	420±46	378±213	
7	78°26'21.84" 30°58'29.64"	Debris slide	8890±978	4001±803	
8	78°25'51.24" 30°57'57.24"	Debris slide	12762±1404	15953±4360	
9	78°25'49.08" 30°57'45.00"	Debris slide	70515±7757	105773±40423	
10	78°25'22.35" 30°57'27.35"	Rockfall	7329±806	9161±2504	
11	78°25'28.97" 30°57'32.37"	Debris slide	1300±143	1625±444	
12	78°24'37.14" 30°56'50.01"	Debris slide	70600±7766	88250±24119	
13	78°24'28.48" 30°56'39.48"	Debris slide	12700±1397	15875±4339	
14	78°24'57.14" 30°57'00.23"	Rockfall	6895±758	3103±623	
15	78°24'26.26" 30°56'35.92"	Rockfall	2350±259	2350±1218	
16	78°24'6.48" 30°56'0.60"	Debris slide	183468±20181	302722±78860	
17	78°23'55.43" 30°55'50.04"	Debris slide	5695±626	18983±6738	
18	78°23'46.65" 30°55'47.65"	Rockfall	773±85	155±80	
19	78°23'38.76" 30°55'41.52"	Debris slide	36368±4000	145472±45696	
20	78°23'48.84" 30°55'44.76"	Debris slide	52846±5813	18496±7743	
21	78°21'33.23" 30°54'10.77"	Debris slide	198061±21787	1188366±292436	
22	78°20'46.70" 30°54'23.05"	Debris slide	215480± 23703	1652013±450472	
23	78°20'18.80" 30°54'23.64"	Rockfall	600±66	540±236	

24	78°20'01.91" 30°54'28.02"	Debris slide	17440±1918	8720±3807	L E S S E R H I M A L A Y A
25	78°19'52.42" 30°54'38.70"	Debris slide	18700±2057	7480±2350	
26	78°19'43.49" 30°54'19.14"	Debris slide	2450±270	613±167	
27	78°19'41.49" 30°54'08.27"	Debris slide	2460±271	615±168	
28	78°19'30.37" 30°53'48.74"	Debris slide	144108±15852	936702±161869	
29	78°19'31.36" 30°53'48.79"	Rockfall	17414±1916	8707±3801	
30	78°18'56.88" 30°53'23.64"	Debris slide	18959±2085	7584±2382	
31	78°18'33.74" 30°52'47.37"	Debris slide	18673±2054	5913±1815	
32	78°18'34.28" 30°52'48.51"	Rockfall	2657±292	531±275	
33	78°18'15.38" 30°52'26.91"	Debris slide	12085±1329	6445±2216	
34	78°14'36.86" 30°51'18.77"	Rockfall	15621±1718	3124±1619	
35	78°16'56.13" 30°49'31.02"	Rockfall	8919±981	1041±671	
36	78°14'38.40" 30°49'11.43"	Rockfall	526±58	210±66	
37	78°14'01.40" 30°49'06.66"	Rockfall	5989±659	2695±541	
38	78°13'43.43" 30°47'07.09"	Debris slide	24747±2722	12374±3382	
39	78°10'13.21" 30°47'42.94"	Debris slide	8533±939	3129±1408	
40	78°10'07.42" 30°47'44.64"	Debris slide	2530±278	1602±840	
41	78°10'00.17" 30°47'48.46"	Debris slide	7929±872	1586±822	
42	78°09'51.92" 30°47'49.39"	Debris slide	1884±207	377±195	
43	78°09'52.18" 30°47'54.29"	Debris slide	6616±728	419±220	
44	78°08'54.12" 30°48'05.48"	Rockfall	8690±956	1014±653	
45	78°09'14.71" 30°47'36.14"	Debris slide	19926±2192	8967±1800	
46	78°08'09.47" 30°47'07.47"	Rockfall	11708±1288	6635±2190	
47	78°07'33.71" 30°47'23.16"	Rockfall	6873±756	5040±1967	
48	78°07'33.71" 30°47'23.16"	Rockfall	4964±546	2482±1084	
49	78°06'52.21" 30°46'45.29"	Rockfall	29385±3232	14693±6415	

50	78°06'33.92" 30°46'21.29"	Rockfall	520±57	260±114	L E S S E R H I M A L A Y A
51	78°06'33.44" 30°46'20.20"	Rockfall	757±83	379±165	
52	78°06'37.37" 30°46'16.92"	Rockfall	376±41	188±82	
53	78°06'21.88" 30°46'04.80"	Rockfall	17970±1977	8985±3923	
54	78°06'13.46" 30°46'10.19"	Rockfall	8801±968	3520±1824	
55	78°06'10.07" 30°46'07.77"	Rockfall	4773±525	1909±989	
56	78°06'06.73" 30°46'04.07"	Rockfall	13348±1468	8009±1971	
57	78°05'33.71" 30°45'09.63"	Debris slide	4848±533	2909±716	
58	78°04'55.87" 30°44'45.02"	Rockfall	2320±255	1392±532	
59	78°04'46.66" 30°42'57.65"	Rockfall	32475±3572	20568±6313	
60	78°04'57.16" 30°42'57.89"	Debris slide	16198±1782	12149±4643	
61	78°04'52.03" 30°42'43.92"	Rockfall	3821±420	2866±1095	
62	78°04'29.86" 30°41'56.13"	Rockfall	34667±3813	34667±17966	
63	78°04'06.86" 30°40'54.70"	Rockfall	7362±810	4417±1688	
64	78°04'14.90" 30°40'38.34"	Rockfall	3488±384	2093±800	
65	78°04'07.06" 30°40'35.32"	Rockfall	16589±1825	11059±5355	
66	78°02'39.92" 30°39'09.81"	Rockfall	1705±188	1023±391	
67	78°02'14.29" 30°38'38.56"	Rockfall	4309±474	2585±988	
68	78°01'44.70" 30°38'35.73"	Rockfall	6251±688	3751±1433	
69	78°01'26.06" 30°38'55.33"	Rockfall	1072±118	643±246	
70	78°01'22.19" 30°38'58.60"	Rockfall	14080±1549	9387±4545	

a: Classification based on Varnes (1978) ; Hungr et al. (2014)

b: Error (±) caused by GE measurement (1.11 %)

c: Error (±) is the product of area ± error and thickness ± error. Thickness error (Std. dev.) corresponds to averaging of field based approximated thickness

BIO- DATA OF THE CANDIDATE

I. List of publications

Published

1. Gupta V., Nautiyal H., Kumar V., **Jamir I.**, and Tandon R.S. (2016) Landslides hazards around Uttarkashi Township, Garhwal Himalaya, after the tragic flash flood in June 2013. *Natural Hazards*, 80, 1689-1707.
2. Gupta V., **Jamir I.**, Kumar V., and Devi M. (2017). Geomechanical characterization of slopes for assessing rockfall hazards between Janki Chatti and Yamunotri Temple, Yamuna valley, Higher Himalaya, India. *Himalayan Geology*, 38 (2), 156-170.
3. **Jamir, I.**, Gupta, V., Kumar, V., and Thong, G. T. (2017). Evaluation of potential surface instability using finite element method in Kharsali Village, Yamuna Valley, Northwest Himalaya. *Journal of Mountain Science*, 14(8), 1666-1676.
4. Kumar V., Gupta V., and **Jamir I.** (2018). Hazard Evaluation of Progressive Pawari Landslide Zone, Kinnaur, Satluj Valley, Higher Himalaya, India. *Natural Hazards*.
5. Kumar V., Gupta V., **Jamir I.** and Chatteraj SL. (2018). Evaluation of Potential landslide damming of Satluj River; Case study of Urni landslide, Kinnaur, Northwest Himalaya. *Geoscience Frontier*.

Under review

6. **Jamir I.**, Gupta V., Thong GT. and Kumar V. (2018). Inter and intra-relationship of landslides; Case study of Yamuna valley, NW Himalaya. *Physical Geography*

Yet to be communicated

7. The influence of tectonics and role of lineaments on slope stability in the Northwest Himalaya, India

II. CONFERENCES ATTENDED AND PAPER PRESENTED

- Presented paper in the 30th *Himalayan-Karakoram-Tibet Workshop (HKT)* Workshop, organized by the Wadia Institute of Himalayan Geology, Dehradun on 6th-8th October, 2015.

- Presented paper in the 2nd *National Geo-research Scholars Meet*, organized by the Wadia Institute of Himalayan Geology, Dehradun on 17th – 20th May, 2017.

III. TRAININGS ATTENDED

- Geological mapping in Chitradurga, conducted by the Geological survey of India (GSI), 2011.
- Rock-Engineering for the Hilly Regions, organized by Department of Civil Engineering, IIT Roorkee, 2015.
- Training programme on the “Introduction to Landslide Site Mapping”, organized by IIT Kanpur, DST, Govt. of India, 2017.
- Training programme on “Monitoring and modeling of large landslides”, organized by Chengdu University of Technology, China on 14th -27th Oct., 2018.